Biophysical Journal
Article

Biophysical Society

Control of Platelet CLEC-2-Mediated Activation by Receptor Clustering and Tyrosine Kinase Signaling

Alexey A. Martyanov,[1,2,3,4] Fedor A. Balabin,[1,2] Joanne L. Dunster,[5] Mikhail A. Panteleev,[1,2,4,6] Jonathan M. Gibbins,[5] and Anastasia N. Sveshnikova[1,2,4,7,*]

[1]Center for Theoretical Problems of Physico-chemical Pharmacology, Russian Academy of Sciences, Moscow, Russia; [2]Dmitry Rogachev National Medical Research Centre of Pediatric Hematology, Oncology and Immunology, Moscow, Russia; [3]Institute for Biochemical Physics, Russian Academy of Sciences, Moscow, Russia; [4]Faculty of Physics, Lomonosov Moscow State University, Moscow, Russia; [5]Institute for Cardiovascular and Metabolic Research, School of Biological Sciences, Harborne Building, University of Reading, Whiteknights, Reading, United Kingdom; [6]Faculty of Biological and Medical Physics, Moscow Institute of Physics and Technology, Dolgoprudnyi, Russia; and [7]Department of Normal Physiology, Sechenov First Moscow State Medical University, Moscow, Russia

ABSTRACT Platelets are blood cells responsible for vascular integrity preservation. The activation of platelet receptor C-type lectin-like receptor II-type (CLEC-2) could partially mediate the latter function. Although this receptor is considered to be of importance for hemostasis, the rate-limiting steps of CLEC-2-induced platelet activation are not clear. Here, we aimed to investigate CLEC-2-induced platelet signal transduction using computational modeling in combination with experimental approaches. We developed a stochastic multicompartmental computational model of CLEC-2 signaling. The model described platelet activation beginning with CLEC-2 receptor clustering, followed by Syk and Src family kinase phosphorylation, determined by the cluster size. Active Syk mediated linker adaptor for T cell protein phosphorylation and membrane signalosome formation, which resulted in the activation of Bruton's tyrosine kinase, phospholipase and phosphoinositide-3-kinase, calcium, and phosphoinositide signaling. The model parameters were assessed from published experimental data. Flow cytometry, total internal reflection fluorescence and confocal microscopy, and western blotting quantification of the protein phosphorylation were used for the assessment of the experimental dynamics of CLEC-2-induced platelet activation. Analysis of the model revealed that the CLEC-2 receptor clustering leading to the membrane-based signalosome formation is a critical element required for the accurate description of the experimental data. Both receptor clustering and signalosome formation are among the rate-limiting steps of CLEC-2-mediated platelet activation. In agreement with these predictions, the CLEC-2-induced platelet activation, but not activation mediated by G-protein-coupled receptors, was strongly dependent on temperature conditions and cholesterol depletion. Besides, the model predicted that CLEC-2-induced platelet activation results in cytosolic calcium spiking, which was confirmed by single-platelet total internal reflection fluorescence microscopy imaging. Our results suggest a refined picture of the platelet signal transduction network associated with CLEC-2. We show that tyrosine kinase activation is not the only rate-limiting step in CLEC-2-induced activation of platelets. Translocation of receptor-agonist complexes to the signaling region and linker adaptor for T cell signalosome formation in this region are limiting CLEC-2-induced activation as well.

SIGNIFICANCE C-type lectin-like receptor II-type (CLEC-2) is a recently discovered platelet receptor implicated in the control of vascular integrity. Here, we computationally reconstructed the regulation of tyrosine kinase and calcium signaling network that controls blood platelet activation via CLEC-2 receptor. We demonstrated that the assembly of the receptors in clusters is the rate-limiting processes in the tyrosine-kinase-associated signal transduction, which could explain the slow rates of platelet activation by CLEC-2. Additionally, we demonstrated for the first time, to our knowledge, that CLEC-2 stimulation leads to cytosolic calcium spiking, with a qualitative change caused by the clustering-affecting influences such as temperature and cholesterol saturation.

INTRODUCTION

The main task of platelets, nonnucleated cellular fragments produced from megakaryocytes in the bone marrow, is the prevention of blood loss upon vessel wall disruption (1). Platelets circulate in the cardiovascular system for

Submitted November 13, 2019, and accepted for publication April 13, 2020.

*Correspondence: agolomy@gmail.com

Editor: Joseph Falke.

https://doi.org/10.1016/j.bpj.2020.04.023

approximately 7 days until they get eliminated in the spleen or liver (2). Alongside their primary role in hemostasis, platelets have been demonstrated to be involved in angiogenesis (3), tissue remodeling (4,5), and leukocyte recruitment under inflammatory conditions (6,7). Platelets respond gradually to various activators (1). Platelet responses to contact with extracellular matrix protein collagen include shape change, granule release, and, in some cases, cell death (8). In contrast, platelet responses to ADP include only shape change and integrin activation (8).

There are two main types of signaling pathways in blood platelets, associated either with G-proteins or with tyrosine kinase signaling (9). Platelet G-protein-coupled receptors govern responses to ADP (P2Y1, P2Y12 receptors), thromboxane A2 (TxA_2), thrombin (protease-activated receptors 1 and 4 (PAR1, PAR4)), epinephrine (α2A), and prostacyclin (IP) (10,11). Platelet receptors that induce tyrosine kinase network of signaling are the receptors for collagen (glycoprotein VI (GPVI)) (8,12) and for IgG (FcγRIIa) (9) and were recently found on platelet receptor C-type lectin-like receptor II-type (CLEC-2) (8). The only confirmed endogenous CLEC-2 ligand is a membrane protein, podoplanin, expressed by the lymphatic endothelial cells (13,14). Therefore, the primary platelet CLEC-2 physiological function is considered to be the separation of blood and lymphatic systems (15–18). Other known CLEC-2 agonists are snake venom protein rhodocytin (19,20) and brown seaweed extract fucoidan (21). CLEC-2 also contributes to the maintenance of blood vessel integrity during inflammatory conditions (17,22–25) and has a role in thrombus formation and wound healing (7,23,26–29) and in various pathologies (30–32). This makes CLEC-2 a prospective therapeutic target (7,29,32,33). Thus, systemic understanding of the CLEC-2 signaling is of essential importance.

A distinct feature observed upon platelet activation via CLEC-2 by either podoplanin, rhodocytin, or fucoidan was 1- to 2-min lag-time before activation (21,34). This has been demonstrated using spectrofluorimetric assay of platelet cytosolic calcium (21). However, it is not understood whether platelet CLEC-2 can induce cytosolic calcium spiking, prolonged cytosolic calcium oscillations, or transient increase of cytosolic calcium. The prolonged platelet CLEC-2-induced response may be a consequence of ADP-containing granule secretion and TxA2 synthesis. Another possible cause of the significant activation lag-time is the receptor clustering, as was proposed by Pollitt et al. (34). Indeed, glycosylated extracellular stalk regions (35), as well as the GxxxG region in the transmembrane domain of CLEC-2 (35,36), lead to homodimerization of the recombinant CLEC-2 proteins (35). On the surface of the resting platelets, CLEC-2 is present in both dimeric and monomeric forms (35,36). Upon ligand binding, CLEC-2 undergoes multimerization (36), which might be ligand driven (e.g., tetrameric rhodocytin can bind two copies of single CLEC-2 or two CLEC-2 dimers simultaneously (37)). On the other hand, nonmultimeric podoplanin still induces CLEC-2 cluster formation (38), which implies more complex clustering mechanisms. The platelet responses to CLEC-2 are also highly dependent on actin polymerization and cholesterol presence in the plasma membrane (34,39). However, unlike cholesterol presence, actin cytoskeleton reorganization is not required for CLEC-2 oligomerization (34). Badolia et al. have recently reported that CLEC-2-induced signaling is still detectable after the abrogation of secondary activation (40).

The computational modeling approach could be useful to reveal the sequence of events in CLEC-2-induced platelet activation and identification of rate-limiting steps in this pathway. Mukherjee et al. demonstrated that receptor clustering is significant for the activation of ITAM-bearing receptors (B-cell receptors (BCR) and T cell receptors (TCR)) (41). The significance of platelet receptor clustering was demonstrated experimentally for CLEC-2 (38) and GPVI (42); however, the computational models of GPVI-induced platelet activation do not incorporate the receptor clustering (43,44). Because of their small size, platelets do not possess significant amounts of signaling proteins. For example, there are only 2000 copies of phospholipase Cγ2 (PLCγ2) in platelets ($\sim$500 nM). Even upon strong activation, no more than 25% of signaling proteins become active (44). Thus, it can be claimed that there are less than 100 active signal-transducing proteins in platelets upon weak stimulation. Because of the low amounts of active participants of the signaling cascades in platelets, deterministic modeling might not be capable of providing reliable calculation results. Thus, stochastic approaches are required for platelet models (45–47).

Here, we aimed to reveal the primary events of platelet activation upon stimulation through CLEC-2 by means of computational modeling and experimental analysis. The proposed in silico model described platelet activation starting from ligand binding to CLEC-2 and proceeding until calcium ions release from the dense tubular system. The model predicted that besides tyrosine kinase activity, platelet activation via CLEC-2 is limited by the CLEC-2 receptor clustering in the plasma membrane, the CLEC-2 clustering pattern, and the LAT signalosome formation. Model predictions were supported experimentally by an essential dependence of CLEC-2-induced platelet activation on temperature and by modulation of membrane saturation of cholesterol by methyl-β-cyclodextrin (mβCD). The model also predicted CLEC-2-induced calcium spiking, which was confirmed experimentally using total internal reflection fluorescence microscopy (TIRF microscopy). Our data enable us to propose a refined concept of signal transduction upon platelet activation via CLEC-2.

METHODS

Reagents

The sources of the materials were as follows: calcium-sensitive cell-permeable fluorescent dye Fura-2-AM, Fura Red-AM (Molecular Probes, Eugene, OR), fucoidan from *Fucus vesiculosis*, ADP, PGI_2, EGTA, HEPES, bovine serum albumin (BSA), apyrase grade VII, and mβCD (Sigma-Aldrich, St Louis, MO). VM-64 antibody was a kind gift of Dr. A.V. Mazurov (National Medical Research Centre (NMRC) of Cardiology, Moscow, RF) (48).

Blood collection and platelet isolation

Healthy volunteers, both men and women aged between 18 and 35 years, were recruited into the study. Investigations were performed under the Declaration of Helsinki, and written informed consent was obtained from all donors. Blood was collected into 4.5 mL tubes containing 3.8% sodium citrate (1:9 vol/vol) and supplemented by apyrase (0.1 U/mL). The study was approved by the Independent Ethics Committee at Center for Theoretical Problems of Physico-chemical Pharmacology, Russian Academy of Sciences (CTP PCP RAS; 1_2018-1 from 12.01.2018). Platelets were purified by double centrifugation as described previously (45,49). Briefly, platelet-rich plasma was obtained by centrifugation at 100 $\times$ *g* for 8 min. Platelet-rich plasma was supplemented with additional sodium citrate (27 mM) and centrifuged at 400 $\times$ *g* for 5 min. The resultant supernatant was removed, and platelets were resuspended in Tyrode's buffer (150 mM NaCl, 2.7 mM KCl, 1 mM $MgCl_2$, 0.4 mM NaH_2PO_4, 5 mM HEPES, 5 mM glucose, 0.2% BSA (pH 7.4)). Alternatively, blood was collected in Li-heparin (IMPROVACUTER; Guangzhou Improve Medical Instruments Co., China) or hirudin (Monovette; Sarstedt, Newton, NC) containing vacuum tubes.

Flow cytometry and inhibitory analysis

For continuous flow cytometry experiments, washed platelets were incubated with either 2 μM Fura Red-AM (2 μM of Fura-2) before the final wash for 45 min at room temperature or for 30 min at 37°C in the presence of apyrase (1 U/mL). Platelets were then incubated in buffer A for 10 min and then centrifuged. Whole blood was incubated with either 2 μM Fura Red-AM (or 2 μM of Fluo-3 or Fluo-4 and 2 μM of Fura-2) for 30 min at 37°C in the presence of apyrase (1 U/mL). Whole blood was diluted 20 times with calcium and albumin containing Tyrode's buffer. Samples were diluted to concentration 1000 plt/μL and analyzed using FACS Canto II or FACS Aria (BD Biosciences, San Jose, CA) flow cytometer in a continuous regime with 20-s interruption for the addition of an activator.

Immunoblotting

Human platelets from drug-free volunteers were prepared on the day of the experiment as described previously (50) and suspended in modified Tyrode's-HEPES buffer (134 mM NaCl, 0.34 mM Na_2HPO_4, 2.9 mM KCl, 12 mM $NaHCO_3$, 20 mM HEPES, 5 mM glucose, 1 mM $MgCl_2$ (pH 7.3)) to a density of 1.5 $\times$ 10^9 cells/mL. Stimulation of platelets with 10$\times$ fucoidan (final concentration of 1, 10, or 100 μg/mL) was performed for 0–15–30–60–90–120–150–180–300 s at 25 or 37°C in an aggregometer with continuous stirring (1000 rpm). Reactions were abrogated by addition of 4$\times$ sodium dodecyl sulfate-polyacrylamide gel electrophoresis (SDS-PAGE) sample treatment buffer (200 mM Tris-HCl (pH 6.8), b-MeEtOH 400 mM, SDS 4%, bromophenol blue 0.01%, glycerol 40%). Samples were then heated to 99°C for 10 min and centrifuged at 15,000 $\times$ *g* for 10 min to remove cell debris.

Proteins were separated by SDS-PAGE on 10% gels and transferred to polyvinylidene difluoride membranes that were then blocked by incubation in 5% (w/v) bovine serum albumin dissolved in Tris-buffered saline with Tween 20 (TBS-T). Primary and secondary antibodies were diluted in TBS-T containing 2% (w/v) bovine serum albumin and incubated with polyvinylidene difluoride membranes for 1.5 h at room temperature. Blots were washed four times for 15 min in TBS-T after each incubation with antibodies and then developed using an enhanced chemiluminescence detection system using ECL Prime Western blotting detection reagent. Primary antibodies were used at a concentration of 1 μg/mL (anti-phosphotyrosine PY20) or diluted 1:1000 (anti-tubulin). Horseradish-peroxidase-conjugated secondary antibodies were diluted 1:1000. To control for protein loading, membranes were stripped by washing two times for 30 min in stripping buffer (250 mM glycine, 0.2% SDS, 0.1% Tween-20, (pH 2.2)) twice for 10 min in phosphate-buffered saline (PBS) and two times for 5 min in TBS-T at room temperature. Membranes were then blocked for 30 min by 2% TBS-T BSA solution at room temperature and restained with anti-tubulin antibodies.

Depletion of platelet cholesterol

Cholesterol was depleted from the plasma membrane of platelets by incubation of washed platelets for 15 min with different concentrations of mβCD at 37°C before stimulation as described in Mahammad and Parmryd (51).

Immunofluorescent microscopy

Washed human platelets were activated by fucoidan (100 μg/mL) at 25°C (with or without cholesterol depletion by mβCD) or at 37°C and fixed by 4% paraformaldehyde (PFA) after 30, 60, 90, 120, and 300 s after activation. Platelets incubated with CRP (5 μg/mL) or mQ water for 300 s were used as positive and negative controls, correspondingly. Fixed platelets were washed from PFA by sequential centrifugation, resuspended in PBS-BSA buffer, and adhered to poly-L-lysine (0.1% in mQ; Sigma-Aldrich)-covered glass coverslips for 90 min at 37°C. Nonadherent platelets were removed by gentle rinsing of the coverslips. Fixed platelets on the glass were then permeabilized by 0.2% Triton X-100 in the presence of 2% BSA and 1% goat serum. After permeabilization, platelets were incubated with 1:250 diluted LAT pY1911 (Abcam, Cambridge, MA) antibodies for 90 min at room temperature. After washing primary antibodies off, platelets were incubated with secondary antibodies, conjugated with Fluorescein isothiocyanate (FITC; Imtek, Moscow, RF) for 90 min in the darkroom at room temperature. After washing off secondary antibodies, cells were additionally fixed by adding 4% PFA for 10 min. Samples were then mounted with Dako fluorescence mounting media (Agilent Technologies; Santa Clara, CA). Samples were analyzed by means of Zeiss Axio Observer Z1 microscope (Carl Zeiss, Jena, Germany) in the confocal mode.

Live cell microscopy

For microscopy experiments, platelets were loaded with calcium fluorophores and immobilized by either incubation of platelet suspension in the flow chamber for 5 min or by perfusing whole blood over the surface at a shear rate of 200 s^{-1} for 5 min. For TIRF microscopy, platelets were immobilized either on fucoidan (100 μg/mL) or anti-CD31 (VM-64) (48) and investigated in flow chambers (52). An inverted Nikon Eclipse Ti-E microscope equipped with 100$\times$/1.49 NA TIRF oil objective was used. Cells were observed in DIC and TIRF modes. A 405-nm laser was applied to assess calcium-free Fura-2 fluorescence in a platelet. Calcium concentration was assessed from Fura-2 fluorescence as a ratio of initial/running values, taking exponential bleaching of the dye into account. For temperature fixation, during observation, a lens heater (Bioptechs, Butler, PA) was used.

Data analysis

Nikon NIS-Elements software was used for microscope image acquisition; ImageJ (http://imagej.net/ImageJ) was used for image processing for both

TIRF microscopy and Western blotting and microscopy assays from literature (21,38). For the CLEC-2 cluster size calculation, data were acquired directly from the figures from (38) without additional calibration. The absolute size of CLEC-2 clusters (Fig. S1 *D*) was calculated from the DyLight 594 FcPodoplanin fluorescence intensity (Fig. 5 *A*; (38)), which was assumed to be proportional to the number of receptors per cluster. It has also been assumed that only CLEC-2 monomers and dimers are present on the surface of resting platelets. Flow cytometry data were processed using FlowJo (http://www.flowjo.com/) software. Statistical analysis was performed in Python 3.6.

Model solution and sensitivity analysis

The model, formed of ordinary differential equations (see Supporting Results) with initial variable values (Tables S2, S5, and S7), was integrated using the LSODA method in COPASI software. The stochastic model was solved using stochastic integration methods (combined Adaptive SSA/the τ-leap method (46,53)) implemented in COPASI software, similar to previously published methods (45,54). Parameter estimation was performed using the Genetic Algorithm. Models are given in the Table S9.

Sensitivity score was calculated as $Score = (O_a - O_i)/O_a$, where O_i and O_a represent the model output (e.g., the steady state and time to reach the peak in Syk activity) in respect to the initial parameter set (obtained from parameter fitting) and the adapted parameter, respectively.

RESULTS

Scheme of biochemical reactions underlying our model of CLEC-2-induced platelet activation

The model development was carried out based on the known details of the CLEC-2 signaling network. Briefly, after the binding of CLEC-2 to its ligand, CLEC-2 receptor-ligand complexes rapidly form tight clusters, predominantly in the lipid rafts (35,36). Activated and clustered CLEC-2 molecules can be phosphorylated by platelet Syk tyrosine kinases (55). Although it has been proposed that Src family kinases (SFKs) also participate in the process of CLEC-2 phosphorylation (56,57), here in the model, we considered SFKs merely as a positive mediator for Syk basal activation (17). The inactive Syk rapidly bound two phosphorylated CLEC-2 receptors by two Src homology 2 (SH-2) domains. Association with CLEC-2 resulted in Syk activation and stabilization of CLEC-2 dimers (17,58,59). Binding of SFKs to phosphorylated hemITAM also led to the complete SFK activation, which additionally amplified Syk activation (17,58). Syk activated T cell ubiquitin ligand-2 (TULA-2), which is a negative regulator Syk activation (44). Active Syk and SFKs phosphorylated an adaptor molecule called LAT, leading to LAT signalosome formation (34,40,60), which consists of PLCγ2, phosphoinositide-3-kinase (PI3K), SH2-domain-containing leukocyte phosphoprotein of 76 kDa (SLP-76), and a set of other adaptor proteins. In the LAT signalosome, the PI3K became active and produced phosphoinositol-3,4,5 trisphosphate (PIP_3) from phosphoinositol-4,5 bisphosphate (PIP_2) in the surrounding plasma membrane region. The increase in PIP_3 concentration resulted in Bruton's tyrosine kinase (Btk) attraction to the region and phosphorylation and activation of PLCγ2 (61). Finally, PLCγ2 hydrolyzed PIP_2 and produced inositol-1,4,5 trisphosphate (IP_3). IP_3 induced Ca^{2+} signaling. A brief scheme of platelet CLEC-2 signaling (Fig. 1) described above was the basis of the constructed computational model.

Computational model construction

The computational model of CLEC-2-induced platelet activation was designed according to the scheme above. It consisted of five compartments: extracellular space, plasma

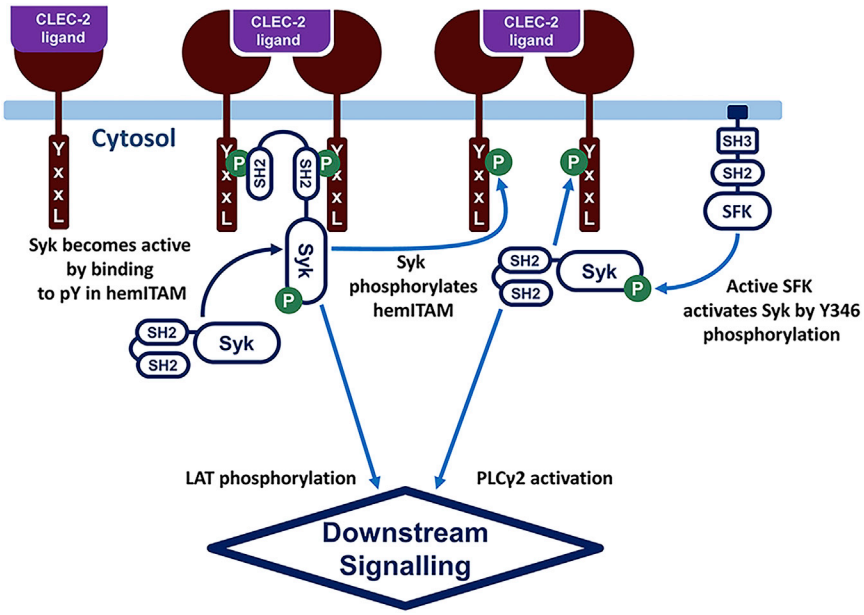

FIGURE 1 CLEC-2-induced signaling in blood platelets. In resting platelets, relatively few Syk kinases are active because of the low SFK activity. Upon ligation of the platelet CLEC-2 and CLEC-2 cluster formation, tyrosine residues in the CLEC-2 cytoplasmic domain (YxxL sequence, hemITAM) become phosphorylated by Syk kinases. Nonactive Syk kinases bind to phosphorylated hemITAM with its SH2 domains and become active via *trans*-autophosphorylation. Accumulation of the active Syk results in downstream platelet activation and calcium signaling. To see this figure in color, go online.

membrane, cytosol, dense tubular system (DTS) membrane, and DTS (Table S1). The model included the following biochemical modules: the "CLEC-2 clustering" module, capturing CLEC-2 ligand binding and cluster formation (Fig. 2 *A*; Tables S2–S4); the "quiescent state" module, capturing CD148 and C-terminal Src kinase (Csk)-mediated SFK activation and Syk primary activation by active SFKs (Fig. 2 *B*; Tables S5 and S6); the "tyrosine kinase" module, capturing CLEC-2 phosphorylation and activation of Syk and SFK kinases (Fig. 2 *C*; Tables S5 and S6); the "LAT-PLCγ2" module, capturing events downstream of activated Syk and SFKs, including phosphorylation of LAT, PI3K and Btk incorporation to the signalosome, PLCγ2 activation, and production of IP_3 (Fig. 2 *D*; Tables S7 and S8); and the "calcium" module, capturing IP_3-induced calcium signaling in platelet cytosol (from Fig. 2 *D*; (45,62)). The underlying systems of differential equations were constructed from current biological knowledge (see above) using the assumptions of either mass action or Henry-Michaelis-Menten kinetics. The probabilities in the corresponding stochastic model were calculated based on the same assumptions. The parameter values were taken from the experimental reports on the corresponding human enzymes, whereas the numbers of proteins per platelet were

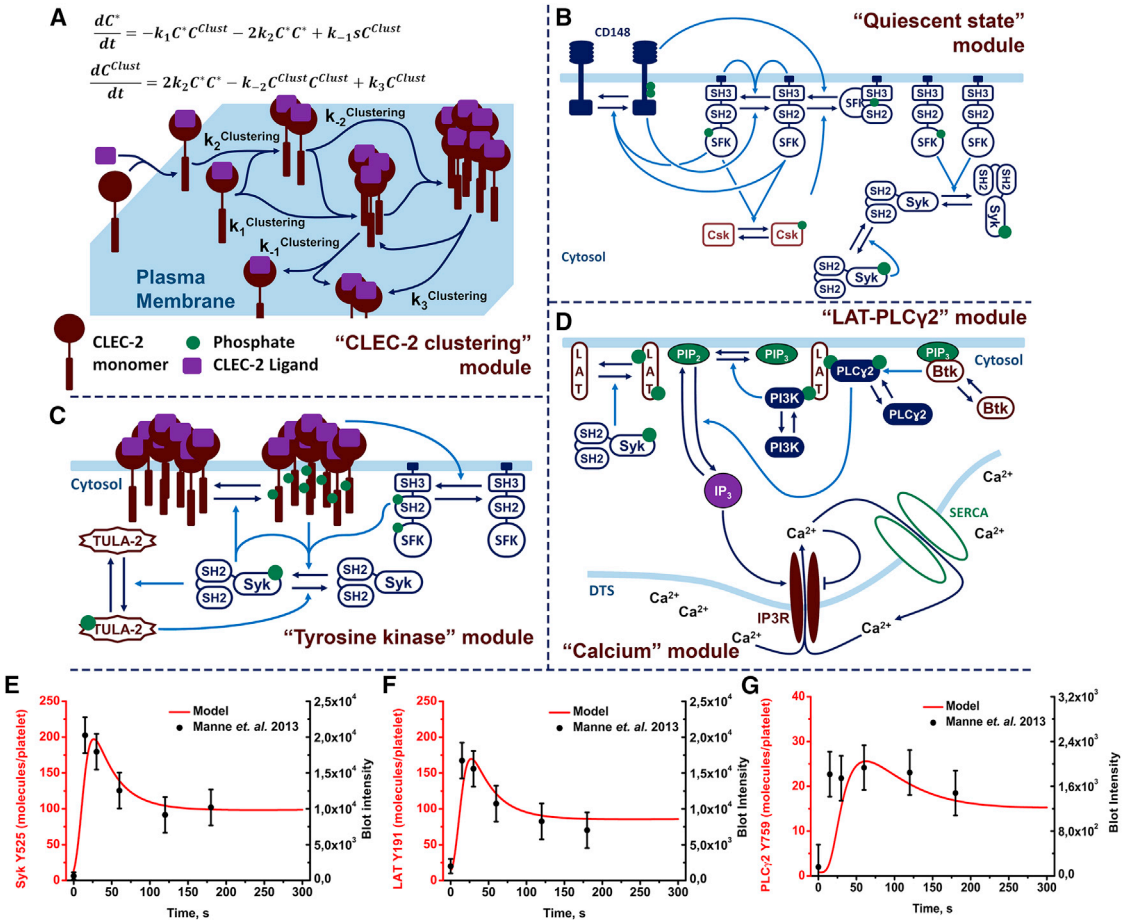

FIGURE 2 Scheme of the model of platelet CLEC-2 signaling. The "CLEC-2 clustering" module (*A*) after CLEC-2 ligation CLEC-2 molecules to formed clusters is shown here. The model of the CLEC-2 clustering is based on Filkova et al. (64). Activated CLEC-2 molecules could form CLEC-2 clusters, which could form larger clusters by binding single-activated CLEC-2 molecules or other clusters. The clusters decayed into cluster and cluster or cluster and single-CLEC-2 molecule. The "quiescent state" module (*B*) shows that active CD148 produces one-third-active SFKs, which are negatively regulated by active Csk. One-third-active SFKs autophosphorylated and became two-thirds-active SFKs. Active CD148 negatively regulated this reaction. All forms of active SFKs mediated CD148, Csk, and Syk activation. Active Syk activated nonactive Syk. The "tyrosine kinase" module (*C*) shows that after cluster formation, active Syk phosphorylated hemITAM in the CLEC-2 cytoplasmic domains. Inactive Syk or two-thirds-active SFKs bound phospho-hemITAMs (two for Syk and one for SFKs) with their SH2 domains and became active. Active Syk also mediated TULA-2 phosphatase activation, which is a negative regulator of Syk activity. "LAT-PLCγ2" module (*D*) shows that active Syk phosphorylated the adaptor protein LAT. PLCγ2 and PI3K bound P-LAT, which activated PI3K. Active PI3K phosphorylated PIP_2 and produced PIP_3, which became a docking site for Btk. Btk activated upon PIP_3 binding and activated PLCγ2. Active PLCγ2 hydrolyzed PIP_2 and produced IP_3. The "calcium" module (*D*) shows that IP_3 activated IP3R on the surface of the DTS. Through active IP3R, free Ca^{2+} ions passed to the cytosol. Ca^{2+} inhibited IP3R as well and returned to the DTS via SERCA. Dark blue lines represented transitions between species; light blue lines represented catalysis. Copy numbers of active Syk (*E*), LAT (*F*), and PLCγ2 (*G*) were fitted to experimental data on fucoidan-induced platelet activation from Manne et al. (21), error bars represent 10% from the experimental values. To see this figure in color, go online.

taken from the published proteomics data (63). The model reactions, equations, and parameter values can be found in Supporting Results.

The "CLEC-2 clustering" module described the process of receptor clustering. Mathematically, this description was performed by two differential equations, based on our previously published study (64). This approach was called the "two-equation" model (Fig. 2 *A*). Its applicability and correspondence to an explicit model of receptor cluster formation (called the "N-equation" model) and experimental data are given in the Fig. S1. The "two-equation" model described the behavior of variables for the concentration of single CLEC-2 molecules and the concentration of CLEC-2 clusters in the plasma membrane (Fig. 2 *A*; Fig. S1 *B*). During the estimation of the "CLEC-2 clustering" module parameters, we identified two distinct patterns of receptor clustering in the "two-equation" model. The first, which could be called "ligand-mediated" cluster formation, suggested that the clustering coincides with receptor ligation. The second, called the "postligation" cluster formation, suggested that the clusters appear after the formation of receptor-ligand complexes. Both patterns will be discussed further in Two Different Clustering Patterns Predicted by the Model. All of the model calculations were performed with "ligand-mediated" cluster formation model, except where otherwise stated.

For the "quiescent state" module, the unknown parameters were tuned to obtain 5% of active Syk kinases and 10% of active SFK kinases at the steady state achieved without CLEC-2 ligand in the system. The CD148 phosphatase and Csk kinase were introduced into the model to maintain this steady state (Fig. 2 *B*). For the "tyrosine kinase" module, we assumed that the first event was the phosphorylation of CLEC-2 in clusters by Syk kinases. The activation of Syk kinases, as well as SFK activation, was assumed to occur depending on the CLEC-2 cluster size. The descriptions of the "LAT-PLCγ2" module and the "calcium" module can be found in the Supporting Results (Fig. 2 *D*). It is noteworthy that the only link between the "calcium" module and the other modules was the IP_3 concentration, which, in its turn, was mediated by active PLCγ2. That is why we chose the number of active PLCγ2 as one of the major model output. A network diagram depicting all of the reactions and parameters of the model is given in Fig. S2. The corresponding Systems Biology Markup Language files can be found in Data S1 (also see Table S9 for details).

The full model was constructed as a sum of the separate models described above without further adjustment of the parameters. The full model appeared to be capable of the correct description of the following experimental data. The predicted numbers of active Syk, SFKs, and the phosphorylated LAT (Fig. 2, *E* and *F*, and Fig. S3, respectively) were in good agreement with available information from experimental literature data (21). However, the predicted numbers of active PLCγ2 described the data less accurately (Fig. 2 *G*), which could be caused by the secondary activation of platelets under the conditions of the experiment.

Two different clustering patterns predicted by the model

In the process of parameter estimation for the "CLEC-2 clustering" module, we identified two different possible sets of parameters from which the model could describe experimental data Pollitt et al. (Figs. 3 and S1 *D*; (38)). The first observed pattern was called a "ligand-mediated" receptor clustering when the rapid receptor dimerization immediately followed the receptors' ligation (Fig. 3 *A*). The "ligand-mediated" receptor-clustering mode corresponds to the ligand-driven receptor-clustering mechanism in vivo. The second pattern, when the receptors' ligation did not directly lead to receptor dimerization, was termed "postligation" (Fig. 3 *A*). This mode corresponded to the assumption that CLEC-2 receptor undergoes additional conformational changes after ligation, which made it more prone to clustering. The comparison of the average cluster size between two different schemes is given in Fig. 3 *B*. Parameter variation results revealed that the maximal size of the CLEC-2 clusters is determined by the total number of CLEC-2 as well as kinetic parameters of the clustering, for both the "ligand-mediated" (Fig. S4, *A–C*) and "postligation" (Fig. S4, *G–L*) clustering regimes. However, in the "ligand-mediated" clustering regime, the maximal CLEC-2 cluster size appeared to be more sensitive to the assessed parameters than in the "postligation" regime (Fig. S4).

With both schemes, the full model predicted cytosolic calcium spiking (Fig. 3 *A*). However, the "postligation" scheme could not be tuned to induce calcium spiking earlier than 200 s after ligand introduction (Fig. 3, *A* and *D*), despite producing a more significant increase in the number of active PLCγ2 (Fig. 3 *C*) and higher concentration of cytosolic calcium in the cell population (Fig. 3 *D*). However, previous experimental data (21) suggested much shorter activation times for CLEC-2-induced platelet activation, and thus, we preferred the "ligation-mediated" scheme. Curiously, a rapid dimerization of ITAM receptors was demonstrated to correlate with the shortened cell activation lag-times elsewhere (41).

Sensitivity analysis of the model

To analyze the influence of unknown parameters and determine the possible rate-limiting steps, we performed a local sensitivity analysis (Fig. 4; Figs. S5–S16). Scaled local sensitivities of the time to reach the peak quantities/concentrations of active Syk (S^*), phosphorylated LAT (L^*), active PLCγ2 (p^*), IP_3 (I_3), and cytosolic Ca^{2+} to all model parameter values were calculated. The results are given in Figs. 4 *A* and S5. Parameters of the "tyrosine kinase" module had the biggest impact on all of the analyzed variables. The "LAT-PLCγ2" module parameters were less influential, and the "CLEC-2

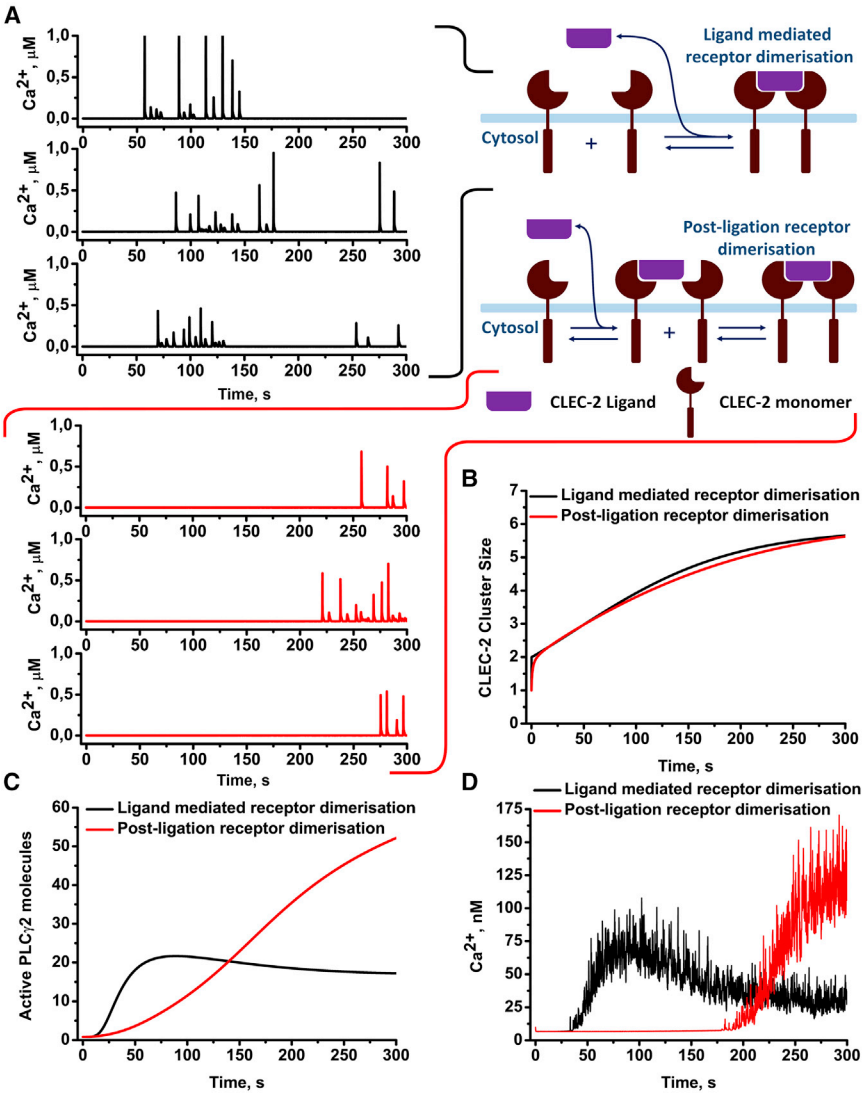

FIGURE 3 Comparison of the receptor-clustering patterns effects on platelet CLEC-2-induced activation. Two patterns of receptor clustering are shown: ligand-mediated receptor clustering (rapid receptor dimerization upon ligation, *black*) and postligation clustering (ligation does not lead to rapid receptor dimerization, *red*). (*A*) Both approaches resulted in cytosolic calcium spiking. However, the postligation model resulted in a significantly delayed activation in comparison with the rapid-dimerization model (*B* and *C*). Averaging of the calcium concentration over 500 stochastic runs of the model also demonstrated that the delayed model demonstrated a significantly delayed but yet amplified response in comparison to the rapid-dimerization model (*D*). To see this figure in color, go online.

clustering" module parameters were the least influential. The "tyrosine kinase" module parameters concerning Syk ($[Syk]_0$, k_{cat}^{Syk}, Km^{Syk}, and k_{S1}^{SH2}) influenced all platelet responses, whereas its parameter for CLEC-2 dephosphorylation rate (Kr^{Phosph}) was the most influential only for S^* (active Syk). Among the "LAT-PLCγ2" module parameters, the most influential parameters were the reverse rate of LAT phosphorylation and LAT concentration (Kr^{LAT}, $[LAT]_0$ for all of the variables, except Syk) and the catalytic parameters of Btk kinase (k_{cat}^{Btk}, Km^{Btk}, for all variables except Btk). Finally, among parameters of the "CLEC-2 clustering" module, k_{-2}, k_{-1}, and k_1, along with CLEC-2 initial concentration, were influential for all responses. Explicit variation of the most influential model parameters for PLCγ2 is given in Fig. 4, *B–M*. Variation of the rest of parameters concerning all of the analyzed variables and sensitivity scores for all of the variables can be found in Figs. S6–S16 and Tables S10–S14, correspondingly. Based on these results, we can conclude that the most influential parameters for all of the analyzed variables concern Syk kinase activation (k_{S1}^{SH2}, k_{cat}^{Syk}, Km^{Syk}). On the other hand, parameters, governing reverse reactions (Kr^{Phosph}, Kr^{LAT}, Kr^{Syk}), as well as parameters concerning TULA-2 activation (Kf_{Syk}^{TULA2}, Kr_{Syk}^{TULA2}, Kr_{TULA2}^{Syk}), also were among the most influential, which highlights the role of the negative regulators of signaling for CLEC-2-induced platelet activation. Finally, local sensitivity analysis also allowed the identification of three rate-limiting reactions: Syk kinase activation, LAT phosphorylation, and CLEC-2 cluster formation. Among these reactions, Syk activation was the most influential.

CLEC-2 agonist fucoidan is capable of evoking calcium response in platelets independently from secondary mediators of signaling

One of the model predictions suggested that CLEC-2 stimulation was sufficient to initiate calcium signaling in

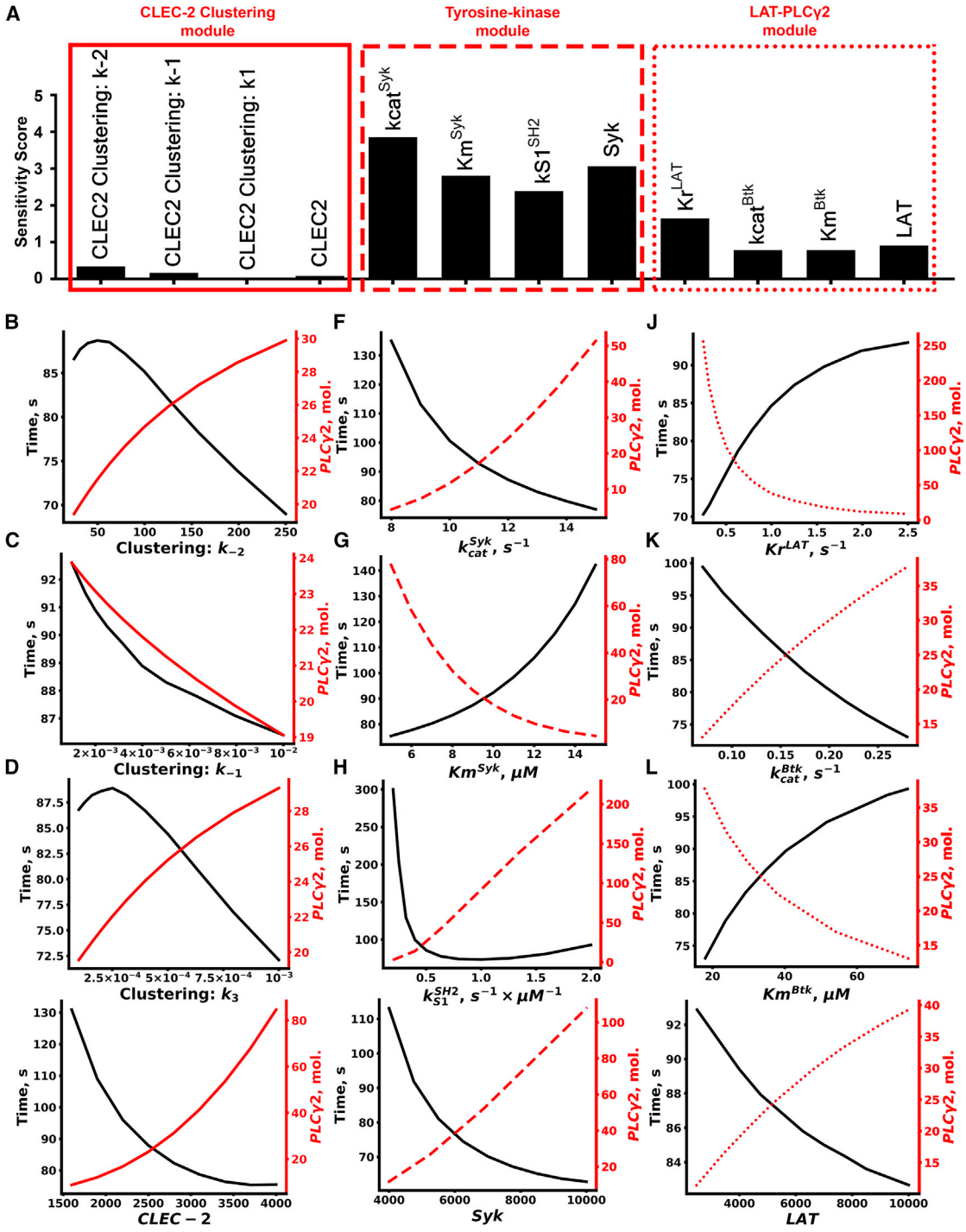

FIGURE 4 Sensitivity analysis and variation of the unknown parameters. Sensitivity scores for the effect of parameter variation on the concentration of active PLCγ2 were calculated (*A*). Explicit variation of the parameters with the highest sensitivity scores for the effect on maximal PLCγ2 number and time to reach the maximum for CLEC-2 clustering k_{-2} (*B*), CLEC-2 clustering k_{-1} (*C*), CLEC-2 clustering k_3 (*D*), CLEC-2 initial number (*E*), turnover rate of Syk kinases (*F*), Michaelis constant of Syk kinases (*G*), forward rate of Syk activation upon SH-2 domain binding to dually phosphorylated hemITAMs (*H*), Syk initial number (*I*), reverse rate of LAT phosphorylation (*J*), turnover rate of Btk (*K*), Michaelis constant of Btk (*L*), and LAT initial number (*M*) are shown. To see this figure in color, go online.

platelets (Fig. 3, *A* and *D*). To test this prediction, we performed flow cytometry experiments on platelets loaded with calcium fluorophore Fura Red (Fig. 5 *A*). To avoid an impact from secondary activation, we preincubated platelets with P2Y1 receptor antagonist MRS2179 (Fig. 5 *A*). To assess the predicted dependence of platelet activation on

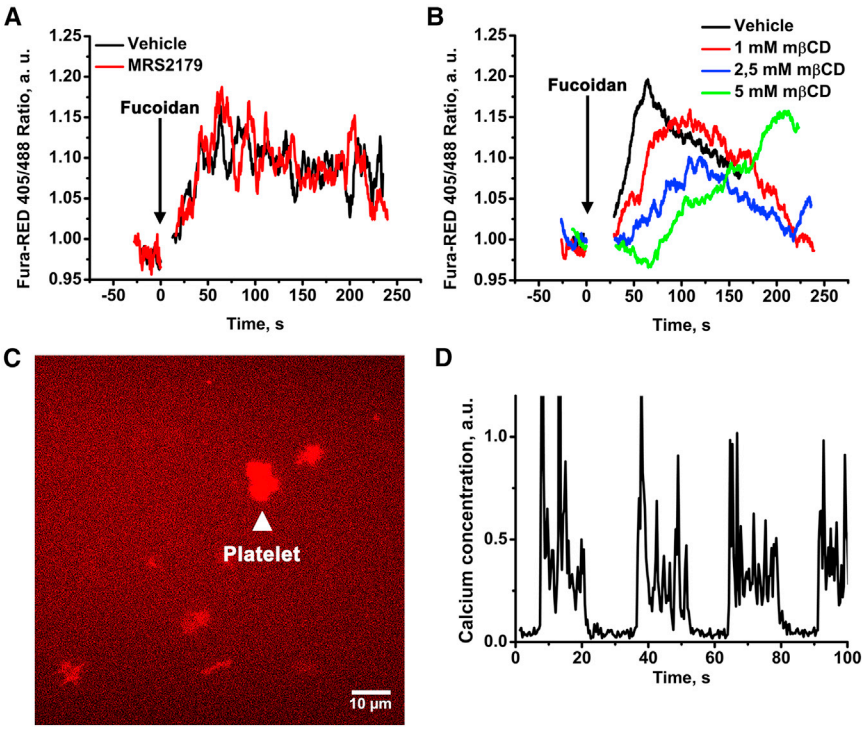

FIGURE 5 CLEC-2-evoked calcium signaling in platelets. Continuous flow cytometry analysis of highly diluted platelet suspension (1×10^3 plt/mL) revealed that CLEC-2 agonist fucoidan-induced calcium response is independent of the presence of MRS2179 (*A*) while being gradually dependent on the concentration of mβCD (*B*). Single-cell analysis using TIRF microscopy revealed that platelets are capable of spreading on fucoidan-covered glass (*C*) and that immobilized fucoidan is capable of evoking calcium oscillations in platelets (*D*). To see this figure in color, go online.

the clustering of CLEC-2, we investigated the influence of membrane cholesterol content on calcium response. Cholesterol molecules determine the stability of membrane regions, and thus, incubation of cells with a cholesterol-binding agent mβCD could disrupt clusters of proteins (51). During experiments, we observed that although high concentrations (5 mM) of mβCD were capable of severe disruption of platelet response to fucoidan (Fig. 5 *B*), relatively low concentrations of mβCD (1 mM) delayed platelet activation without affecting its degree (Fig. 5 *B*). This observation was in agreement with model predictions (Fig. 3 *D*), supporting rapid clustering pattern for CLEC-2 (Fig. 3 *A*). To test the prediction of the model that fucoidan induces rare calcium spiking in platelets instead of a stationary increase in calcium concentration (Fig. 3 *A*), we performed analysis of single-cell calcium signaling using fluorescence microscopy (Fig. 5, *C* and *D*). Washed Fura-Red-loaded platelets spread on fucoidan-covered glass (Fig. 5 *C*), which resulted in prolonged calcium spiking (Fig. 5 *D*). This observation supported the model prediction that fucoidan is capable of calcium spiking induction.

Impact of the medium temperature and plasma membrane fluidity on CLEC-2 induced calcium response in platelet suspension

We have performed further investigation of fucoidan-induced intracellular signaling in platelets in the presence of mβCD and temperature variation to test the model predictions on the role of the receptor-clustering process. At both room (25°C) and body (37°C) temperature, activation of platelets with fucoidan led to an increase in cytosolic Ca^{2+} concentration (Fig. 6 *A*). However, at 25°C, this increase occurred at 100 s, whereas at 37°C, it was significantly more rapid and occurred at 60 s. Preincubation of platelets with mβCD further delayed the increase in the concentration of cytosolic calcium both at 25°C (240 s) and at 37°C (105 s) (Fig. 6 *B*). It should be noted that temperature variation did not affect the activation of platelets by low concentrations (2 μM) of ADP (Fig. S17).

Single-cell analysis by means of immunofluorescent microscopy revealed that at 37°C, clustered fractions of phosphorylated LAT, which are known markers of cholesterol-enriched microdomains in the platelet membrane (34), appeared at 30 s, and the amount of phosphorylated LAT reached its maximal values by 60 s (Fig. 6 *C*; Fig. S18). It is noteworthy that at most time points, the bright phosphorylated LAT (LATp) fluorescence spots could be observed. The lower medium temperature and cholesterol depletion by 1 mM mβCD resulted in delayed LATp phosphorylation and decreased clustering (Figs. S19 and S20, correspondingly). Platelets activated by C-reactive protein exhibited the most significant increase in LATp phosphorylation after 300 s (Fig. S21). The "CLEC-2 clustering" module parameter variation (k_1 and k_3 decrease and k_{-2} increase) allowed us to accurately describe the decrease in LAT phosphorylation upon temperature lowering and cholesterol depletion (Fig. 6 *C*; Table S15).

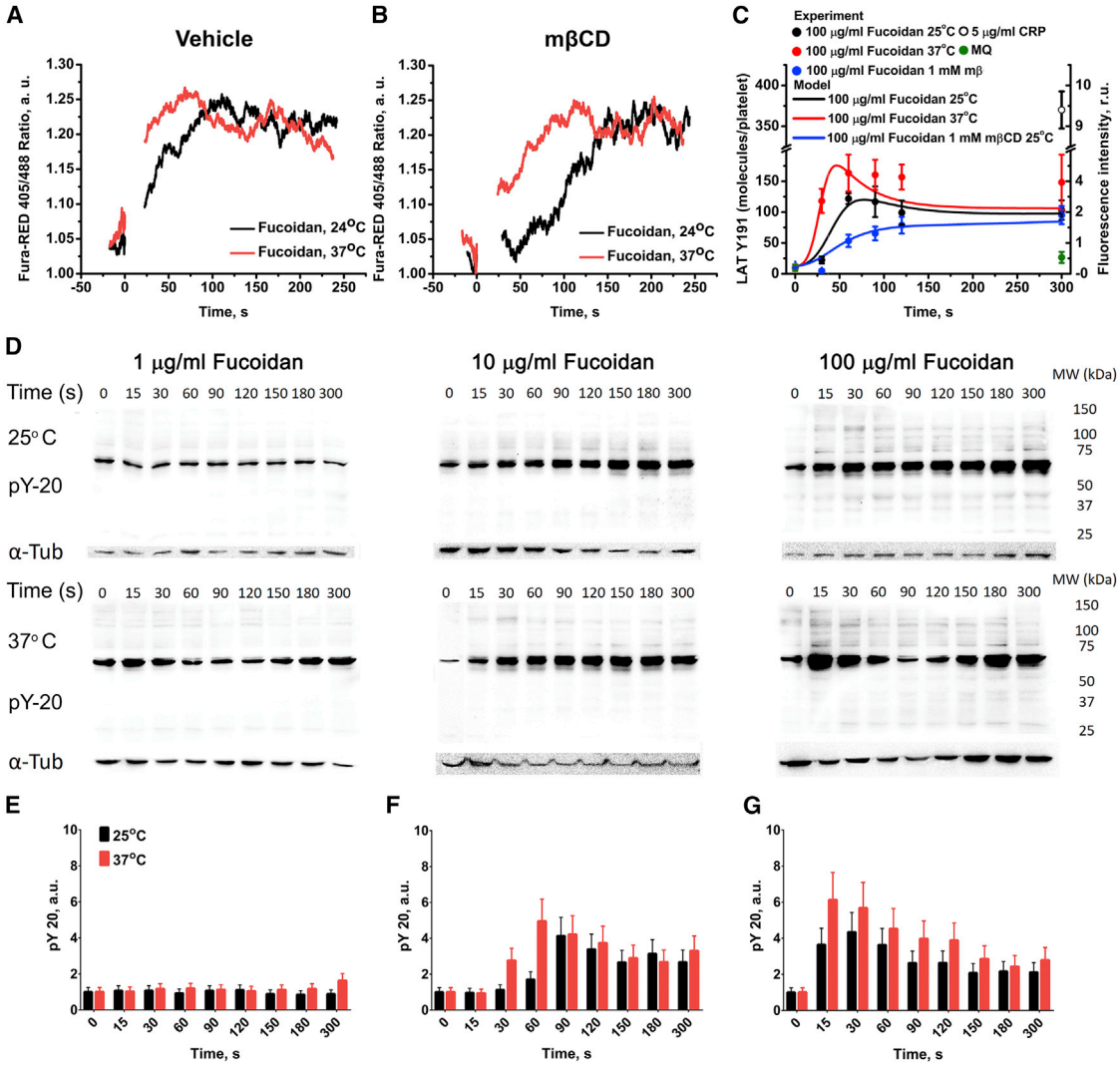

FIGURE 6 Platelet CLEC-2 signaling is dependent on temperature conditions. Flow cytometry assay of CLEC-2 induced signaling in platelets after activation by 100 μg/mL of fucoidan. Activation at 25°C was significantly slower than at 37°C (*A*). Disruption of lipid rafts by mβCD delayed activation (*B*). Each curve represents data from at least three experiments. (*C*) Comparison of the immunofluorescent assays with computational model predictions describing the dependence of platelet CLEC-2-induced activation from medium temperature and cholesterol presence in the cell membrane. Each experimental time point is averaged over 50 platelets. Error barrs represent SEM. (*D–G*) Immunoblot assay of CLEC-2-induced signaling is shown (*D* shows raw data); platelets were activated by 1(*E*), 10(*G*), and 100(*F*) μg/mL of fucoidan at 25 or 37°C. Samples for analysis were taken 0, 15, 30, 60, 90, 120, 150, 180, and 300 s after activation. Murine anti-human-phosphotyrosine primary antibodies (PY-20 clone) were used. Anti-tubulin primary antibodies were used as loading control after stripping. A typical experiment is shown for one out of $n = 3$ different donors, error bars represent SD. To see this figure in color, go online.

To investigate which part of the CLEC-2 signaling cascade is influenced by the temperature changes, we performed immunoblotting analysis of tyrosine phosphorylation level in platelets activated by fucoidan at room and body temperature (Fig. 6, *D–G*). Washed human platelets at a concentration of 1.5×10^9/mL in modified Tyrode's buffer (no BSA and no Ca^{2+}) were incubated with fucoidan for 0–5 min at given temperature conditions. Samples were taken at 15- to 30-s time intervals and analyzed by immunoblotting with anti-phosphotyrosine antibody PY20, as described in Methods. The analysis shows that 1 μg/mL of fucoidan does not induce significant activation. On the other hand, both 10 and 100 μg/mL of fucoidan induced tyrosine phosphorylation with peak values at 90 and 30 s, respectively. The increase in temperature significantly shortened the lag-times of phosphorylation to 60 and 15 s, respectively. Thus, we can conclude that the temperature variation influences the activity of tyrosine kinases as well as calcium signaling. This result is in agreement with the model prediction that the rate of CLEC-2 clustering determines the time-lapse to peak platelet activation.

Impact of the medium temperature on CLEC-2 induced calcium response in single cells

TIRF microscopy of immobilized single-calcium-sensitive-dye-loaded platelets was performed to investigate the nature

of the cytosolic calcium increase observed in flow cytometry. We utilized two experimental settings. In the first setting, platelets were immobilized on VM64 (anti-CD31 clone (48)) antibody (Fig. 7, *A–D*), and the fucoidan solution in Tyrode's buffer was washed over the surface. Platelets developed cytosolic calcium spiking with varying intensities (Fig. 7, *A* and *C*). Frequent cytosolic calcium spiking intensified by 50 s after fucoidan addition (Fig. 7, *A–D*). Maximal calcium concentration in the spikes as well as spike frequency corresponded with the model predictions (Fig. 5 *A*). Comparison between fucoidan-induced calcium spiking between 25 (Fig. 7 *A*) and 37°C (Fig. 7 *C*) shows that the frequency of spiking increases at body temperature, and there is also a noticeable increase in amplitude. This result corresponds to the prediction that fucoidan-induced platelet activation could be influenced by the temperature-dependent parameters: receptor translocation and enzyme turnover rates. Together, these data corroborate the model predictions that 1) fucoidan induces calcium spiking in platelets and 2) fucoidan-induced activation of platelets is significantly influenced by temperature. It could be noticed that although the amplitudes of the calcium spikes remained around the same values at different temperatures (Fig. 7 *F*), the interspike time intervals were significantly shorter at 37°C than at 25°C (Fig. 7 *E*). This observation corresponded with the model prediction that an increase in CLEC-2 clustering rates in the membrane lead to an increase in cytosolic calcium spiking (Fig. S22).

DISCUSSION

Here, we aimed at investigation of primary regulatory mechanisms of platelet CLEC-2-induced activation by means of comprehensive computational systems biology modeling. Our model accurately reproduced literature data on platelet activation by CLEC-2 agonists fucoidan, rhodocytin, and podoplanin. The model gave a set of predictions. First, a rapid CLEC-2 clustering upon ligation was required for platelet activation by CLEC-2 agonists, which corresponded to data from Mukherjee et al. (41) and our experiments with mβCD-treated platelets (Fig. 5 *B*). Second, CLEC-2 ligands are capable of inducing cytosolic calcium spiking independent of platelet secondary activation, which corresponded to data from Badolia et al. (40) and our experiments with MRS2179 (Figs. 5 *A* and 6, *A* and *B*). Third, the sensitivity analysis of the model has revealed a key role of Syk kinases in the CLEC-2 signaling cascade (Fig. 3), which was in perfect agreement with Hughes et al. (17) and Séverin et al.

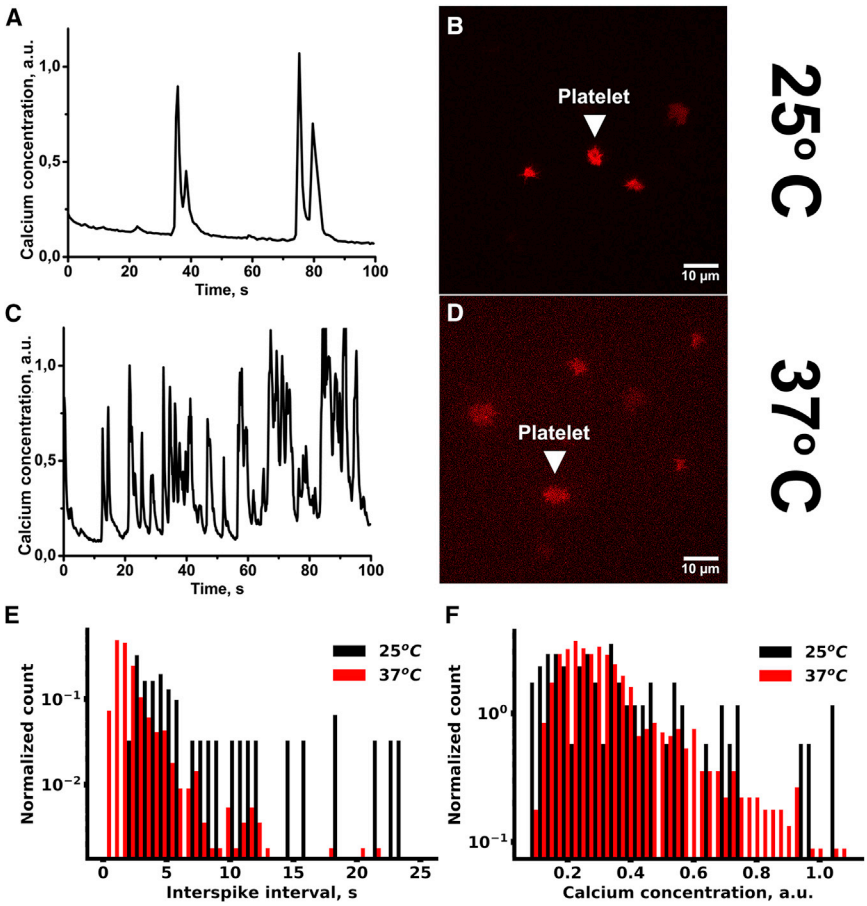

FIGURE 7 Cytosolic calcium spiking induced by fucoidan in single cells. Platelets were loaded with Fura-2, immobilized on VM-64 (*A–D*), and then illuminated by 405-nm laser. Cytosolic calcium concentration was recalculated from Fura-2 fluorescence (see Methods). Washed platelets were immobilized on the VM64 antibody (*A–D*). At time point "0," the fucoidan solution at 100 μg/mL was added. Cytosolic calcium spiking (*A* and *C*) and whole-cell fluorescence (*B* and *D*) were monitored at room temperature (*A* and *B*) or 37°C (*C* and *D*). Representative curves are shown out of $n = 10$. (*E* and *F*) Intervals between calcium spikes (*E*) and calcium concentration per spike (*F*), spread on VM-64 and activated by fucoidan at 25°C (*black*) or 37°C (*red*), are shown. Data were collected from 20 cells. To see this figure in color, go online.

(55). Finally, the CLEC-2 clustering and LAT signalosome formation appeared to be the rate-limiting steps in signal propagation in addition to tyrosine kinase activities. This proposition was supported by our experiments at different temperature conditions alongside different mβCD concentrations (Figs. 6 and 7).

During model development, we applied mathematical equations from our previously published model of platelet aggregation (64) to describe the process of receptor clustering (*"two-equation" model*, Fig. S1 *B*). The "two-equation" model described experimental data on CLEC-2 receptor clustering, as well as the computational results of a more conventional model of receptor clustering (*"N-equation" model*, Fig. S1 *A*). Two possible receptor-clustering patterns distinctive in the sequence of dimerization and ligation of receptors were identified. However, only the inclusion of the pattern with rapid dimerization in the model allowed it to reproduce an experimentally observed calcium response (Fig. 3, *C* and *D*). The "ligand-mediated receptor dimerization" clustering pattern was in line with experimental data describing the capability of the CLEC-2 ligand to promote receptor clustering (35–37). Furthermore, this result was in agreement with previously published data on other ITAM-bearing receptors (41). On the other hand, CLEC-2 clustering upon activation by monomeric ligands (e.g., podoplanin) has been reported (38), which should correspond to "postligation" clustering, assuming conformational changes in the CLEC-2 structure upon ligation.

The analysis of the model predicted a central role of the Syk tyrosine kinase for CLEC-2 signaling cascade (Fig. 4 *A*). This prediction corresponded to previously published data on CLEC-2 stimulation in platelets pretreated with PRT-060318 (56), as well as CLEC-2 stimulation of platelets of mice deficient in Syk-activating SH-2 domains (17). Sensitivity analysis has also revealed that, in addition to the tyrosine kinase activity, the PLCγ2 activity and receptor clustering, to a lesser extent, are the rate-limiting steps as well (Fig. 4). It is noteworthy that the parameters concerning dephosphorylation of signaling were as influential as the parameters concerning the activation of kinases (Fig. 4; Fig. S5). This result emphasizes the role of the negative regulators of intracellular signaling for CLEC-2-induced platelet activation.

More accurate analysis of the parts of the platelet response influenced by the parameters revealed that, although the activity of tyrosine kinases had the most impact on every response, only CLEC-2 clustering influenced the time-lapse to peak concentration while only moderately affecting the number of active signaling proteins. This observation was supported by the decrease in platelet activation time with temperature increase or mβCD supplementation (Fig. 6, *A* and *B*). A similar effect could be expected from GPVI signaling, which also requires clustering of receptors. Indeed, when GPVI cluster formation was affected by losartan, a delay in platelet response to collagen appeared (65).

To test the model predictions that CLEC-2 clustering is one of the rate-limiting processes for the CLEC-2 signaling cascade, we investigated the influence of two membrane-fluidity-changing agents on platelet activation. First, we utilized incubation of platelets with a cholesterol-binding agent mβCD, which changes membrane cholesterol saturation, and thus directly increases the fluidity of the membranes. We observed a faster platelet response to CLEC-2 agonists in the presence of mβCD (Figs. 5 *B* and 6 *B*). However, these results were in disagreement with previously published work (60) in which CLEC-2 signaling was shown to be independent of lipid rafts, and the lipid raft role was proposed mainly for secondary signaling. On the other hand, in Manne et al. (60), platelets were incubated with mβCD for an hour, and this could have led to the reintroduction of cholesterol in the signaling region (51). The dose-dependent response to mβCD, obtained upon incubation for 15 min in our work (Fig. S3 B), proves the membrane fluidity to be of significance for primary CLEC-2 response.

The second way to influence the rate of CLEC-2 clustering utilized here was a variation in the environment temperature. The temperature decrease from 37 to 25°C resulted in a prolonged delay after activation (Figs. 6 and 7). This result could not be considered as a direct confirmation of the receptor-clustering impact because it is well known that the temperature affects the turnover numbers of enzymes (66,67) to the same degree as the rates of diffusion (68,69). Experimental data on immunofluorescence microscopy additionally demonstrated impairment of LAT signalosome formation upon temperature decrease and cholesterol depletion (Fig. 6 *C*; Figs. S18–S20). Based on the model predictions, this is justified by the alterations in the receptor cluster formation at different conditions (Fig. 6 *C*). Furthermore, the fact that the applied decrease in temperature did not affect the degree of activation is in agreement with the model prediction that the receptor clustering affects only the times of activation, whereas tyrosine kinase activity controls both the time and the degree of activation (Fig. 4, *B–E*; Fig. S8). Additionally, we demonstrated that such a temperature variation has no significant effect on ADP-induced platelet activation, confirming the hypothesis that receptor clustering is specifically important for tyrosine kinase signaling (Fig. S17).

Among the main features of the model was its capability to work both in stochastic and in deterministic modes. The applicability of stochastic modeling to platelets is based on the fact that even at maximal degrees of activation upon CLEC-2 stimulation, amounts of crucial signaling proteins do not exceed 200 (Syk, LAT, PLCγ2).

Although the experimental data supported our model predictions, some limitations should be noted. Although it has been shown that fucoidan is capable of activating platelet CLEC-2 (21), it has been demonstrated recently that

fucoidan might be activating GPVI and platelet endothelial aggregation receptor 1 (PEAR-1) as well (70,71). However, PEAR-1 and GPVI participation in fucoidan-induced platelet activation has been demonstrated by aggregometry (70), in which the effects of secondary mediators of signaling are prevailing (34). Authors of Kardeby et al. (70) also report that fucoidan is not inducing calcium signaling in platelets solely by implicating spectrofluorimetry, which is insensitive to weak calcium signaling.

The confirmations of model predictions here are limited to experiments with isolated platelets. A large part of the model predictions is concerned with kinase activity not routinely assessed for single cells. For the experiments with immunoblotting, the distinction between primary and secondary signaling for tyrosine phosphorylation assays is not evident. Additional experiments on the roles of tyrosine kinases in CLEC-2 signaling, as well as further model development (direct inclusion of the protein-tyrosine phosphatase 1B (PTP1B) phosphatase) and investigation of cooperativity between CLEC-2 and GPVI, should be the subject of further studies.

The fact that the motion of proteins drives CLEC-2 activation in the plasma membrane and the assembly of signaling complexes demonstrated here allows us to take a new perspective on all receptors that perform clustering after activation or are associated with specific lipid microdomains. The knowledge of the underlying mechanisms of receptor cluster assembly will push forward understanding of molecular signaling in all types of eukaryotic cells, as well as the development of new antithrombotic agents specifically targeting receptor cluster formation.

SUPPORTING MATERIAL

Supporting Material can be found online at https://doi.org/10.1016/j.bpj.2020.04.023.

AUTHOR CONTRIBUTIONS

A.A.M. developed the model, performed simulations, performed experiments (flow cytometry, immunoblotting, immunofluorescent microscopy), analyzed the data, and wrote the article. F.A.B. performed single-cell microscopy experiments. J.M.G. and J.L.D. analyzed the data and edited the article. M.A.P. supervised the project and edited the article. A.N.S. planned model development and research, analyzed the data, performed experiments (microscopy), and edited the article.

ACKNOWLEDGMENTS

We thank Prof. F.I. Ataullakhanov (CTP PCP RAS, Moscow, RF), Dr. A.V. Mazurov (NMRC of Cardiology, Moscow, RF), and Dr. N.E. Ustuzhanina (Zelinsky Institute of Organic Chemistry RAS, Moscow, RF) for reagents used during preliminary experiments and valuable discussions. We are grateful to Dr. A.V. Pichugin (Federal Medical Biological Agency, Moscow, RF) for advice and Miss V.N. Kaneva for assistance during flow cytometry data collection. We are grateful to Dr. S.I. Obydennyi for the advice and support during confocal microscopy data collection.

The study was supported by the Russian Science Foundation grant 17-74-20045.

REFERENCES

1. Versteeg, H. H., J. W. M. Heemskerk, …, P. H. Reitsma. 2013. New fundamentals in hemostasis. *Physiol. Rev.* 93:327–358.
2. van der Meijden, P. E. J., and J. W. M. Heemskerk. 2019. Platelet biology and functions: new concepts and clinical perspectives. *Nat. Rev. Cardiol.* 16:166–179, Published online November 14, 2018.
3. Repsold, L., R. Pool, …, A. M. Joubert. 2017. An overview of the role of platelets in angiogenesis, apoptosis and autophagy in chronic myeloid leukaemia. *Cancer Cell Int.* 17:89.
4. Nurden, A. T. 2007. Platelets and tissue remodeling: extending the role of the blood clotting system. *Endocrinology.* 148:3053–3055.
5. Gawaz, M., and S. Vogel. 2013. Platelets in tissue repair: control of apoptosis and interactions with regenerative cells. *Blood.* 122:2550–2554.
6. Ed Rainger, G., M. Chimen, …, G. B. Nash. 2015. The role of platelets in the recruitment of leukocytes during vascular disease. *Platelets.* 26:507–520.
7. Hitchcock, J. R., C. N. Cook, …, A. F. Cunningham. 2015. Inflammation drives thrombosis after Salmonella infection via CLEC-2 on platelets. *J. Clin. Invest.* 125:4429–4446.
8. Watson, S. P., J. M. J. Herbert, and A. Y. Pollitt. 2010. GPVI and CLEC-2 in hemostasis and vascular integrity. *J. Thromb. Haemost.* 8:1456–1467.
9. Stalker, T. J., D. K. Newman, …, L. F. Brass. 2012. Platelet signaling. *Handb. Exp. Pharmacol* 59–85.
10. Gurbel, P. A., A. Kuliopulos, and U. S. Tantry. 2015. G-protein-coupled receptors signaling pathways in new antiplatelet drug development. *Arterioscler. Thromb. Vasc. Biol.* 35:500–512.
11. FitzGerald, G. A. 1991. Mechanisms of platelet activation: thromboxane A_2 as an amplifying signal for other agonists. *Am. J. Cardiol.* 68:11B–15B.
12. Gibbins, J. M., M. Okuma, …, S. P. Watson. 1997. Glycoprotein VI is the collagen receptor in platelets which underlies tyrosine phosphorylation of the Fc receptor γ-chain. *FEBS Lett.* 413:255–259.
13. Suzuki-Inoue, K., Y. Kato, …, Y. Ozaki. 2007. Involvement of the snake toxin receptor CLEC-2, in podoplanin-mediated platelet activation, by cancer cells. *J. Biol. Chem.* 282:25993–26001.
14. Christou, C. M., A. C. Pearce, …, C. A. O'Callaghan. 2008. Renal cells activate the platelet receptor CLEC-2 through podoplanin. *Biochem. J.* 411:133–140.
15. Bertozzi, C. C., A. A. Schmaier, …, M. L. Kahn. 2010. Platelets regulate lymphatic vascular development through CLEC-2-SLP-76 signaling. *Blood.* 116:661–670.
16. Suzuki-Inoue, K., O. Inoue, …, Y. Ozaki. 2010. Essential in vivo roles of the C-type lectin receptor CLEC-2: embryonic/neonatal lethality of CLEC-2-deficient mice by blood/lymphatic misconnections and impaired thrombus formation of CLEC-2-deficient platelets. *J. Biol. Chem.* 285:24494–24507.
17. Hughes, C. E., B. A. Finney, …, S. P. Watson. 2015. The N-terminal SH2 domain of Syk is required for (hem)ITAM, but not integrin, signaling in mouse platelets. *Blood.* 125:144–154.
18. Herzog, B. H., J. Fu, …, L. Xia. 2013. Podoplanin maintains high endothelial venule integrity by interacting with platelet CLEC-2. *Nature.* 502:105–109.
19. Huang, T. F., C. Z. Liu, and S. H. Yang. 1995. Aggretin, a novel platelet-aggregation inducer from snake (Calloselasma rhodostoma) venom, activates phospholipase C by acting as a glycoprotein Ia/IIa agonist. *Biochem. J.* 309:1021–1027.
20. Shin, Y., and T. Morita. 1998. Rhodocytin, a functional novel platelet agonist belonging to the heterodimeric C-type lectin family, induces

platelet aggregation independently of glycoprotein Ib. *Biochem. Biophys. Res. Commun.* 245:741–745.

21. Manne, B. K., T. M. Getz, …, S. P. Kunapuli. 2013. Fucoidan is a novel platelet agonist for the C-type lectin-like receptor 2 (CLEC-2). *J. Biol. Chem.* 288:7717–7726.
22. Boulaftali, Y., P. R. Hess, …, W. Bergmeier. 2013. Platelet ITAM signaling is critical for vascular integrity in inflammation. *J. Clin. Invest.* 123:908–916.
23. Hughes, C. E., L. Navarro-Núñez, …, S. P. Watson. 2010. CLEC-2 is not required for platelet aggregation at arteriolar shear. *J. Thromb. Haemost.* 8:2328–2332.
24. Bender, M., F. May, …, B. Nieswandt. 2013. Combined in vivo depletion of glycoprotein VI and C-type lectin-like receptor 2 severely compromises hemostasis and abrogates arterial thrombosis in mice. *Arterioscler. Thromb. Vasc. Biol.* 33:926–934.
25. Gros, A., V. Syvannarath, …, B. Ho-Tin-Noé. 2015. Single platelets seal neutrophil-induced vascular breaches via GPVI during immune-complex-mediated inflammation in mice. *Blood.* 126:1017–1026.
26. May, F., I. Hagedorn, …, B. Nieswandt. 2009. CLEC-2 is an essential platelet-activating receptor in hemostasis and thrombosis. *Blood.* 114:3464–3472.
27. Inoue, O., K. Hokamura, …, Y. Ozaki. 2015. Vascular smooth muscle cells stimulate platelets and facilitate thrombus formation through platelet CLEC-2: implications in atherothrombosis. *PLoS One.* 10:e0139357.
28. Pike, L. J. 2009. The challenge of lipid rafts. *J. Lipid Res.* 50 (*Suppl*):S323–S328.
29. Payne, H., T. Ponomaryov, …, A. Brill. 2017. Mice with a deficiency in CLEC-2 are protected against deep vein thrombosis. *Blood.* 129:2013–2020.
30. Shirai, T., O. Inoue, …, K. Suzuki-Inoue. 2017. C-type lectin-like receptor 2 promotes hematogenous tumor metastasis and prothrombotic state in tumor-bearing mice. *J. Thromb. Haemost.* 15:513–525.
31. Kato, Y., M. K. Kaneko, …, H. Narimatsu. 2008. Molecular analysis of the pathophysiological binding of the platelet aggregation-inducing factor podoplanin to the C-type lectin-like receptor CLEC-2. *Cancer Sci.* 99:54–61.
32. O'Rafferty, C., G. M. O'Regan, …, O. P. Smith. 2015. Recent advances in the pathobiology and management of Kasabach-Merritt phenomenon. *Br. J. Haematol.* 171:38–51.
33. Chang, Y.-W., P. W. Hsieh, …, C.-P. Tseng. 2015. Identification of a novel platelet antagonist that binds to CLEC-2 and suppresses podoplanin-induced platelet aggregation and cancer metastasis. *Oncotarget.* 6:42733–42748.
34. Pollitt, A. Y., B. Grygielska, …, S. P. Watson. 2010. Phosphorylation of CLEC-2 is dependent on lipid rafts, actin polymerization, secondary mediators, and Rac. *Blood.* 115:2938–2946.
35. Watson, A. A., C. M. Christou, …, C. A. O'Callaghan. 2009. The platelet receptor CLEC-2 is active as a dimer. *Biochemistry.* 48:10988–10996.
36. Hughes, C. E., A. Y. Pollitt, …, S. P. Watson. 2010. CLEC-2 activates Syk through dimerization. *Blood.* 115:2947–2955.
37. Watson, A. A., J. A. Eble, and C. A. O'Callaghan. 2008. Crystal structure of rhodocytin, a ligand for the platelet-activating receptor CLEC-2. *Protein Sci.* 17:1611–1616.
38. Pollitt, A. Y., N. S. Poulter, …, S. P. Watson. 2014. Syk and Src family kinases regulate C-type lectin receptor 2 (CLEC-2)-mediated clustering of podoplanin and platelet adhesion to lymphatic endothelial cells. *J. Biol. Chem.* 289:35695–35710.
39. Inoue, K., Y. Ozaki, …, T. Morita. 1999. Signal transduction pathways mediated by glycoprotein Ia/IIa in human platelets: comparison with those of glycoprotein VI. *Biochem. Biophys. Res. Commun.* 256:114–120.
40. Badolia, R., V. Inamdar, …, S. P. Kunapuli. 2017. G_q pathway regulates proximal C-type lectin-like receptor-2 (CLEC-2) signaling in platelets. *J. Biol. Chem.* 292:14516–14531.
41. Mukherjee, S., J. Zhu, …, A. Weiss. 2013. Monovalent and multivalent ligation of the B cell receptor exhibit differential dependence upon Syk and Src family kinases. *Sci. Signal.* 6:ra1.
42. Poulter, N. S., A. Y. Pollitt, …, S. M. Jung. 2017. Clustering of glycoprotein VI (GPVI) dimers upon adhesion to collagen as a mechanism to regulate GPVI signaling in platelets. *J. Thromb. Haemost.* 15:549–564.
43. Dunster, J. L., A. J. Unsworth, …, A. Y. Pollitt. 2020. Interspecies differences in protein expression do not impact the spatiotemporal regulation of glycoprotein VI mediated activation. *J. Thromb. Haemost.* 18:485–496.
44. Dunster, J. L., F. Mazet, …, M. J. Tindall. 2015. Regulation of early steps of GPVI signal transduction by phosphatases: a systems biology approach. *PLoS Comput. Biol.* 11:e1004589.
45. Sveshnikova, A. N., A. V. Balatskiy, …, M. A. Panteleev. 2016. Systems biology insights into the meaning of the platelet's dual-receptor thrombin signaling. *J. Thromb. Haemost.* 14:2045–2057.
46. Gillespie, D. T. 2007. Stochastic simulation of chemical kinetics. *Annu. Rev. Phys. Chem.* 58:35–55.
47. Dunster, J. L., M. A. Panteleev, …, A. N. Sveshnikova. 2018. Mathematical techniques for understanding platelet regulation and the development of new pharmacological approaches. *Methods Mol. Biol.* 1812:255–279.
48. Mazurov, A. V., D. V. Vinogradov, …, V. N. Smirnov. 1991. A monoclonal antibody, VM64, reacts with a 130 kDa glycoprotein common to platelets and endothelial cells: heterogeneity in antibody binding to human aortic endothelial cells. *Thromb. Haemost.* 66:494–499.
49. Panteleev, M. A., N. M. Ananyeva, …, E. L. Saenko. 2005. Two subpopulations of thrombin-activated platelets differ in their binding of the components of the intrinsic factor X-activating complex. *J. Thromb. Haemost.* 3:2545–2553.
50. Gibbins, J. M. 2004. Study of tyrosine kinases and protein tyrosine phosphorylation BT. *In* Platelets and Megakaryocytes: Volume 2: Perspectives and Techniques. J. M. Gibbins and M. P. Mahaut-Smith, eds. Humana Press, pp. 153–167.
51. Mahammad, S., and I. Parmryd. 2015. Cholesterol depletion using methyl-β-cyclodextrin. *Methods Mol. Biol.* 1232:91–102.
52. Lawrence, M. B., L. V. McIntire, and S. G. Eskin. 1987. Effect of flow on polymorphonuclear leukocyte/endothelial cell adhesion. *Blood.* 70:1284–1290.
53. Pahle, J. 2009. Biochemical simulations: stochastic, approximate stochastic and hybrid approaches. *Brief. Bioinform.* 10:53–64.
54. Balabin, F. A., and A. N. Sveshnikova. 2016. Computational biology analysis of platelet signaling reveals roles of feedbacks through phospholipase C and inositol 1,4,5-trisphosphate 3-kinase in controlling amplitude and duration of calcium oscillations. *Math. Biosci.* 276:67–74.
55. Séverin, S., A. Y. Pollitt, …, S. P. Watson. 2011. Syk-dependent phosphorylation of CLEC-2: a novel mechanism of hem-immunoreceptor tyrosine-based activation motif signaling. *J. Biol. Chem.* 286:4107–4116.
56. Manne, B. K., R. Badolia, …, S. P. Kunapuli. 2015. Distinct pathways regulate Syk protein activation downstream of immune tyrosine activation motif (ITAM) and hemITAM receptors in platelets. *J. Biol. Chem.* 290:11557–11568.
57. Fuller, G. L. J., J. A. E. Williams, …, A. C. Pearce. 2007. The C-type lectin receptors CLEC-2 and Dectin-1, but not DC-SIGN, signal via a novel YXXL-dependent signaling cascade. *J. Biol. Chem.* 282:12397–12409.
58. Bradshaw, J. M. 2010. The Src, Syk, and Tec family kinases: distinct types of molecular switches. *Cell. Signal.* 22:1175–1184.
59. Tsang, E., A. M. Giannetti, …, J. M. Bradshaw. 2008. Molecular mechanism of the Syk activation switch. *J. Biol. Chem.* 283:32650–32659.
60. Manne, B. K., R. Badolia, …, S. P. Kunapuli. 2015. C-type lectin like receptor 2 (CLEC-2) signals independently of lipid raft microdomains in platelets. *Biochem. Pharmacol.* 93:163–170.

61. Baba, Y., and T. Kurosaki. 2011. Impact of Ca2+ signaling on B cell function. *Trends Immunol.* 32:589–594.

62. Sveshnikova, A. N., F. I. Ataullakhanov, and M. A. Panteleev. 2015. Compartmentalized calcium signaling triggers subpopulation formation upon platelet activation through PAR1. *Mol. Biosyst.* 11:1052–1060.

63. Burkhart, J. M., M. Vaudel, …, R. P. Zahedi. 2012. The first comprehensive and quantitative analysis of human platelet protein composition allows the comparative analysis of structural and functional pathways. *Blood.* 120:e73–e82.

64. Filkova, A. A., A. A. Martyanov, …, A. N. Sveshnikova. 2019. Quantitative dynamics of reversible platelet aggregation: mathematical modelling and experiments. *Sci. Rep.* 9:6217.

65. Jiang, P., S. Loyau, …, M. Jandrot-Perrus. 2015. Inhibition of glycoprotein VI clustering by collagen as a mechanism of inhibiting collagen-induced platelet responses: the example of losartan. *PLoS One.* 10:e0128744.

66. Robinson, P. K. 2015. Enzymes: principles and biotechnological applications. *Essays Biochem.* 59:1–41.

67. Struvay, C., and G. Feller. 2012. Optimization to low temperature activity in psychrophilic enzymes. *Int. J. Mol. Sci.* 13:11643–11665.

68. Medda, L., M. Monduzzi, and A. Salis. 2015. The molecular motion of bovine serum albumin under physiological conditions is ion specific. *Chem. Commun. (Camb.).* 51:6663–6666.

69. Saha, S., I.-H. Lee, …, S. Mayor. 2015. Diffusion of GPI-anchored proteins is influenced by the activity of dynamic cortical actin. *Mol. Biol. Cell.* 26:4033–4045.

70. Kardeby, C., K. Fälker, …, M. Grenegård. 2019. Synthetic glycopolymers and natural fucoidans cause human platelet aggregation via PEAR1 and GPIbα. *Blood Adv.* 3:275–287.

71. Alshehri, O. M., S. Montague, …, S. P. Watson. 2015. Activation of glycoprotein VI (GPVI) and C-type lectin-like receptor-2 (CLEC-2) underlies platelet activation by diesel exhaust particles and other charged/hydrophobic ligands. *Biochem. J.* 468:459–473.

Biophysical Journal, Volume *118*

Supplemental Information

Control of Platelet CLEC-2-Mediated Activation by Receptor Clustering and Tyrosine Kinase Signaling

Alexey A. Martyanov, Fedor A. Balabin, Joanne L. Dunster, Mikhail A. Panteleev, Jonathan M. Gibbins, and Anastasia N. Sveshnikova

1. Supporting results

1.1. Quiescent state reactions incorporated in our model of CLEC-2-induced platelet activation.

The quiescent state of platelet's tyrosine kinase network is supported by a set of phosphatases, among which CD148 (also known as DEP-1 or PTPRJ) has a dominant role (1–3). Here we assume that SFK can exist in four different states which differ in the degree of activation: non-active SFK (Y527 phosphorylated), a third (1/3) active SFK (Y527 dephosphorylated), two thirds (2/3) active (Y416 phosphorylated) and fully active SFK (Y416 phosphorylated and bound to a phosphorylated tyrosine by its SH-2 domain) (4). Non-active SFK is transferred to the 1/3 active state by active CD148 phosphatases (2, 4). On the contrary, 1/3 active SFK can be deactivated by active Csk kinases, which phosphorylate SFK at Y527 (2, 5). 1/3 active SFK turn to a 2/3 active state via autophosphorylation on Y416 (2). This transition is negatively regulated by the active CD148 (1, 2, 4, 6). We assume that fully active SFK are not produced in the quiescent state due to the absence of the phosphorylated receptor molecules. All types of active SFK mediate phosphorylation of CD148 at Y1311 (6), which results in CD148 activation. On the other side, all types of active SFK also mediate Csk activation (7, 8). It is noteworthy that Csk activation in platelets is not regulated directly by SFK. Namely, SFK phosphorylates a protein called paxillin adapter, which binds Csk and this results in Csk activation (7). Active SFK phosphorylates Syk at Y346, which results in Syk initial activation (9).

It is noteworthy that in *in vivo* experiments with $SFK^{-/-}$ mice CLEC-2 phosphorylation was present upon stimulation by rhodocytin, while further signal propagation was significantly weakened (10). Furthermore, Hughes *et al.* 2015 demonstrated that for CLEC-2 signalling SFK acts mostly as a positive mediator of Syk basal activation (9).

1.2. A detailed description of the model construction in a modular fashion

The "CLEC-2 clustering" module (Fig. 2A) consists of variables for concentrations of CLEC-2 in free, ligand-bound and cluster forms (3 variables, all located in the plasma membrane), fucoidan (1 variable, located in the extracellular space) and 7 parameters, among which 4 concern receptor clustering.

In order to describe cluster formation, we initially used an "N-equation" model (Fig. S1A), which could capture the behavior of the receptor clusters of all sizes (where N is the size of the largest cluster). "N-equation" model of clustering contains 4 parameters: single receptor association and dissociation with clusters rates (k_1, k_{-1}, respectively) and two clusters association and dissociation rates (k_2, k_{-2}, respectively) (11). Formation of clusters of all sizes was described using mass-action kinetics. For example, behaviouor of cluster of size three was described by the following equation:

$$\frac{d[3R]}{dt} = k_1([2R] \times [R] - [3R] \times [R]) + k_{-1}([4R] - [3R]) + k_2([2R] \times [R] - [3R] \times [2R]) + k_{-2}([5R] - [3R]).$$

Average cluster size ($\sum_{i=1}^{n} c_i i \Big/ \sum_{i=1}^{n} c_i$, where c_i – The concentration of the cluster of size i), predicted by the model, was fitted to the data from (12). Calculated distribution of cluster sizes at 300s (Fig. S1C) show that the dimerised receptor concentration is prevailing, while a small fraction of receptors remains in a non-dimerized state.

Although the "N-equation" model could capture the literature data, it was poorly applicable to stochastic calculations. Thus, in order to describe receptor clustering, we utilised a "2-equation model" (13) to describe results obtained by the "N-equation" model.

2-equation model contains 5 parameters, which were determined in the process of fitting the 2-equation model to "N-equation" model, which, in turn, was fitted to experimental data from (12) (for equations and parameter values see Tables S2-S4). Average cluster size was calculated as $s = (C_0^* - C^*) \Big/ C^{Clust}$, where C_0^* - initial concentration of non-clustered CLEC-2 species, C_0^* - transient concentration of the non-clustered CLEC-2 and C^{Clust} – transient CLEC-2 cluster concentration.

Both the full model and 2-equation model were capable of accurately simulating available literature data (Fig. S1D). Furthermore, the number of single receptor molecules, predicted by "2-equation" model, corresponded to the value, predicted by "N-equation" model. Based on these results, we considered "2-equation" model applicable for the description of receptor clustering. Thus, "2-equation" model was used in all further calculations.

The "Quiescent state" module (Fig. 2B) of the model consists of variables for concentrations of CD148 phosphatase in active and passive states (2 variables); Csk in active and passive states (2 variables); SFK in a set of gradually active states: non-active, 1/3 active and 2/3 active (3 variables); Syk kinases in active and passive states (2 variables); TULA-2 in active and passive states (2 variables). "Quiescent state" module contains 19 parameters, common with "Tyrosine kinase" module. The initial concentrations of the species (Table S5) were at steady-state values for the module. The "Quiescent state" module was tuned in order to obtain 5% active Syk kinases required for CLEC-2 phosphorylation (9, 10) and 10% of SFKs (Kr^{CD148}, Kr^{Csk}, Kr^{Syk} parameters were estimated). The parameters of the reactions are given in Table S6.

The "Tyrosine kinase" module (Fig. 2C) of the model consists of variables for concentrations of active and inactive Syk kinases (2 variables); SFK in gradually active states: non active, one-third, two-thirds and fully active (4 variables); clustered non phosphorylated and clustered phosphorylated CLEC-2 receptors (2 variables); active and non-active TULA-2 (2 variables).

The unknown parameters of the module (Kr^{CLEC2}, k_{S1}^{SH2}, Kr_{TULA2}^{Syk}, Kf_{Syk}^{TULA2}, Kr_{Syk}^{TULA2}) were estimated by fitting number of active Syk to data from (14), and the number of Y416 phosphorylated SFK to data from (15) (Fig. 2E and S3, correspondingly).

The "LAT-PLCγ2" module (Fig. 2D) consists of variables for concentrations of active Syk (1 variable); phosphorylated and non-phosphorylated LAT (2 variables); LAT-PLCγ2 complexes (1 variable); LAT-PLCγ2-PI3K complexes (1 variable); phosphoinositides (IP_3, PIP_2 and PIP_3, 3 variables); active and non-active Btk (2 variables). The "LAT-PLCγ2" module contains 16 parameters. Unknown parameters (Kr^{LAT}, Kr^{PLC}, k_1^{Btk}, Kr^{PIP_3}) were estimated by fitting numbers of phosphorylated LAT and active PLCγ2 to data from (14) (Fig. 2F and 2G, correspondingly). Initial concentrations of the species in the model and parameter values with equations of the model can be found in tables S7 and S8, correspondingly. The model of Ca^{2+} release (Fig. 2D, "Calcium" module) is described in our previous work (16, 17). It is noteworthy that IP_3 concentration in the model of CLEC-2 signalling is a sole link to calcium module and no other positive or negative feedbacks exist in the model. Thus, being the sole generator of IP_3, active PLCγ2 was selected as the main output of the model.

2. Supporting Tables.

Table S1. Geometric region details.

Geometric region details			
Name	Parameter	Value	Ref.
The volume of extracellular space	V_{EC}	3.3 μl	(18)
Size of plasmatic membrane	S_{PM}	45 μm^2	(19) Rate of $\frac{S_{PM}}{V_{Cyt}}$ is conserved from (20)
Volume of cytosol	V_{Cyt}	4.5 fl	
Juxtamembrane Volume	V_{JM}	1 fl	An artificial parameter used to preserve dimensions in multi-compartment reactions
Size of the DTS membrane	V_{IM}	1 fl	(19)
The volume of the DTS	V_{DTS}	1.5 fl	

Table S2. "CLEC-2 clustering" module: initial conditions.

Compartment	Species	Variable	Value	Ref.
EC	Ligand	Lig	$2 * 10^{14}$	(14)
PM	Free CLEC-2 molecules	R	2000	(21)
	CLEC-2 molecules, bound to an activator	R^*	0	
	Clustered CLEC-2 molecules	R_C^*	1	

	Phosphorylated CLEC-2 molecules	R_P^*		
	All clustered CLEC-2 molecules	$R_C = R_P^* + R_C^*$		

Table S3. "CLEC-2 clustering" module: receptor ligation.

Name	Reaction		Equation	Parameters	Ref.
CLEC-2 ligation	M_1	$R + Lig \leftrightarrows R^*$	$S_{PM} \times V_{EC} \times Kf^{Lig} \times Lig \times R - S_{PM} \times Kr^{Lig} \times R^*$	$Kf^{Lig} = 1\ s^{-1} \times \mu mol^{-1}$ $Kr^{Lig} = 0.0302\ s^{-1}$	this work

Table S4. "CLEC-2 clustering" module: receptor clustering description (rapid-receptor dimerisation).

Name	Reaction	Equation	Parameters (ligand-mediated dimerisation)	Parameters (post-ligation dimerisation)	Ref.
Non-clustered CLEC-2	$R^* \leftrightarrows R_C^*$	$\frac{dR^*}{dt} = -k_1 R_C R^* - 2k_2 R^* R^* + k_{-1} R_C s$	$k_1 = 12324.611\ s^{-1} \times \mu mol^{-1}$ $k_{-1} = 0.0116\ s^{-1} \times \mu mol^{-1}$ $k_2 = 985236\ s^{-1} \times \mu mol^{-1}$	$k_1 = 619.65\ s^{-1} \times \mu mol^{-1}$ $k_{-1} = 0.00205\ s^{-1}$ $k_2 = 8.496\ s^{-1} \times \mu mol^{-1}$	(13)
			s – average cluster size		
Clustered CLEC-2		$\frac{dR_C^*}{dt} = k_2 R^* R^* - k_{-2} R_C R_C + k_3 R_C$	$k_{-2} = 348.26\ s^{-1} \times \mu mol^{-1}$ $k_3 = 2.7 \times 10^{-6}\ s^{-1}$	$k_{-2} = 0.00017\ s^{-1} \times \mu mol^{-1}$ $k_3 = 0.0106\ s^{-1}$	

Table S5. "Tyrosine kinase" and "Quiescent state" module: initial conditions.

Compartment	Species	Variable	Value	Ref.
PM	Non-active SFK (Y527 phosphorylated)	F_P	36800	(22)
	1/3 active SFK	F		
	2/3 active SFK (Y416 phosphorylated)	F^P		
	Active SFK (Y416 phosphorylated, SH2 bound)	F_*^P		
	Non-active CD148	D	3600	
	Active CD148 (Y1311)	D^*		
Cytosol	Non-active Csk	Cs	11500	
	Active Csk	Cs^*		
	Non-active Syk	S	5000	
	Active Syk (Y346 or Y525 phosphorylated)	S^*		
	Non-active TULA-2	T	8000	
	Active TULA-2	T^*		

Table S6. "Tyrosine kinase" and "Quiescent state" module: equations and parameters.

Name	Reaction		Equation	Parameters	Ref.
CD 148 activation	K_1	$D \leftrightarrows D^*$	$S_{PM} \times \left(\frac{\left(\frac{F \times S_{PM}}{V_{JM}} \times kcat_{cat}^{Src} / 3 + \frac{F^P \times S_{PM}}{V_{JM}} \times 2 \times kcat_{cat}^{Src} / 3 + \frac{F_*^P \times S_{PM}}{V_{JM}} \times kcat_{cat}^{Src} \right)}{Km^{Src} + \frac{D \times S_{PM}}{V_{JM}}} \right) \times D - S_{PM} \times Kr^{CD148} \times D^*$	$k_{cat}^{Src} = 2.1\ s^{-1}$ $Km^{Src} = 3\ \mu M$	(4, 23)
				$Kr^{CD148} = 90.8\ s^{-1}$	*
Csk activation	K_2	$Cs \leftrightarrows Cs^*$	$S_{PM} \times \left(\frac{\left(\frac{F \times S_{PM}}{V_{JM}} \times kcat_{cat}^{Src} / 3 + \frac{F^P \times S_{PM}}{V_{JM}} \times 2 \times kcat_{cat}^{Src} / 3 + \frac{F_*^P \times S_{PM}}{V_{JM}} \times kcat_{cat}^{Src} \right)}{Km^{Src} + \frac{Cs \times S_{PM}}{V_{JM}}} \right) \times Cs - S_{PM} \times Kr^{CD148} \times Cs^*$	$k_{cat}^{Src} = 2.1\ s^{-1}$ $Km^{Src} = 3\ \mu M$	(4, 23)
				$Kr^{Csk} = 1.0\ s^{-1}$	*
SFK activation 1	K_3	$F_P \leftrightarrows F$	$S_{PM} \times \left(\frac{\frac{D^* \times S_{PM}}{V_{JM}} \times k_{cat}^{CD148}}{Km^{CD148} + \frac{F_P \times S_{PM}}{V_{JM}}} \right) \times F_P - S_{PM} \times \left(\frac{\frac{Cs^* \times S_{PM}}{V_{JM}} \times k_{cat}^{Csk}}{Km^{Csk} + \frac{F \times S_{PM}}{V_{JM}}} \right) \times F$	$k_{cat}^{CD148} = 9.7\ s^{-1}$ $Km^{CD148} = 9.1\ mM$	(24)
				$k_{cat}^{Csk} = 1.9\ s^{-1}$ $Km^{Csk} = 10\ \mu M$	(8)
	K_4	$F \leftrightarrows F^P$		$k_{cat}^{Src} = 2.1\ s^{-1}$ $Km^{Src} = 3\ \mu M$	(4, 23)

SFK activation 2			$S_{PM} \times \left(\frac{\left(\frac{F \times S_{PM}}{V_{JM}} \times kcat_{cat}^{Src}/_3 + \frac{F^P \times S_{PM}}{V_{JM}} \times 2 \times kcat_{cat}^{Src}/_3 + \frac{F_*^P \times S_{PM}}{V_{JM}} \times kcat_{cat}^{Src} \right)}{Km^{Src} + \frac{F \times S_{PM}}{V_{JM}}} \right) \times F - S_{PM} \times \left(\frac{\frac{D^* \times S_{PM}}{V_{JM}} \times k_{cat}^{CD148}}{Km^{CD148} + \frac{F^P \times S_{PM}}{V_{JM}}} \right) \times F^P$	$k_{cat}^{CD148} = 9.7\ s^{-1}$ $Km^{CD148} = 9.1\ mM$	(24)
SFK activation 3	K_5	$F^P \leftrightarrows F_*^P$	$S_{PM} \times s \times k_{SF1}^{SH2} \times 2 \times R_P^* \times F^P - S_{PM} \times kD_{SFK}^{SH2} \times k_{SF1}^{SH2} \times F_*^P$	*s – average cluster size* $k_{SF1}^{SH2} = 0.6\ \mu m^2 \times s^{-1} \times \mu mol^{-1}$ $kD_{SFK}^{SH2} = 10^{-6}\ \mu mol/\mu m^2 \times s^{-1}$	* (25)
TULA-2 activation	K_6	$T \leftrightarrows T^*$	$V_{Cyt} \times Kf_{Syk}^{TULA-2} \times S^* \times T - V_{Cyt} \times Kr_{Syk}^{TULA-2} \times T^*$	$Kf_{Syk}^{TULA2} = 0.1 \mu M^{-1} \times s^{-1}$ $Kr_{Syk}^{TULA2} = 0.007\ s^{-1}$	*
CLEC-2 phosphorylation	K_7	$R_C^* \leftrightarrows R_P^*$	$S_{PM} \times \left(\frac{S^* \times k_{cat}^{Syk}}{Km^{Syk} + \frac{R_C^* \times S_{PM}}{V_{JM}}} \right) \times R_C^* - S_{PM} \times Kr^{Phosph} \times R_P^*$	$k_{cat}^{Syk} = 11.85\ s^{-1}$ $Km^{Syk} = 9.1\ \mu M$ $Kr^{Phosph} = 0.21\ s^{-1}$	(26) *
Syk activation	K_8	$S \leftrightarrows S^*$	$V_{Cyt} \times \frac{s \times k_{S1}^{SH2} \times S_{PM} \times R_P^*}{V_{JM}} \times \left(\frac{S^* \times k_{cat}^{Syk}}{Km^{Syk} + \frac{S \times S_{PM}}{V_{JM}}} \right) \times S - V_{Cyt} \times \left(kD_{Syk}^{SH2} \times k_{S1}^{SH2} + Kr^{Syk} + Kr_{TULA2}^{Syk} \times T^* \right) \times S^*$	*s – average cluster size* $k_{S1}^{SH2} = 0.47\ s^{-1} \times \mu M^{-1}$ $k_{cat}^{Syk} = 11.85\ s^{-1}$ $Km^{Syk} = 9.1\ \mu M$ $kD_{Syk}^{SH2} = 0.176\ \mu M$ $Kr^{Syk} = 10\ s^{-1}$ $Kr_{TULA2}^{Syk} = 7.5\ s^{-1} \times \mu M^{-1}$	* (26) (27) *

Table S7. "LAT-PLCγ2" module: initial conditions.

Compartment	Species	Variable	Value	Ref.
PM	LAT	L	4900	(22)
	Phosphorylated LAT	L^*		
	LAT-PLCγ2 complexes	Lp		
	LAT-PLCγ2- PI3K complexes	LP		
	PIP_2	I_1	200 μM	(19)
	PIP_3	I_2		
	Active Btk	B^*	0	(22)
	Active PLCγ2	p^*		
Cytosol	Non-active PI3K	P	1900	
	Non-active PLCγ2	p	2000	
	Non-active Btk	B	11100	
	IP_3	I_3	0.05 nM	(19)

Table S8. "LAT-PLCγ2" module: equations and parameters.

Name	Reaction		Equation	Parameters	Ref.
LAT phosphoryl	PL_1	$L \leftrightarrows L^*$		$k_{cat}^{Syk} = 11.85\ s^{-1}$ $Km^{Syk} = 9.1\ \mu M$	(4, 23)

ation by Syk			$S_{PM} \times \left(\frac{S^* \times k_{cat}^{Syk}}{Km^{Syk} + \frac{L \times S_{PM}}{V_{JM}}} \right) \times L - S_{PM} \times Kr^{LAT} \times (L^* + Lp + LP + p^*)$	$Kr^{LAT} = 1.41\ s^{-1}$	*
LAT-PLCγ2 complex formation	PL_2	$p \leftrightarrows Lp$	$S_{PM} \times k_1^{Lp} \times L^* \times p - S_{PM} \times kD_{Lp} \times k_1^{Lp} \times (Lp + LP + p^*)$	$k_1^{Lp} = 0.9 \mu M^{-1} \times s^{-1}$	*
				$kD_{Lp} = 0.15\ \mu M$	(25)
LAT-PLCγ2-PI3K complex formation	PL_3	$P \leftrightarrows LP$	$S_{PM} \times k_1^{LP} \times Lp \times P - S_{PM} \times kD_{LP} \times k_1^{LP} \times LP$	$k_1^{LP} = 4.2\ \mu M^{-1} \times s^{-1}$	*
				$kD_{LP} = 0.22\ \mu M$	(25)
PIP_3 production	PL_4	$I_1 \leftrightarrows I_2$	$S_{PM} \times \left(\frac{\frac{LP \times S_{PM}}{V_{JM}} \times k_{cat}^{PI3K}}{Km^{PI3K} + \frac{I_1 \times S_{PM}}{V_{JM}}} \right) \times I_1 - S_{PM} \times Kr^{PIP_3} \times (I_2 + B^*)$	$k_{cat}^{PI3K} = 2.82\ s^{-1}$	*
				$Km^{PI3K} = 11\ \mu M$	(19)
				$Kr^{PIP_3} = 0.44\ s^{-1}$	*
Btk activation	PL_5	$B \leftrightarrows B^*$	$S_{PM} \times k_1^{BI} \times I_2 \times B - S_{PM} \times kD_{BI} \times k_1^{BI} \times B^*$	$k_1^{BI} = 0.51\ \mu M^{-1} \times s^{-1}$	*
				$kD_{BI} = 0.64\ \mu M$	(25)
PLCγ2 activation	PL_6	$Lp \leftrightarrows p^*$	$S_{PM} \times \left(\frac{\frac{B^* \times S_{PM}}{V_{JM}} \times k_{cat}^{Btk}}{Km^{Btk} + \frac{Lp \times S_{PM}}{V_{JM}}} \right) \times Lp - S_{PM} \times Kr^{PLC} \times p^*$	$k_{cat}^{Btk} = 0.14\ s^{-1}$	(4, 28)
				$Km^{Btk} = 37\ \mu M$	
				$Kr^{PLC} = 8.6 \times 10^{-3}\ s^{-1}$	*
IP_3 production	PL_7	$I_1 \leftrightarrows I_3$	$S_{PM} \times \left(\frac{\frac{p^* \times S_{PM}}{V_{JM}} \times k_{cat}^{PLC\gamma 2} \times (Ca)}{Km^{PLC\gamma 2} + (Ca)} \right) \times I_1 - V_{Cyt} \times Kr^{IP_3} \times I_3$	$k_{cat}^{PLC\gamma 2} = 30.5\ s^{-1}$	*
				$Km^{PLC\gamma 2} = 0.78\ \mu M$	
				$Kr^{IP_3} = 60\ s^{-1}$	

Detailed calcium module description is given in (19).

Table S9. Models in COPASI Software.

Model of platelet CLEC-2 induced activation with rapid, ligand-induced receptor dimerisation	CLEC2_rapidclust.xml
Model of platelet CLEC-2 induced activation with post-ligation receptor dimerisation	CLEC2_altclust.xml

Table S10. Sensitivity scores of the most influential parameters for the number of active Syk kinases at the point of maximal activation.

Module	Parameter name	Variable	Value	Variation limits	Sensitivity Score
"CLEC-2 clustering" module	CLEC-2 clustering: k_{-2}	k_{-2}	$348.26\ s^{-1} \times \mu mol^{-1}$	25 – 250	0.077
	CLEC-2 clustering: k_{-1}	k_{-1}	$0.0116\ s^{-1} \times \mu mol^{-1}$	0.001 – 0.01	0.044
	CLEC-2 clustering: k_1	k_1	$12324.611\ s^{-1} \times \mu mol^{-1}$	5000 – 50000	0.014
"Tyrosine kinase" module	the forward rate of Syk activation by SH-2 domains	k_{S1}^{SH2}	$0.47\ s^{-1} \times \mu M^{-1}$	0.2 – 2	1.21245
	reverse rate of CLEC-2 phosphorylation	Kr^{Phosph}	$0.21\ s^{-1}$	0.05 - 0.5	1.10722
	the turnover rate of Syk kinases	k_{cat}^{Syk}	$11.85\ s^{-1}$	5 – 15	1.10362
	Michaelis constant of Syk kinases	Km^{Syk}	$9.1\ \mu M$	5 – 15	0.997198

	reverse rate of Syk activation by SFK kinases	Kr^{Syk}	$10\ s^{-1}$	5 – 25	0.775836
	Syk deactivation by TULA-2 rate	Kr_{TULA2}^{Syk}	$7.5\ s^{-1} \times \mu M^{-1}$	2 – 20	0.734043
	the forward rate of TULA-2 activation by Syk	Kf_{Syk}^{TULA2}	$0.1\mu M^{-1} \times s^{-1}$	0.05 - 0.5	0.559938
	reverse rate of TULA-2 activation by Syk	Kr_{Syk}^{TULA2}	$0.007\ s^{-1}$	0.01 - 0.1	0.21001
	the turnover rate of SFK kinases	k_{cat}^{Src}	$2.1\ s^{-1}$	0.5 – 5	0.17258
	Michaelis constant of CD148	Km^{CD148}	$9.1\ mM$	4550 - 18200	0.010652
	reverse rate of CD148 activation	Kr^{CD148}	$90.8\ s^{-1}$	40 - 200	0.010623
	the turnover rate of CD148	k_{cat}^{CD148}	$9.7\ s^{-1}$	4 - 20	0.010536
	Syk initial number	S	5000	2500 - 10000	1.46352
	TULA-2 initial number	T	8000	3750 - 15000	0.680195
	SFK initial number	F_P	36800	10000 - 40000	0.010381
Comp. Sizes	platelet cytosol volume	V_{Cyt}	$4.5\ fl$	2.25 – 9	1
	plasma membrane area	S_{PM}	$45\ \mu m^2$	25 - 90	0.152712

Table S11. Sensitivity scores of the most influential parameters for the number of phosphorylated LAT at the point of maximal activation.

Module	Parameter name	Variable	Value	Variation limits	Sensitivity Score
"CLEC-2 clustering" module	CLEC-2 clustering: k_{-2}	k_{-2}	$348.26\ s^{-1} \times \mu mol^{-1}$	25 – 250	0.080092
	CLEC-2 clustering: k_{-1}	k_{-1}	$0.0116\ s^{-1} \times \mu mol^{-1}$	0.001 – 0.01	0.035984
	CLEC-2 clustering: k_1	k_1	$12324.611\ s^{-1} \times \mu mol^{-1}$	5000 – 50000	0.01352
	CLEC-2 initial number	R	2000	1000-4000	0.061893
"Tyrosine kinase" module	turnover rate of Syk kinases	k_{cat}^{Syk}	$11.85\ s^{-1}$	5 – 15	2.34692
	Michaelis constant of Syk kinases	Km^{Syk}	$9.1\ \mu M$	5 – 15	1.71089
	the forward rate of Syk activation by SH-2 domains	k_{S1}^{SH2}	$0.47\ s^{-1} \times \mu M^{-1}$	0.2 – 2	1.53089
	reverse rate of Syk activation by SFK kinases	Kr^{Syk}	$10\ s^{-1}$	5 – 25	1.37626
	reverse rate of CLEC-2 phosphorylation	Kr^{Phosph}	$0.21\ s^{-1}$	0.05 - 0.5	1.07892

	Syk deactivation by TULA-2 rate	Kr_{TULA2}^{Syk}	$7.5\ s^{-1} \times \mu M^{-1}$	2 – 20	0.531341
	the forward rate of TULA-2 activation by Syk	Kf_{Syk}^{TULA2}	$0.1\mu M^{-1} \times s^{-1}$	0.05 - 0.5	0.348428
	the turnover rate of SFK kinases	k_{cat}^{Src}	$2.1\ s^{-1}$	0.5-5	0.136494
	reverse rate of TULA-2 activation by Syk	Kr_{Syk}^{TULA2}	$0.007\ s^{-1}$	0.01 - 0.1	0.05687
	Syk SH-2 domains kD	kD_{Syk}^{SH2}	$0.176\ \mu M$	0.05-0.5	0.011793
	Syk initial number	S	5000	2500 - 10000	1.91275
	TULA-2 initial number	T	8000	3750 - 15000	0.369641
"LAT-PLCγ2" module	reverse rate of LAT phosphorylation	Kr^{LAT}	$1.41\ s^{-1}$	0.25 - 2.5	0.983638
	LAT initial number	L	4900	2500 - 10000	0.544366
Comp. Sizes	plasma membrane area	S_{PM}	$45\ \mu m^2$	25 - 90	0.39402

Table S12. Sensitivity scores of the most influential parameters for the number of active PLCγ2 at point of maximal activation.

Module	Parameter name	Variable	Value	Variation limits	Sensitivity Score
"CLEC-2 clustering" module	CLEC-2 clustering: k_{-2}	k_{-2}	$348.26\ s^{-1} \times \mu mol^{-1}$	25 – 250	0.129158
	CLEC-2 clustering: k_{-1}	k_{-1}	$0.0116\ s^{-1} \times \mu mol^{-1}$	0.001 – 0.01	0.062745
	CLEC-2 clustering: k_1	k_1	$12324.611\ s^{-1} \times \mu mol^{-1}$	5000 – 50000	0.021921
	CLEC-2 clustering: k_3	k_3	$2.7 \times 10^{-6}\ s^{-1}$	0.0001 – 0.001	0.011867
	CLEC-2 initial number	R	2000	1000-4000	0.08554
"Tyrosine kinase" module	turnover rate of Syk kinases	k_{cat}^{Syk}	$11.85\ s^{-1}$	5 – 15	3.86148
	Michaelis constant of Syk kinases	Km^{Syk}	$9.1\ \mu M$	5 – 15	2.8085
	the forward rate of Syk activation by SH-2 domains	k_{S1}^{SH2}	$0.47\ s^{-1} \times \mu M^{-1}$	0.2 – 2	2.38768
	reverse rate of Syk activation by SFK kinases	Kr^{Syk}	$10\ s^{-1}$	5 – 25	2.0621
	reverse rate of CLEC-2 phosphorylation	Kr^{Phosph}	$0.21\ s^{-1}$	0.05 - 0.5	1.78911
	Syk deactivation by TULA-2 rate	Kr_{TULA2}^{Syk}	$7.5\ s^{-1} \times \mu M^{-1}$	2 – 20	0.993338
	the forward rate of TULA-2 activation by Syk	Kf_{Syk}^{TULA2}	$0.1\mu M^{-1} \times s^{-1}$	0.05 - 0.5	0.681899
	the turnover rate of SFK kinases	k_{cat}^{Src}	$2.1\ s^{-1}$	0.5-5	0.262073

	reverse rate of TULA-2 activation by Syk	Kr_{Syk}^{TULA2}	$0.007\ s^{-1}$	0.01 - 0.1	0.16055
	Syk SH-2 domains kD	kD_{Syk}^{SH2}	$0.176\ \mu M$	0.05-0.5	0.0173905
	Syk initial number	S	5000	2500 - 10000	3.00666
	TULA-2 initial number	T	8000	3750 - 15000	0.765108
"LAT-PLCγ2" module	reverse rate of LAT phosphorylation	Kr^{LAT}	$1.41\ s^{-1}$	0.25 - 2.5	1.6537
	the turnover rate of Btk	k_{cat}^{Btk}	$0.14\ s^{-1}$	0.07 - 0.28	0.795997
	Michaelis constant of Btk	Km^{Btk}	$37\ \mu M$	18 - 74	0.793626
	the turnover rate of PI3K	k_{cat}^{PI3K}	$2.82\ s^{-1}$	1.4 - 5.65	0.70601
	reverse rate of PIP_3 production by PI3K	Kr^{PIP_3}	$0.44\ s^{-1}$	0.2 - 0.9	0.691281
	reverse rate of PLCγ2 activation	Kr^{PLC}	$8.6 \times 10^{-3}\ s^{-1}$	0.005 - 0.05	0.260846
	PLCγ2 kD from phosphorylated LAT	kD_{Lp}	$0.15\ \mu M$	0.075 - 0.3	0.146303
	Michaelis constant of PI3K	Km^{PI3K}	$11\ \mu M$	5.5 - 22	0.0369431
	the forward rate of Btk activation upon PIP_3 binding	k_1^{BI}	$0.51\ \mu M^{-1} \times s^{-1}$	0.25 - 1	0.0113054
	PI3K kD from phosphorylated LAT	kD_{LP}	$0.22\ \mu M$	0.11 - 0.44	0.0108299
	LAT initial number	L	4900	2500 - 10000	0.912258
	Btk initial number	B	11100	5000 - 25000	0.796234
	PLCγ2 initial number	p	2000	1000 - 4000	0.152649
	PI3K initial number	P	1900	950 - 3800	0.0115858
Comp. Sizes	plasma membrane area	S_{PM}	$45\ \mu m^2$	25 - 90	0.73603

Table S13. Sensitivity scores of the most influential parameters for the IP_3 concentration at the point of maximal activation.

Module	Parameter name	Variable	Value	Variation limits	Sensitivity Score
"CLEC-2 clustering" module	CLEC-2 clustering: k_{-2}	k_{-2}	$348.26\ s^{-1} \times \mu mol^{-1}$	25 – 250	0.190352
	CLEC-2 clustering: k_{-1}	k_{-1}	$0.0116\ s^{-1} \times \mu mol^{-1}$	0.001 – 0.01	0.092191
	CLEC-2 clustering: k_1	k_1	$12324.611\ s^{-1} \times \mu mol^{-1}$	5000 – 50000	0.032406
	CLEC-2 clustering: k_3	k_3	$2.7 \times 10^{-6}\ s^{-1}$	0.0001 – 0.001	0.0175
	CLEC-2 initial number	R	2000	1000-4000	0.126508
	turnover rate of Syk kinases	k_{cat}^{Syk}	$11.85\ s^{-1}$	5 – 15	5.71225

"Tyrosine kinase" module	Michaelis constant of Syk kinases	Km^{Syk}	$9.1\ \mu M$	5 – 15	4.12844
	the forward rate of Syk activation by SH-2 domains	k_{S1}^{SH2}	$0.47\ s^{-1} \times \mu M^{-1}$	0.2 – 2	3.52858
	reverse rate of Syk activation by SFK kinases	Kr^{Syk}	$10\ s^{-1}$	5 – 25	3.03843
	reverse rate of CLEC-2 phosphorylation	Kr^{Phosph}	$0.21\ s^{-1}$	0.05 - 0.5	2.6302
	Syk deactivation by TULA-2 rate	Kr_{TULA2}^{Syk}	$7.5\ s^{-1} \times \mu M^{-1}$	2 – 20	1.45979
	the forward rate of TULA-2 activation by Syk	Kf_{Syk}^{TULA2}	$0.1 \mu M^{-1} \times s^{-1}$	0.05 - 0.5	1.00145
	the turnover rate of SFK kinases	k_{cat}^{Src}	$2.1\ s^{-1}$	0.5-5	0.386137
	reverse rate of TULA-2 activation by Syk	Kr_{Syk}^{TULA2}	$0.007\ s^{-1}$	0.01 - 0.1	0.235098
	Syk SH-2 domains kD	kD_{Syk}^{SH2}	$0.176\ \mu M$	0.05-0.5	0.025556
	reverse rate of CD148 activation	Kr^{CD148}	$90.8\ s^{-1}$	40 - 200	0.011223
	the turnover rate of CD148	k_{cat}^{CD148}	$9.7\ s^{-1}$	4 - 20	0.010769
	Michaelis constant of CD148	Km^{CD148}	$9.1\ mM$	4550 - 18200	0.010616
	Syk initial number	S	5000	2500 - 10000	4.44675
	TULA-2 initial number	T	8000	3750 - 15000	1.12288
	SFK initial number	F_P	36800	10000 - 40000	0.010622
"LAT-PLCγ2" module	reverse rate of LAT phosphorylation	Kr^{LAT}	$1.41\ s^{-1}$	0.25 - 2.5	2.43175
	reverse rate of IP_3 production	Kr^{IP_3}	$60\ s^{-1}$	20 – 100	1.47202
	the turnover rate of Btk	k_{cat}^{Btk}	$0.14\ s^{-1}$	0.07 - 0.28	1.17565
	Michaelis constant of Btk	Km^{Btk}	$37\ \mu M$	18 - 74	1.17029
	the turnover rate of PI3K	k_{cat}^{PI3K}	$2.82\ s^{-1}$	1.4 - 5.65	1.03907
	reverse rate of PIP_3 production by PI3K	Kr^{PIP_3}	$0.44\ s^{-1}$	0.2 - 0.9	1.01565
	reverse rate of PLCγ2 activation	Kr^{PLC}	$8.6 \times 10^{-3}\ s^{-1}$	0.005 - 0.05	0.382328
	PLCγ2 kD from phosphorylated LAT	kD_{Lp}	$0.15\ \mu M$	0.075 - 0.3	0.215728
	Michaelis constant of PI3K	Km^{PI3K}	$11\ \mu M$	5.5 - 22	0.054275
	the forward rate of Btk activation upon PIP_3 binding	k_1^{BI}	$0.51\ \mu M^{-1} \times s^{-1}$	0.25 - 1	0.016936

	PI3K kD from phosphorylated LAT	kD_{LP}	$0.22\ \mu M$	0.11 - 0.44	0.015487
	LAT initial number	L	4900	2500 - 10000	1.3449
	Btk initial number	B	11100	5000 - 25000	1.17598
	PLCγ2 initial number	p	2000	1000 - 4000	0.225426
	PI3K initial number	P	1900	950 - 3800	0.016803
Comp. Sizes	plasma membrane area	S_{PM}	$45\ \mu m^2$	25 - 90	2.70157

Table S14. Sensitivity scores of the most influential parameters for the calcium concentration at the point of maximal activation.

	$k_1;\ s^{-1} \times \mu mol^{-1}$	$k_{-2};\ s^{-1} \times \mu mol^{-1}$	$k_3;\ s^{-1}$
37ºC	13924.4	348.26	2.7×10^{-6}
25ºC	2249	251.16	1.8×10^{-6}
25ºC, 1mM mβCD	164	208.07	1×10^{-6}

Table S15. "CLEC-2 clustering" module parameters, corresponding to different activatory conditions.

System of differential equations corresponding to the biochemical reactions incorporated in the stochastic model:

$$\frac{dLig}{dt} \times V_{EC} = -M_1 \quad (1)$$

$$\frac{dR}{dt} \times S_{PM} = -M_1 \quad (2)$$

$$\frac{dR^*}{dt} \times S_{PM} = M_1 + TS5_1 \quad (3)$$

$$\frac{dR_C^*}{dt} \times S_{PM} = TS5_2 - K_7 \quad (4)$$

$$\frac{dR_P^*}{dt} \times S_{PM} = K_7 \quad (5)$$

$$\frac{dD}{dt} \times S_{PM} = -K_1 \quad (6)$$

$$\frac{dD^*}{dt} \times S_{PM} = K_1 \quad (7)$$

$$\frac{dCs}{dt} \times V_{Cyt} = -K_2 \quad (8)$$

$$\frac{dCs^*}{dt} \times V_{Cyt} = K_2 \quad (9)$$

$$\frac{dF_P}{dt} \times S_{PM} = -K_3 \quad (10)$$

$$\frac{dF}{dt} \times S_{PM} = K_3 - K_4 \quad (11)$$

$$\frac{dF^P}{dt} \times S_{PM} = K_4 - K_5 \quad (12)$$

$$\frac{dF_*^P}{dt} \times S_{PM} = K_5 \quad (13)$$

$$\frac{dT}{dt} \times V_{Cyt} = -K_6 \quad (14)$$

$$\frac{dT^*}{dt} \times V_{Cyt} = K_6 \quad (15)$$

$$\frac{dS}{dt} \times V_{Cyt} = -K_8 \quad (16)$$

$$\frac{dS^*}{dt} \times V_{Cyt} = K_8 \quad (17)$$

$$\frac{dL}{dt} \times S_{PM} = -PL_1 \quad (18)$$

$$\frac{dL^*}{dt} \times S_{PM} = PL_1 \quad (19)$$

$$\frac{dLp}{dt} \times S_{PM} = PL_2 - PL_6 \quad (20)$$

$$\frac{dLP}{dt} \times S_{PM} = PL_3 \quad (21)$$

$$\frac{dp}{dt} \times V_{Cyt} = -PL_2 \quad (22)$$

$$\frac{dP}{dt} \times V_{Cyt} = -PL_3 \quad (23)$$

$$\frac{dI_1}{dt} \times S_{PM} = -PL_4 - PL_7 \quad (24)$$

$$\frac{dI_2}{dt} \times S_{PM} = PL_4 \quad (25)$$

$$\frac{dB}{dt} \times V_{Cyt} = -PL_5 \quad (26)$$

$$\frac{dB^*}{dt} \times S_{PM} = PL_5 \quad (27)$$

$$\frac{dp^*}{dt} \times S_{PM} = PL_6 \quad (28)$$

$$\frac{dI_3}{dt} \times V_{Cyt} = PL_7 \quad (29)$$

3. Supporting Figures

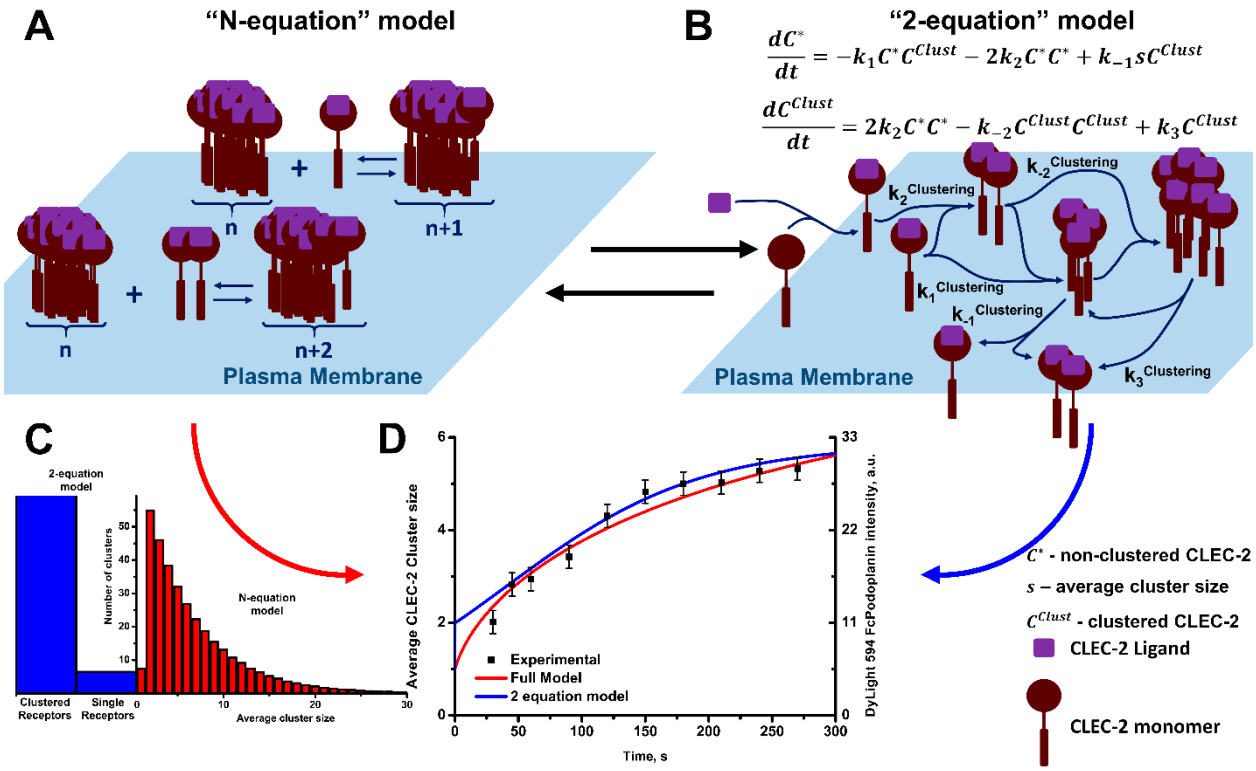

Figure S1. CLEC-2 receptor clustering models. In order to describe platelet CLEC-2 receptor clustering two approaches were used: N-equation model of receptor clustering, which describes behavior of the clusters of the receptors of each size explicitly (A – scheme, C- average cluster size) – (11) and 2-equation model, that describes behavior of the receptor clusters in general (B) – (13). Both models were capable of describing experimental data showing the clustering of CLEC-2, calculated from absolute fluorescent intensity data (12) under the assumption that only CLEC-2 monomers and dimers are present on the surface of resting platelets (29) (D). More simplistic approach – 2-equation model – was used for the construction of the complete model of CLEC-2 signalling, because it both allowed to describe experimental data and to reduce computational complexity.

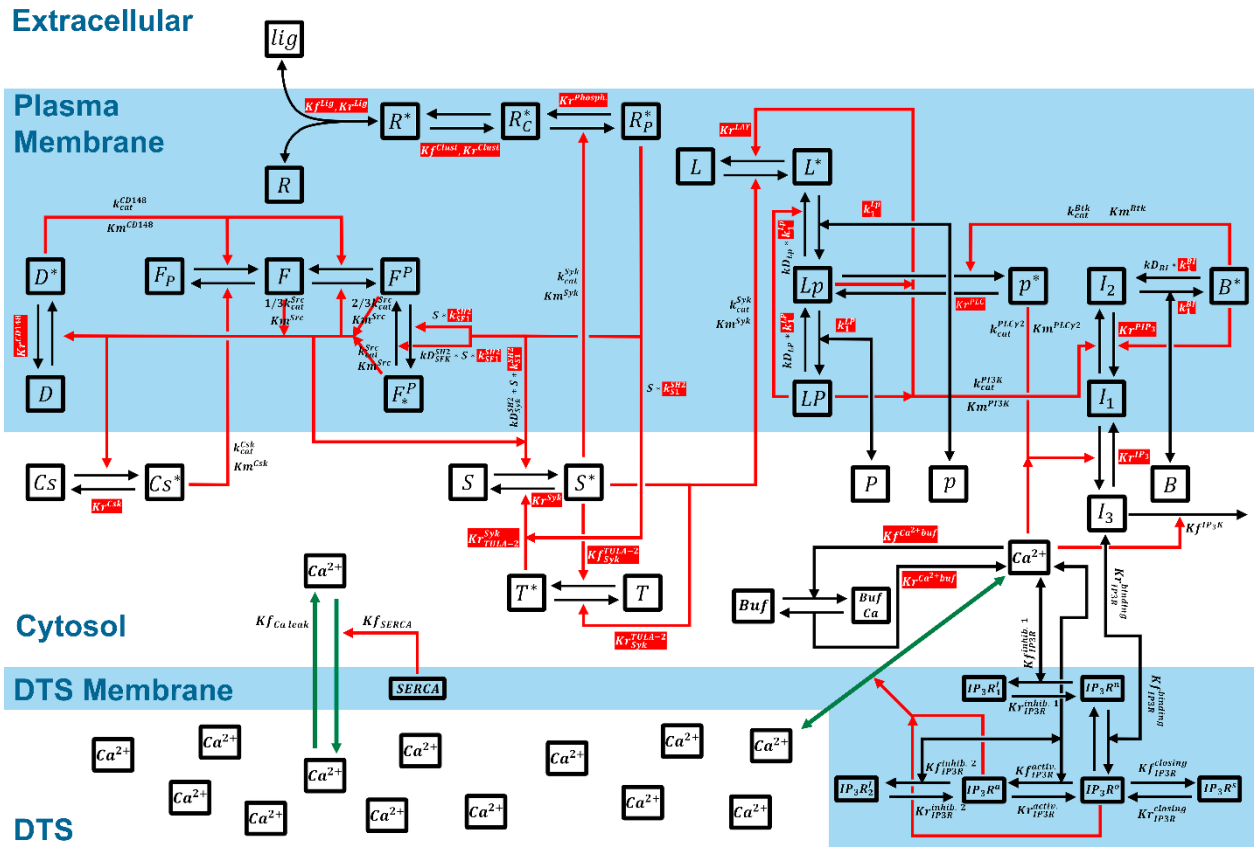

Figure S2. Network diagram of the platelet CLEC-2 signalling model. Black lines represent transitions between the different state of the incorporated species. Red lines represent catalysis. Green lines represent calcium ions transitions from DTS to the cytosol. Unknown parameter values are highlighted in red. All parameter values can be found in Supplementary Tables S4,5,7,9.

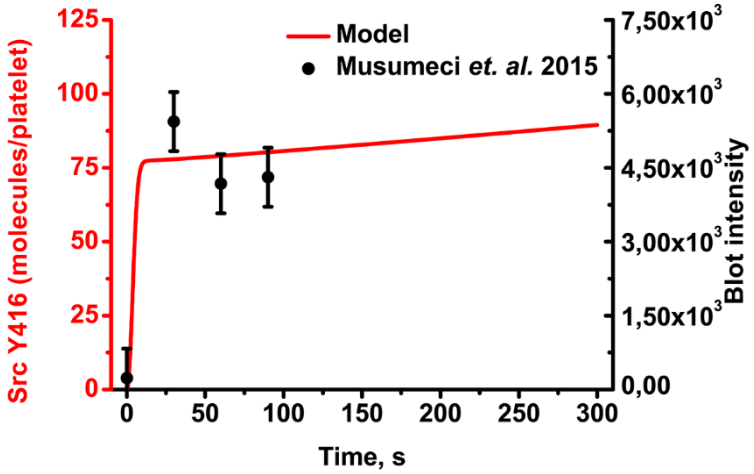

Figure S3. Model validation. Comparison of the numbers of Y416 phosphorylated amount of SFK predicted by the model to experimental data available from the literature (15).

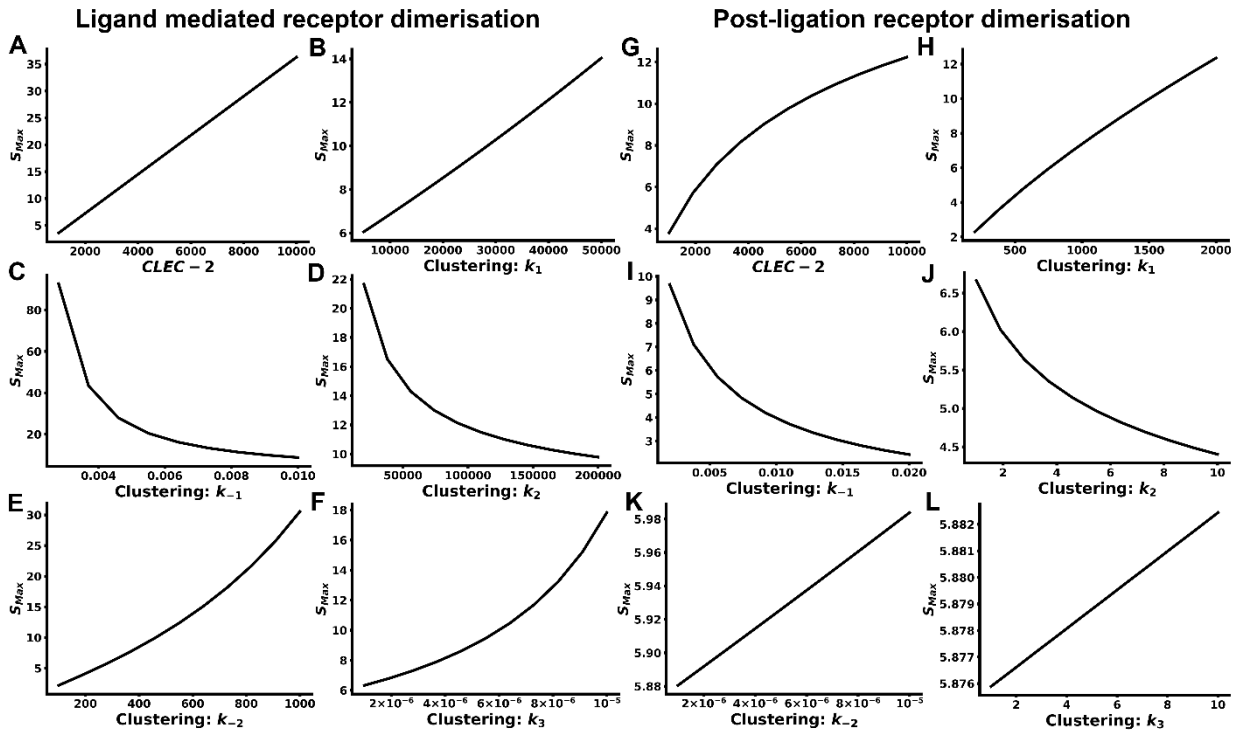

Figure S4. Explicit variation of the parameters of the "CLEC-2 clusteri ng module". (A-C) Impact of the "CLEC-2 clustering" parameters on maximal CLEC-2 cluster size (S_{Max}) in "Ligand mediated receptor dimerisation" mode: CLEC-2 initial number (A), CLEC-2 clustering k_1 (B), CLEC-2 clustering k_{-1} (C), CLEC-2 clustering k_2 (D), CLEC-2 clustering k_{-2} (E), CLEC-2 clustering k_3 (F). (G-L) Impact of the "CLEC-2 clustering" parameters on maximal CLEC-2 cluster size (S_{Max}) in "Ligand mediated receptor dimerisation" mode: CLEC-2 initial number (G), CLEC-2 clustering k_1 (H), CLEC-2 clustering k_{-1} (I), CLEC-2 clustering k_2 (J), CLEC-2 clustering k_{-2} (K), CLEC-2 clustering k_3 (L).

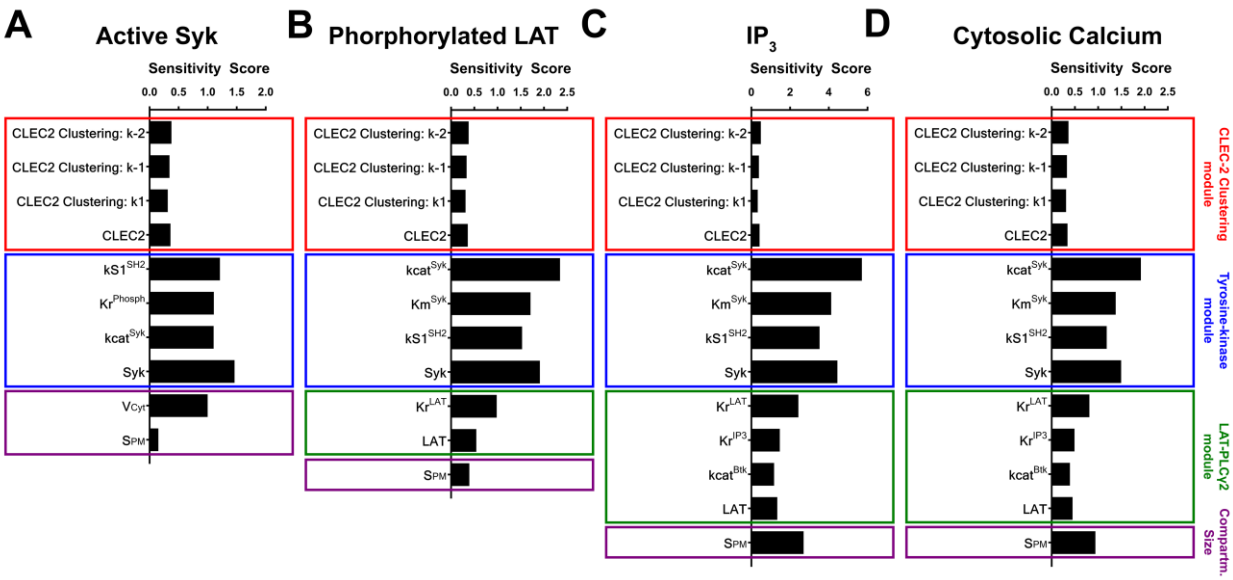

Figure S5. Local sensitivity analysis. Sensitivity score of the most influential parameters from each of the module and the most influential initial concentration, concerning: number of active Syk kinases (A), number of phosphorylated LAT (B), IP_3 concentration (C), cytosolic calcium concentration (D). Red colour highlights "CLEC-2 clustering" module, blue – "Tyrosine kinase" module, green – "LAT-PLCγ2" module, purple – initial volumes of the model compartments.

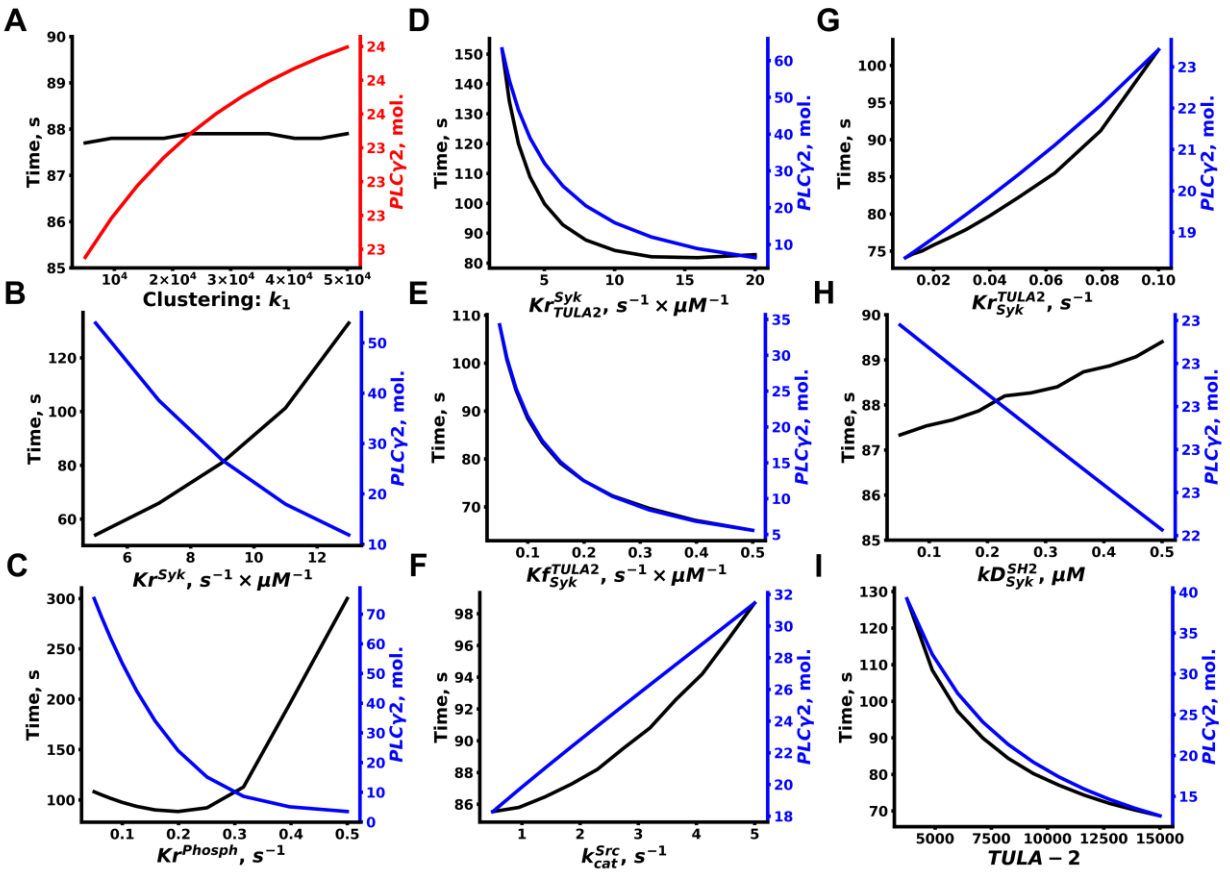

Figure S6. Explicit variation of the parameters with the sensitivity score above 0.01 for effect on maximal amount of active PLCγ2 and time to maximum (from CLEC-2 clustering k_1 to TULA-2 initial concentration). CLEC-2 clustering k_1 (A), reverse rate of Syk activation by SFK kinases (B), reverse rate of CLEC-2 phosphorylation (C), Syk deactivation by TULA-2 rate (D), forward rate of TULA-2 activation by Syk (E), turnover rate of SFK kinases (F), reverse rate of TULA-2 activation by Syk (G), Syk SH-2 domains kD from phosphorylated tyrosine residues in hemITAM sequences (H), TULA-2 initial number (I). Red colour highlights "CLEC-2 clustering" module, blue – "Tyrosine kinase" module.

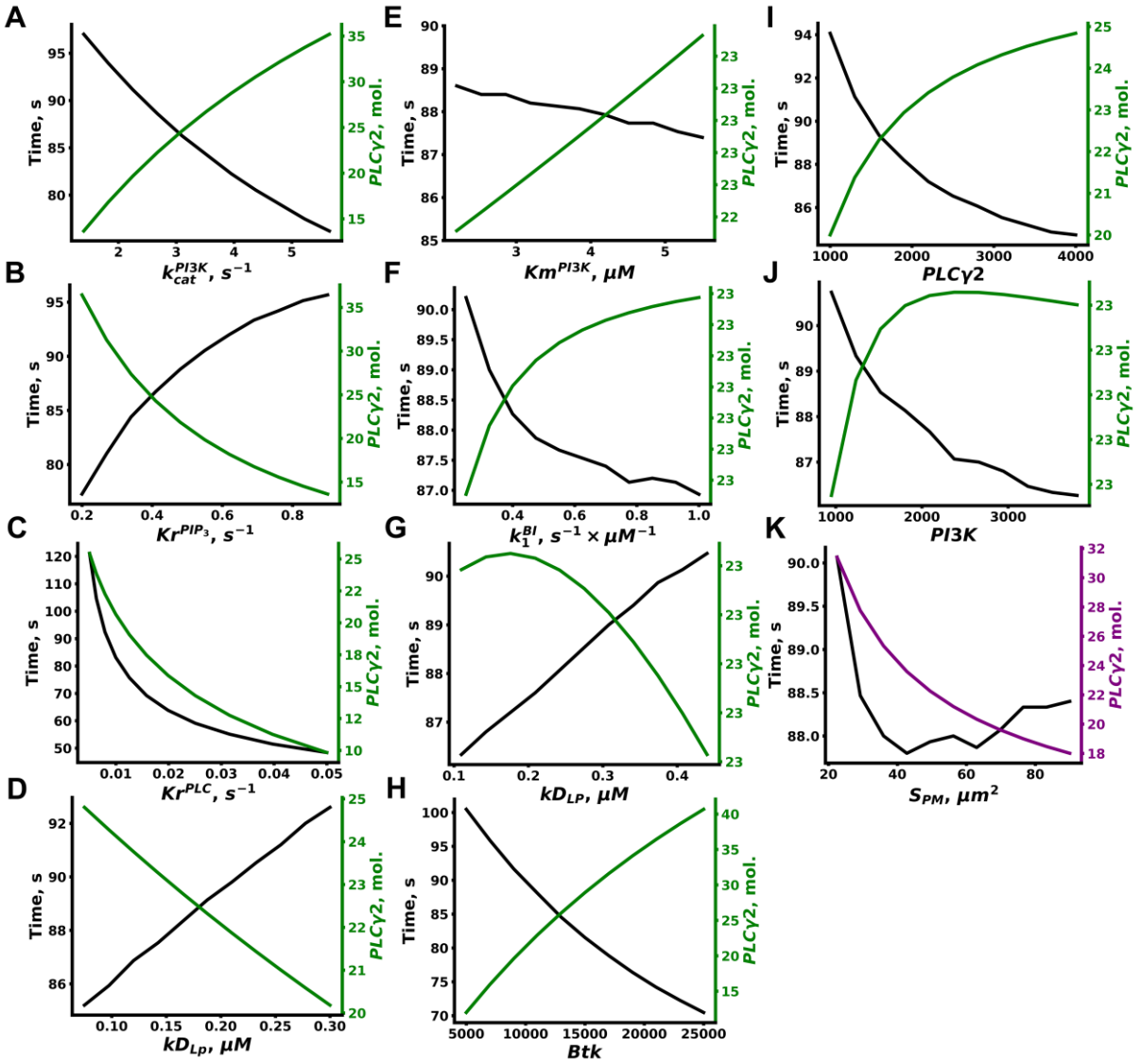

Figure S7. Explicit variation of the parameters with the sensitivity score above 0.01 for effect on maximal amount of active PLCγ2 and time to maximum (from PI3K turnover rate to plasma membrane area). PI3K turnover rate (A), reverse rate of PIP_3 production by PI3K (B), reverse rate of PLCγ2 activation (C), PLCγ2 kD from phosphorylated LAT (D), Michaelis constant of PI3K (E), forward rate of Btk activation upon PIP_3 binding (F), PI3K kD from phosphorylated LAT (G), Btk initial number (H), PLCγ2 initial number (I), PI3K initial number (J), plasma membrane area (K). Green – "LAT-PLCγ2" module, purple – initial volumes of the model compartments.

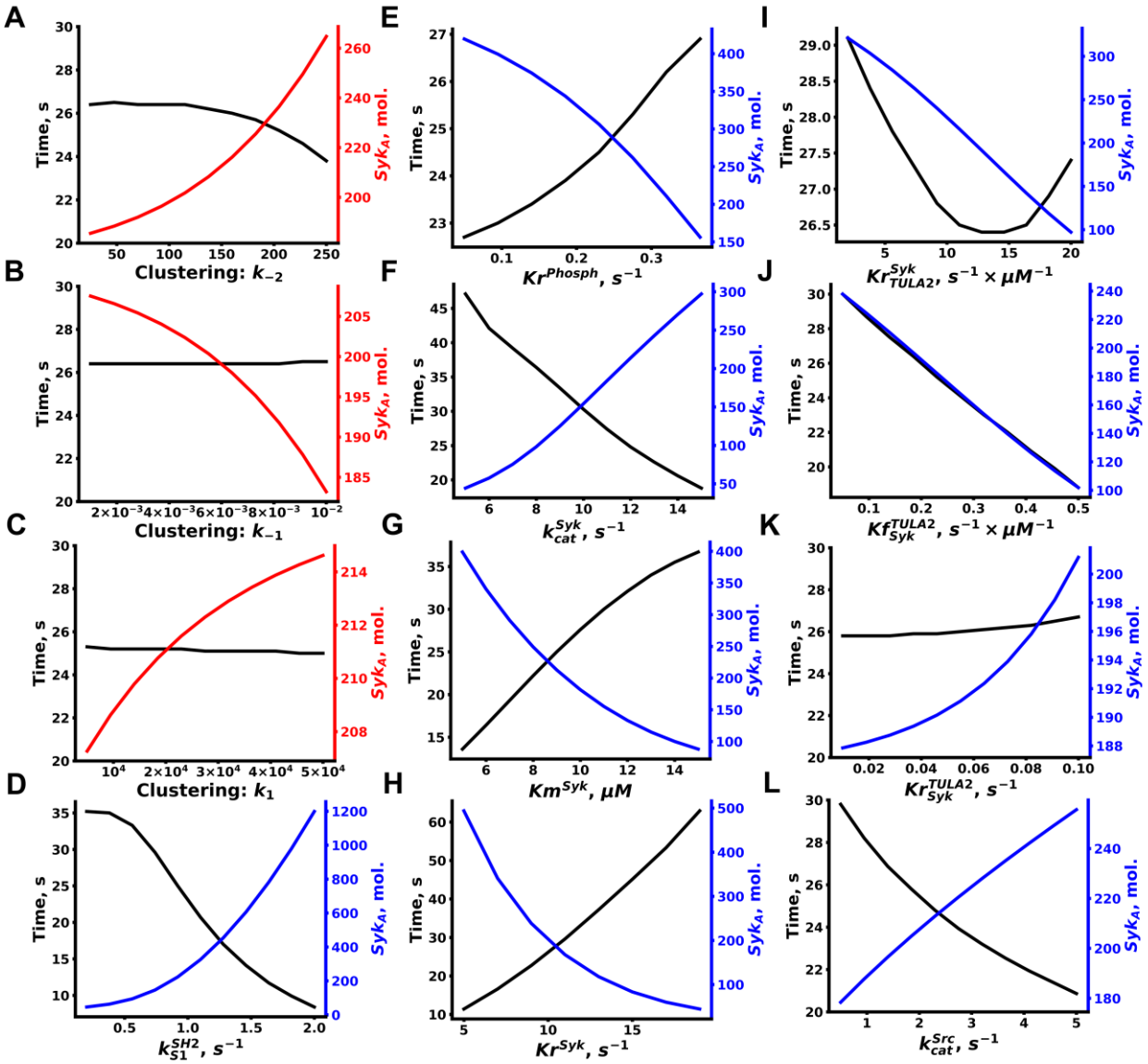

Figure S8. Explicit variation of the parameters with the sensitivity score above 0.01 for effect on maximal amount of active Syk kinases and time to maximum (from CLEC-2 clustering k_{-2} to turnover rate of SFK). CLEC-2 clustering k_{-2} (A), CLEC-2 clustering k_{-1} (B), CLEC-2 clustering k_1 (C), forward rate of Syk activation upon SH-2 domain binding to dually phosphorylated hemITAMs (D), reverse rate of CLEC-2 phosphorylation (E), turnover rate of Syk kinases (F), Michaelis constant of Syk kinases (G), reverse rate of Syk activation by SFK kinases (H), Syk deactivation by TULA-2 rate (I), forward rate of TULA-2 activation by Syk (J), reverse rate of TULA-2 activation by Syk (K), turnover rate of SFK kinases (L). Red colour highlights "CLEC-2 clustering" module, blue – "Tyrosine kinase" module.

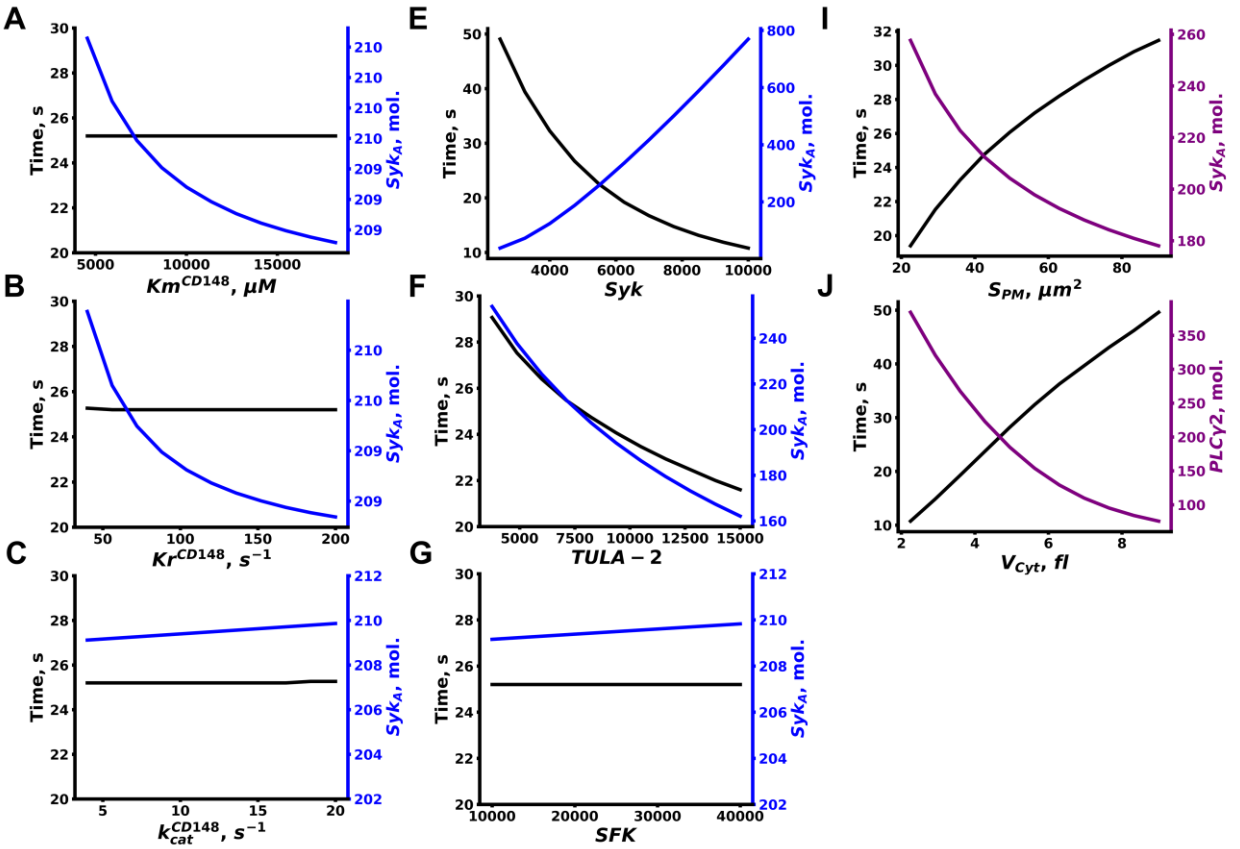

Figure S9. Explicit variation of the parameters with the sensitivity score above 0.01 for effect on maximal amount of active Syk kinases and time to maximum (from Michaelis constant of CD148 to platelet cytosol volume). Michaelis constant of CD148 (A), reverse rate of CD148 activation (B), turnover rate of CD148 (C), Syk initial number (D), TULA-2 initial number (E), SFK initial number (F), plasma membrane area (I), platelet cytosol volume (J). Blue – "Tyrosine kinase" module, purple – initial volumes of the model compartments.

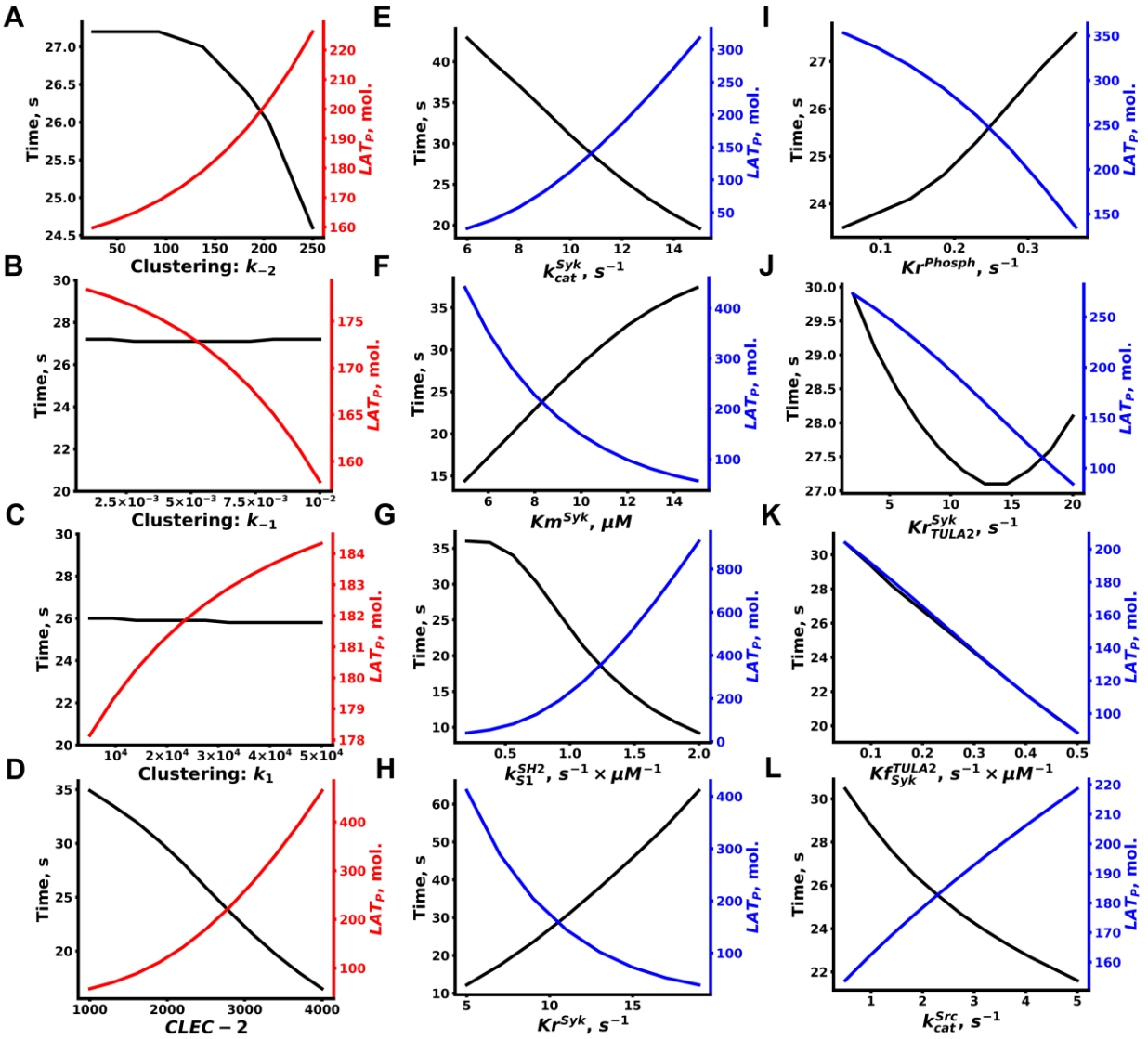

Figure S10. Explicit variation of the parameters with the sensitivity score above 0.01 for effect on maximal amount of phosphorylated LAT and time to maximum (from CLEC-2 clustering k_{-2} to turnover rate of SFK). CLEC-2 clustering k_{-2} (A), CLEC-2 clustering k_{-1} (B), CLEC-2 clustering k_1 (C), CLEC-2 initial number (D), turnover rate of Syk kinases (E), Michaelis constant of Syk kinases (F), forward rate of Syk activation upon SH-2 domain binding to dually phosphorylated hemITAMs (G), reverse rate of Syk activation by SFK kinases (H), reverse rate of CLEC-2 phosphorylation (I), Syk deactivation by TULA-2 rate (J), forward rate of TULA-2 activation by Syk (K), turnover rate of SFK kinases (L). Red colour highlights "CLEC-2 clustering" module, blue – "Tyrosine kinase" module.

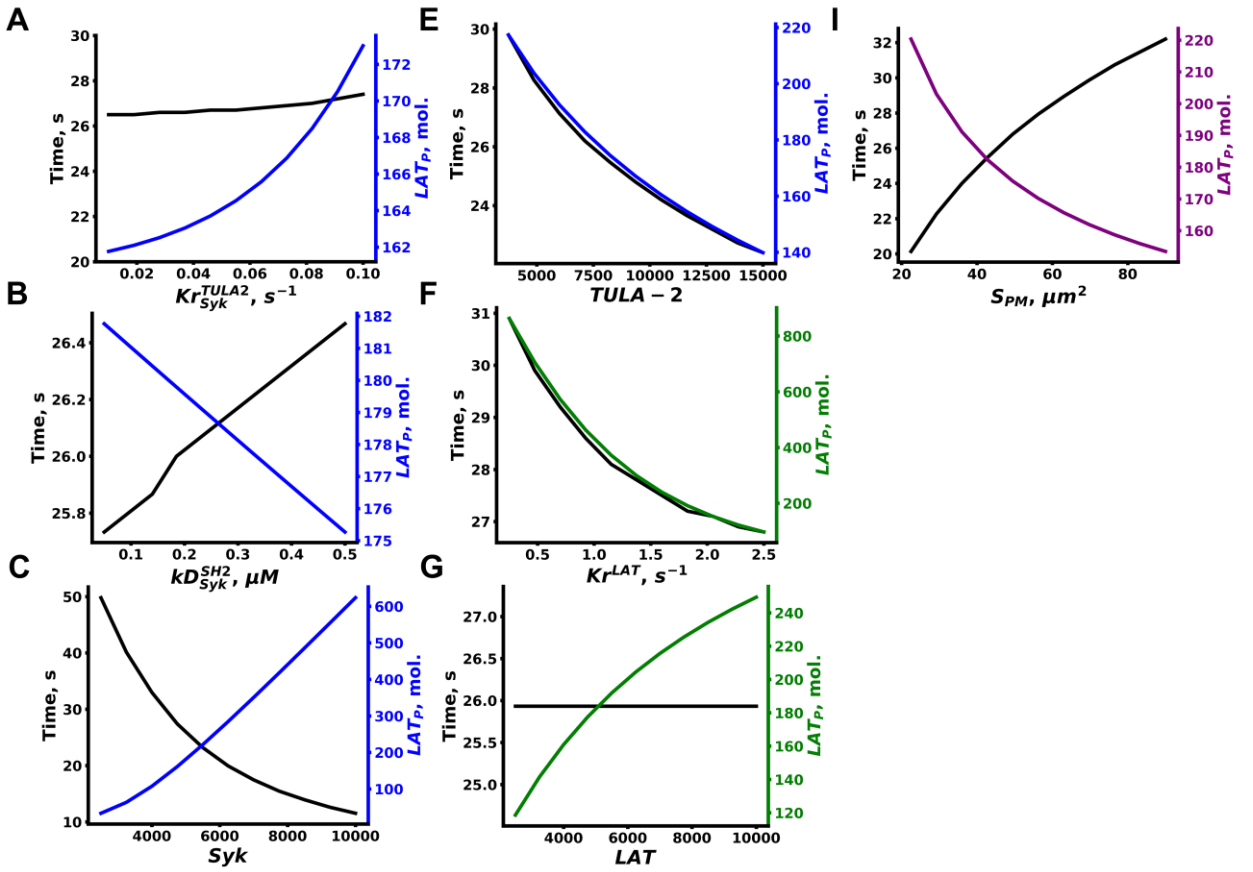

Figure S11. Explicit variation of the parameters with the sensitivity score above 0.01 for effect on maximal amount of phosphorylated LAT and time to maximum (from the reverse rate of TULA-2 activation by Syk to plasma membrane area). Reverse rate of TULA-2 activation by Syk (A), Syk SH-2 domains kD from phosphorylated tyrosine residues in hemITAM sequences (B), Syk initial number (C), TULA-2 initial number (D), reverse rate of LAT phosphorylation (F), LAT initial number (G), plasma membrane area (I). Blue – "Tyrosine kinase" module, green – "LAT-PLCγ2" module, purple – initial volumes of the model compartments.

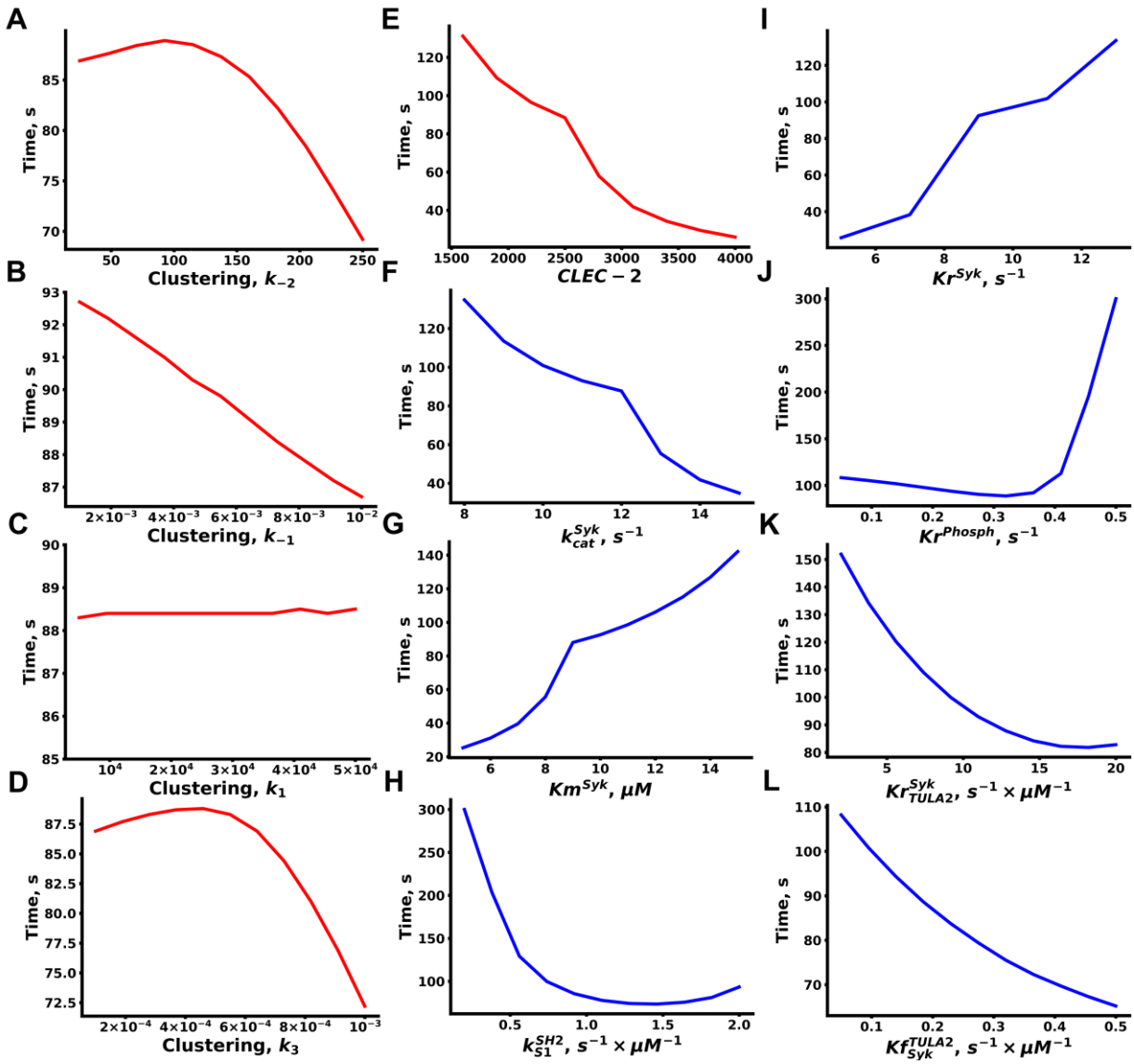

Figure S12. Explicit variation of the parameters with the sensitivity score above 0.01 for effect on the maximal concentration of IP_3 and time to maximum (from CLEC-2 clustering k_{-2} to forward rate of TULA-2 activation by Syk). Inflexion point on the graph corresponds to the initiation of calcium oscillations. CLEC-2 clustering k_{-2} (A), CLEC-2 clustering k_{-1} (B), CLEC-2 clustering k_1 (C), CLEC-2 clustering k_3 (D), CLEC-2 initial number (E), turnover rate of Syk kinases (F), Michaelis constant of Syk kinases (G), forward rate of Syk activation upon SH-2 domain binding to dually phosphorylated hemITAMs (H), reverse rate of Syk activation by SFK kinases (I), reverse rate of CLEC-2 phosphorylation (J), Syk deactivation by TULA-2 rate (K), forward rate of TULA-2 activation by Syk (L). Red colour highlights "CLEC-2 clustering" module, blue – "Tyrosine kinase" module.

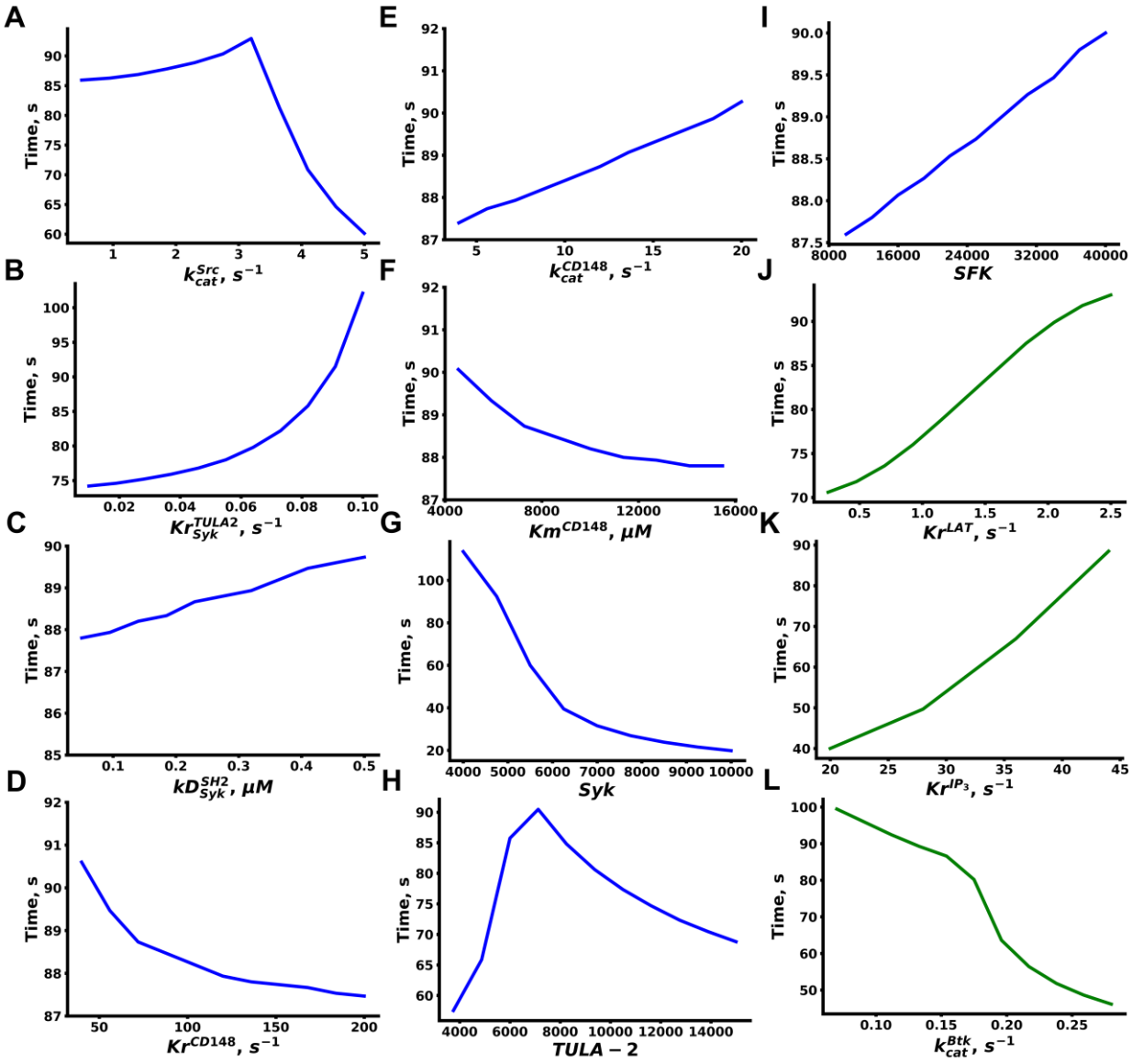

Figure S13. Explicit variation of the parameters with the sensitivity score above 0.01 for effect on the maximal concentration of IP_3 and time to maximum (turnover rate of SFK to turnover rate of Btk). Inflexion point on the graph corresponds to the initiation of calcium oscillations. Turnover rate of SFK (A), reverse rate of TULA-2 activation by Syk (B), Syk SH-2 domains kD from phosphorylated tyrosine residues in hemITAM sequences (C), reverse rate of CD148 activation (D), turnover rate of CD148 (E), Michaelis constant of CD148 (F), Syk initial number (G), TULA-2 initial number (H), SFK initial number (I), reverse rate of LAT phosphorylation (J), reverse rate of IP_3 production (K), turnover rate of Btk (L). Blue – "Tyrosine kinase" module, green – "LAT-PLCγ2" module.

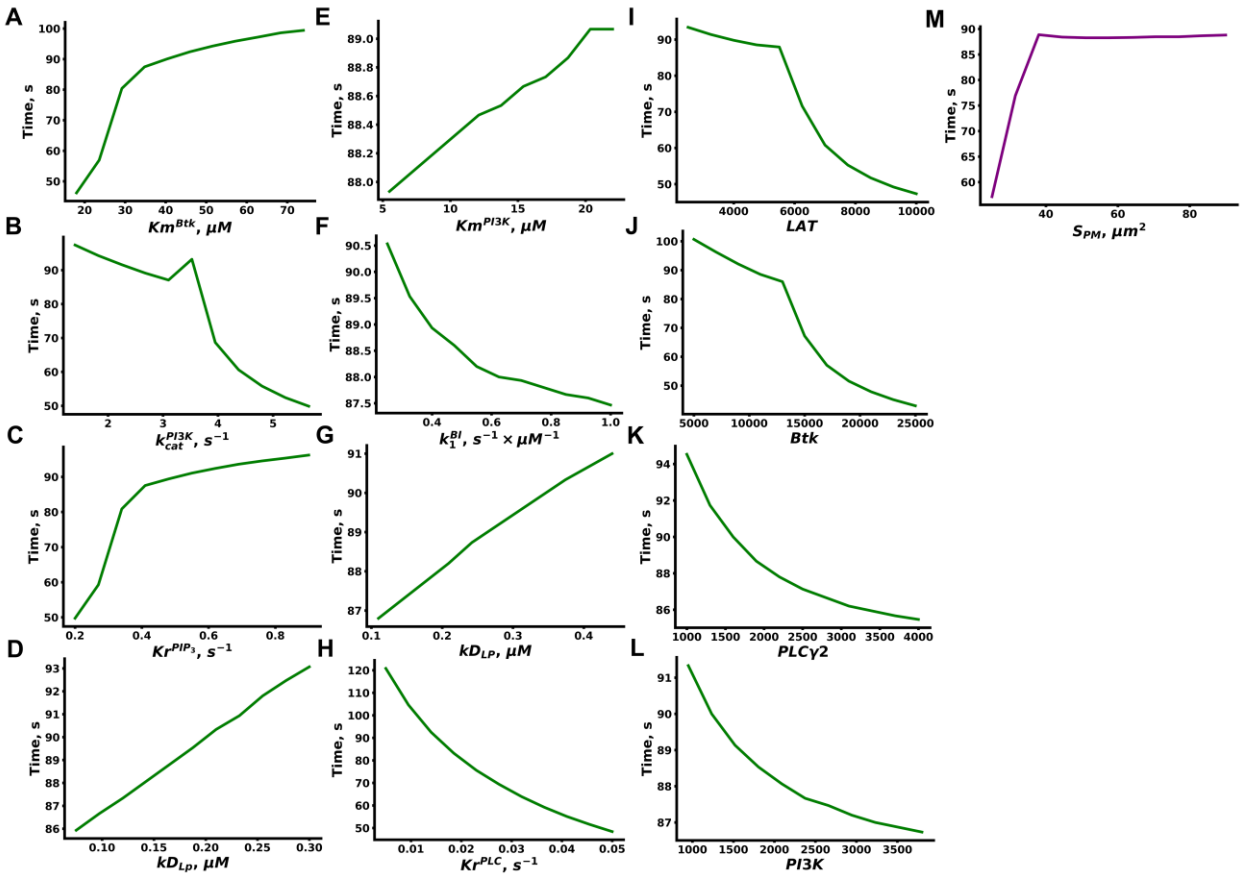

Figure S14. Explicit variation of the parameters with the sensitivity score above 0.01 for effect on the maximal concentration of IP_3 and time to maximum (from Michaelis constant of Btk to plasma membrane area). Inflexion point on the graph corresponds to the initiation of calcium oscillations. Michaelis constant of Btk (A), turnover rate of PI3K (B), reverse rate of PIP_3 production by PI3K (C), PLCγ2 kD from phosphorylated LAT (D), Michaelis constant of PI3K (E), forward rate of Btk activation upon PIP_3 binding (F), PI3K kD from phosphorylated LAT (G), reverse rate of PLCγ2 activation (H), LAT initial number (I), Btk initial number (J), PLCγ2 initial number (K), PI3K initial number (L), plasma membrane area (M). Green – "LAT-PLCγ2" module, purple – initial volumes of the model compartments.

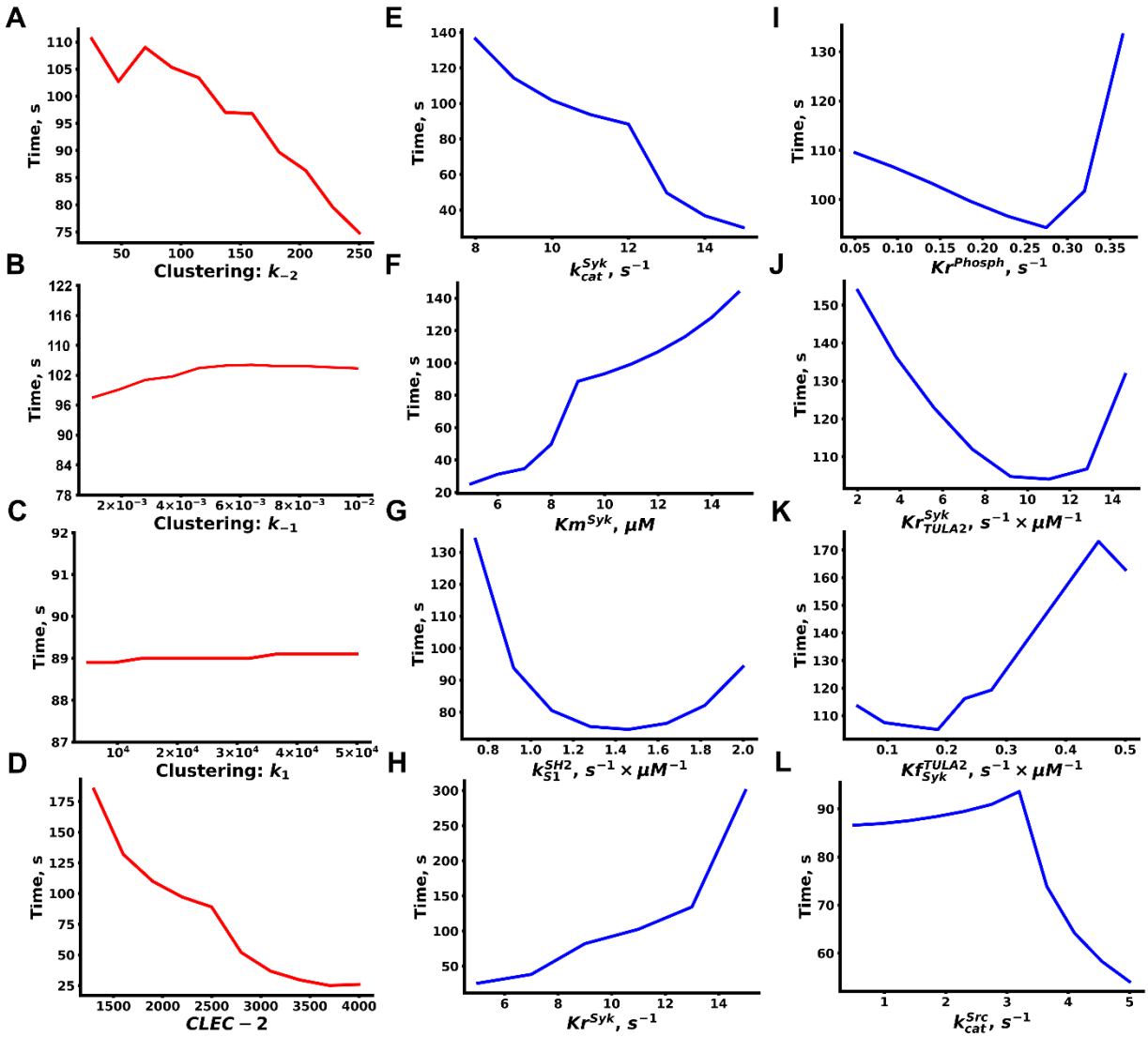

Figure S15. Explicit variation of the parameters with the sensitivity score above 0.01 for effect on the maximal concentration of cytosolic calcium and time to maximum (from CLEC-2 clustering k_{-2} to turnover rate of SFK). Inflexion point on the graph corresponds to the initiation of calcium oscillations. CLEC-2 clustering k_{-2} (A), CLEC-2 clustering k_{-1} (B), CLEC-2 clustering k_1 (C), CLEC-2 initial number (D), turnover rate of Syk kinases (E), Michaelis constant of Syk kinases (F), forward rate of Syk activation upon SH-2 domain binding to dually phosphorylated hemITAMs (G), reverse rate of Syk activation by SFK kinases (H), reverse rate of CLEC-2 phosphorylation (I), Syk deactivation by TULA-2 rate (J), forward rate of TULA-2 activation by Syk (K), turnover rate of SFK (L). Red colour highlights "CLEC-2 clustering" module, blue – "Tyrosine kinase" module.

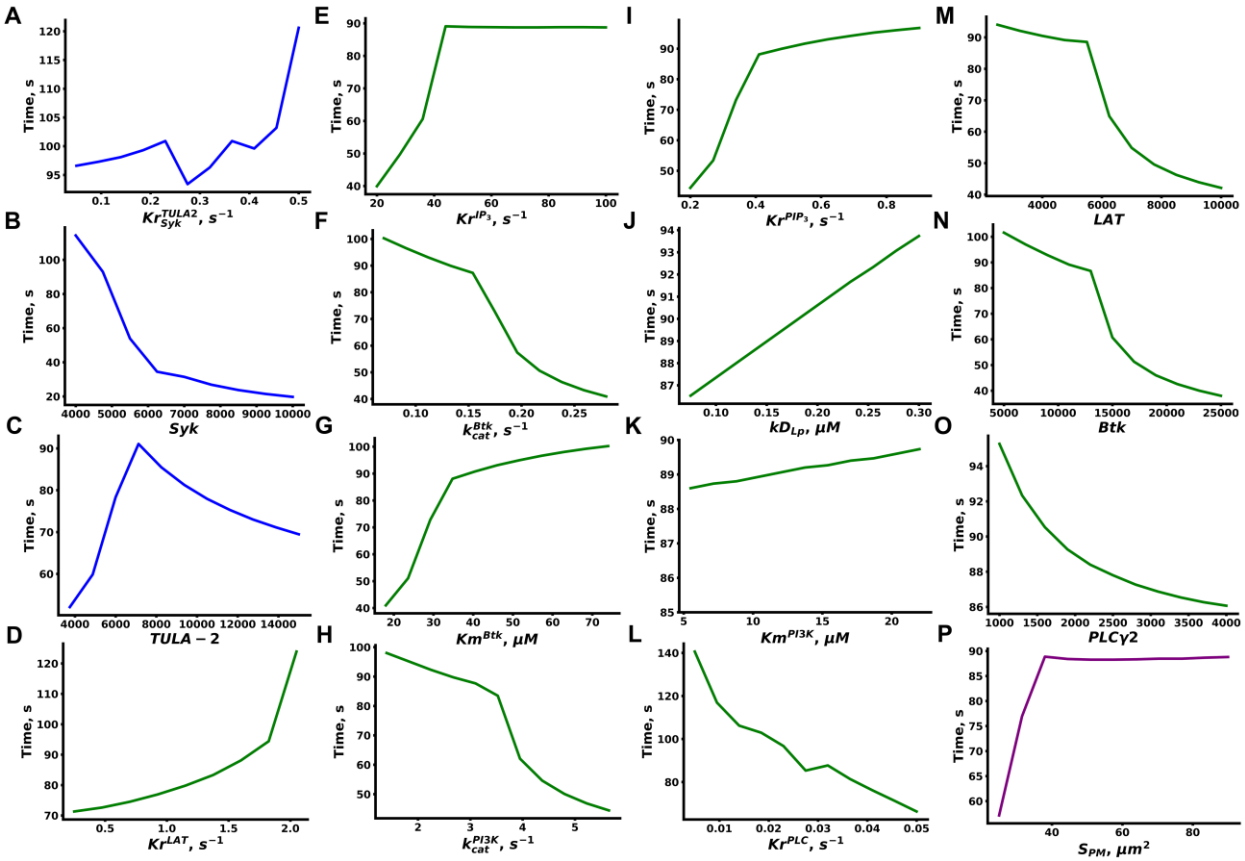

Figure S16. Explicit variation of the parameters with the sensitivity score above 0.01 for effect on the maximal concentration of cytosolic calcium and time to maximum (turnover rate of SFK to turnover rate of Btk). Inflexion point on the graph corresponds to the initiation of calcium oscillations. Reverse rate of TULA-2 activation by Syk (A), Syk initial number (B), TULA-2 initial number (C), reverse rate of LAT phosphorylation (D), reverse rate of IP_3 production (E), turnover rate of Btk (F), Michaelis constant of Btk (G), turnover rate of PI3K (H), reverse rate of PIP_3 production by PI3K (I), PLCγ2 kD from phosphorylated LAT (D) (J), Michaelis constant of PI3K (K), reverse rate of PLCγ2 activation (L), LAT initial number (M), Btk initial number (N), PLCγ2 initial number (O), plasma membrane area (P).

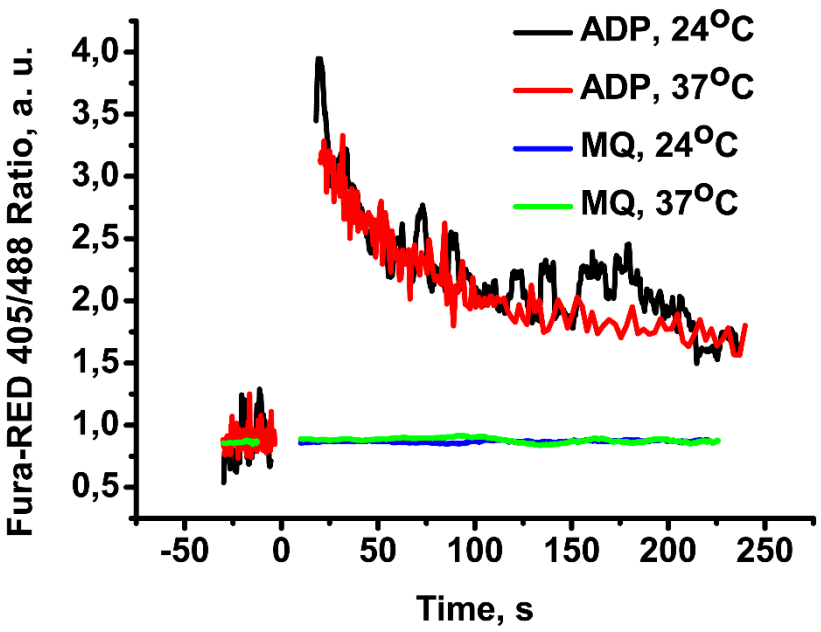

Figure S17. Activation of platelets by 2µM ADP was independent of temperature conditions.

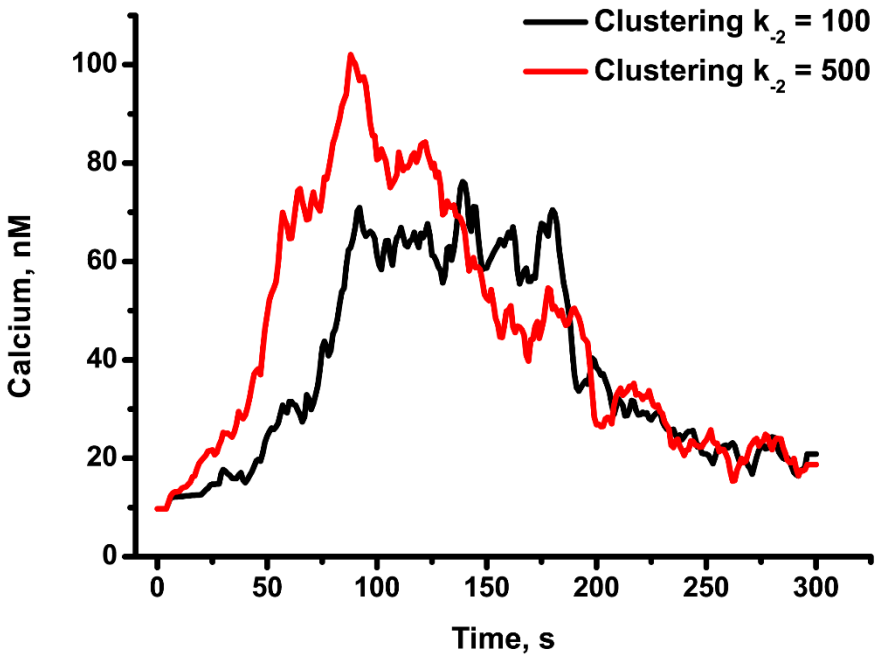

Figure S18. CLEC-2 induced calcium response in platelets, averaged over 100 stochastic runs at different CLEC-2 cluster formation rates.

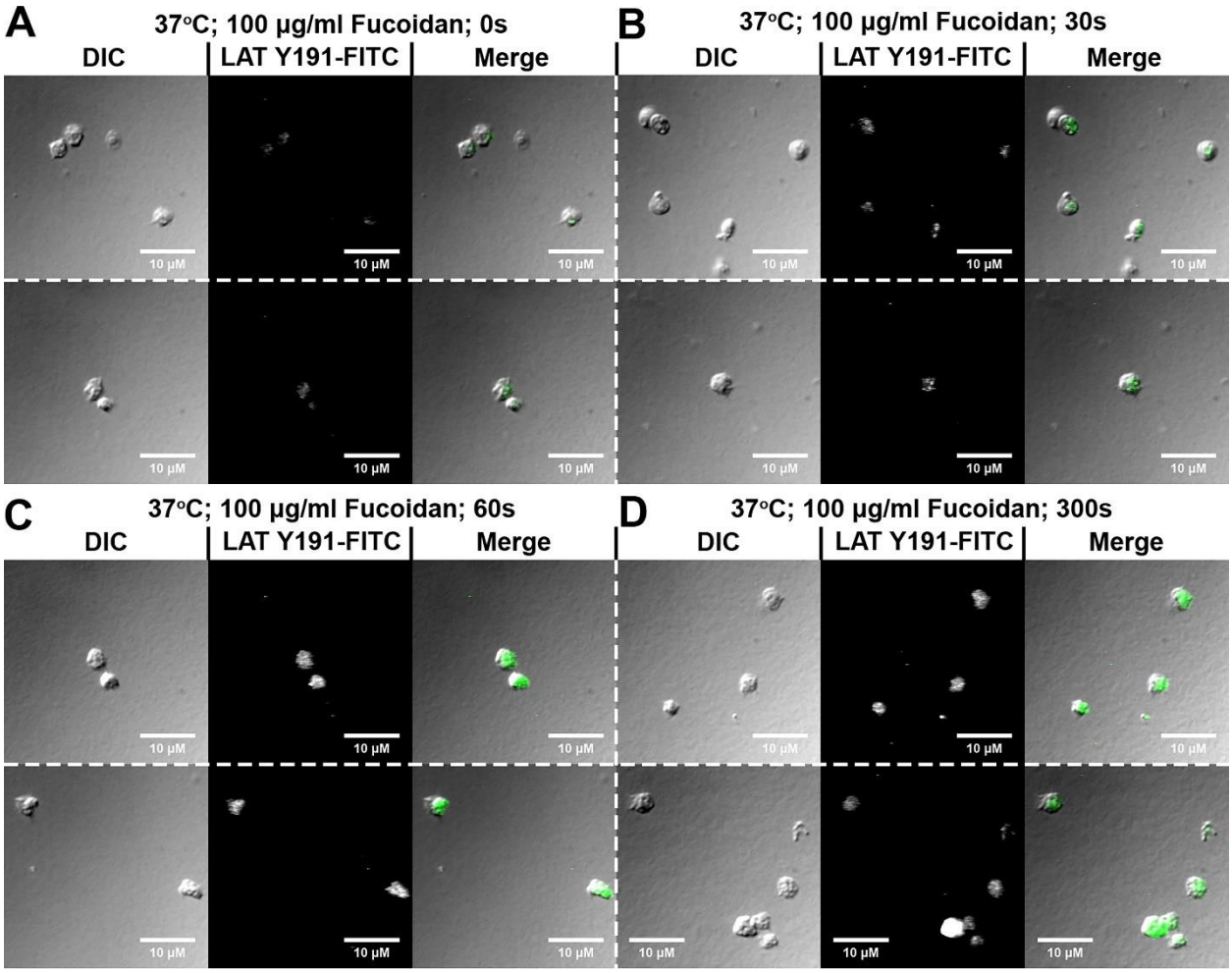

Figure S19. Immunefluorescence of platelets activated by 100 µg/ml Fucoidan at 37°C, fixed at different time-points and stained for phosphorylated LAT. (A) Resting platelets; (B) 30 second incubation with the activator; (C) 60 second incubation with the activator; (D) 300 second incubation with the activator.

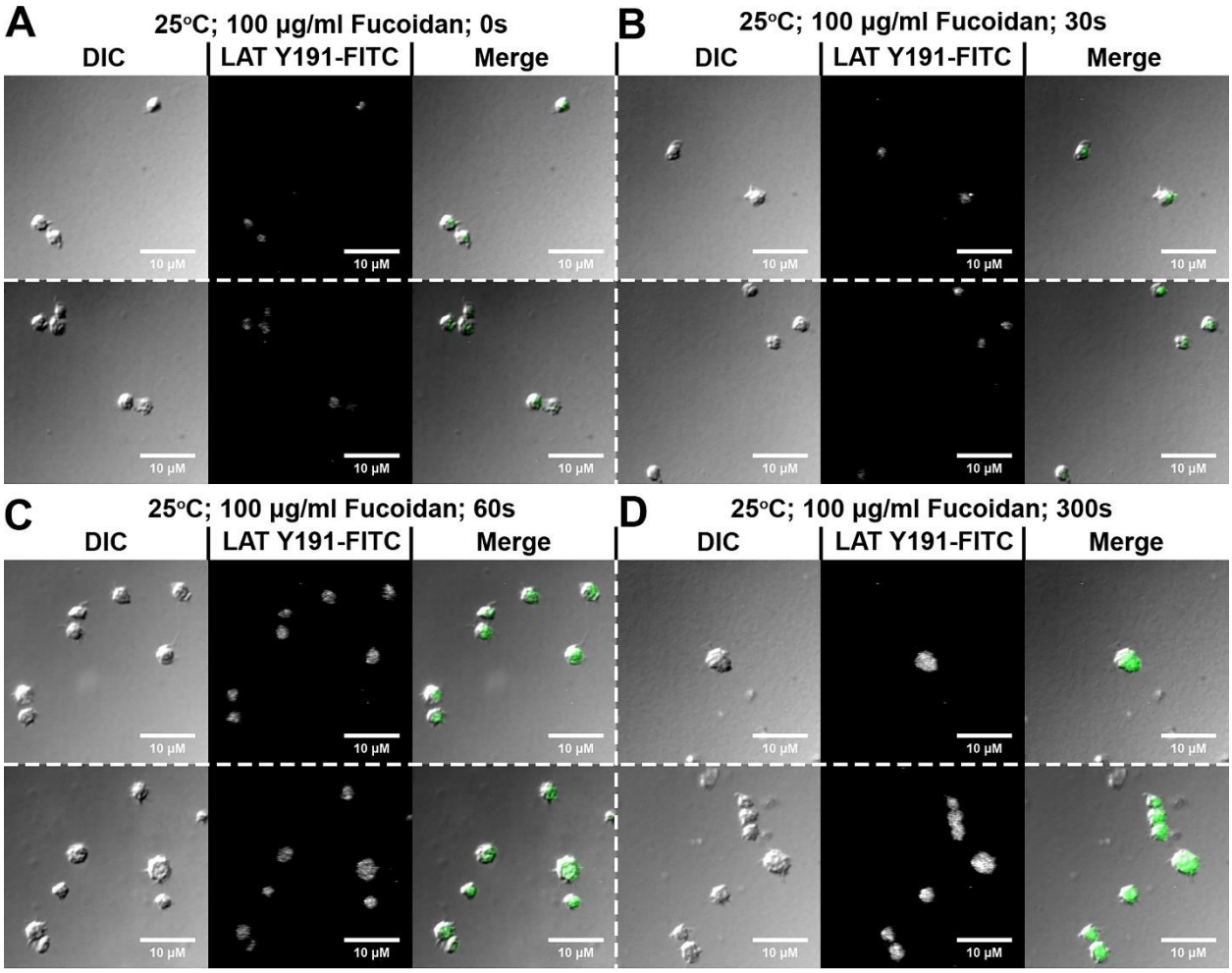

Figure S20. Immunefluorescence of platelets activated by 100 µg/ml Fucoidan at 25°C, fixed at different time-points and stained for phosphorylated LAT. (A) Resting platelets; (B) 30 second incubation with the activator; (C) 60 second incubation with the activator; (D) 300 second incubation with the activator.

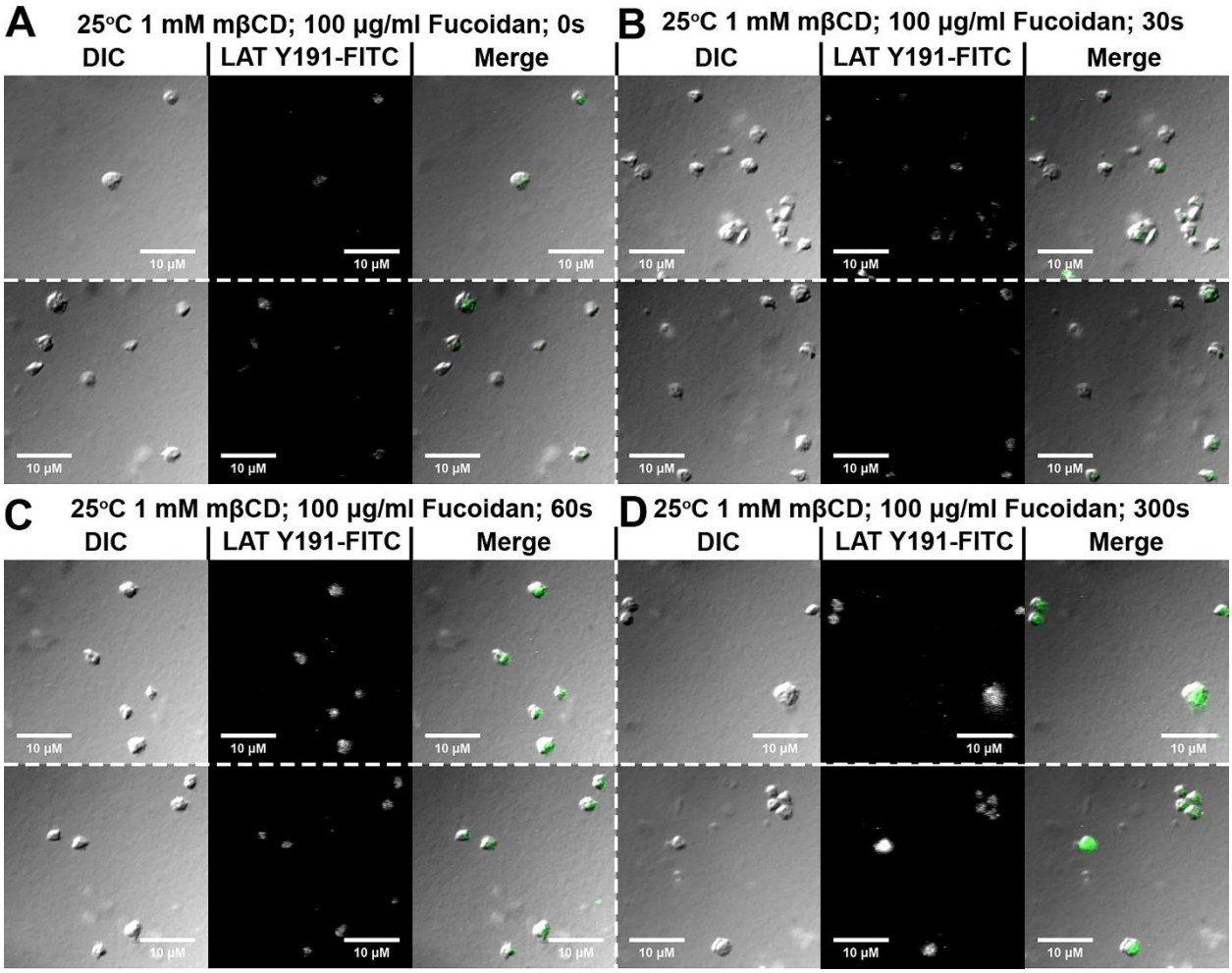

Figure S21. Immunefluorescence of cholesterol depleted platelets activated by 100 µg/ml Fucoidan at 25°C, fixed at different time-points and stained for phosphorylated LAT. (A) Resting platelets; (B) 30 second incubation with the activator; (C) 60 second incubation with the activator; (D) 300 second incubation with the activator.

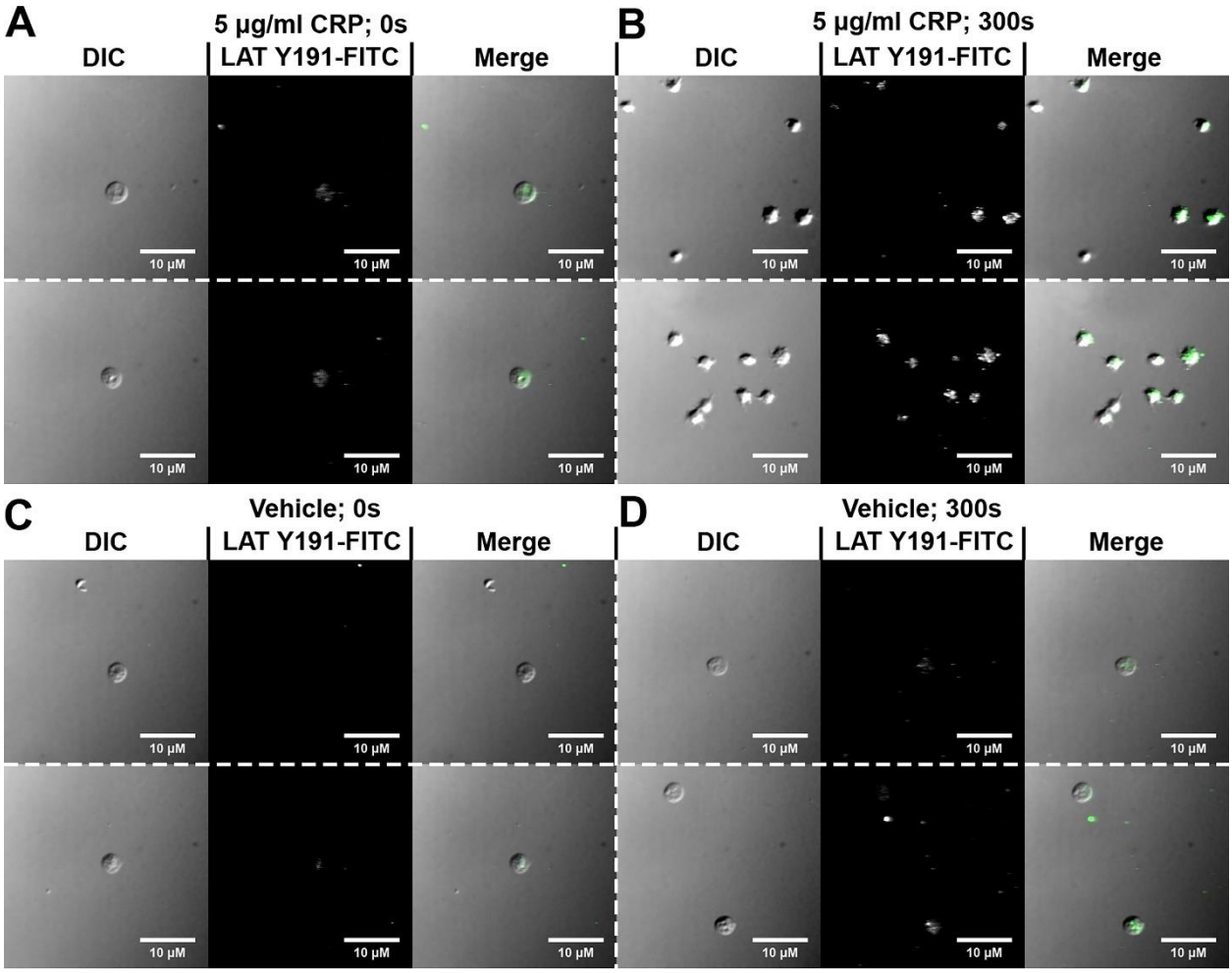

Figure S22. Immunefluorescence of platelets activated either by 5 µg/ml CRP or incubated with MQ, fixed at different time-points and stained for phosphorylated LAT. (A) Resting platelets; (B) 300 second incubation with the activator; (C) resting platelets; (D) 300 second incubation with MQ.

4. Supporting references

1. Mori, J., Y.J. Wang, S. Ellison, S. Heising, B.G. Neel, M.L. Tremblay, S.P. Watson, and Y.A. Senis. 2012. Dominant role of the protein-tyrosine phosphatase CD148 in regulating platelet activation relative to protein-tyrosine phosphatase-1B. Arterioscler. Thromb. Vasc. Biol. 32: 2956–2965.

2. Senis, Y.A., A. Mazharian, and J. Mori. 2014. Src family kinases: at the forefront of platelet activation. Blood. 124: 2013–2024.

3. Coxon, C.H., M.J. Geer, and Y.A. Senis. 2017. ITIM receptors: More than just inhibitors of platelet activation. Blood. 129: 3407–3418.

4. Bradshaw, J.M. 2010. The Src, Syk, and Tec family kinases: Distinct types of molecular switches. Cell. Signal. 22: 1175–1184.

5. Tiganis, T., and A.M. Bennett. 2007. Protein tyrosine phosphatase function: the substrate perspective. Biochem. J. 402: 1 LP – 15.

6. Spring, K., C. Chabot, S. Langlois, L. Lapointe, N.T.N. Trinh, C. Caron, J.K. Hebda, J. Gavard, M. Elchebly, and I. Royal. 2012. Tyrosine phosphorylation of DEP-1/CD148 as a mechanism controlling Src kinase activation, endothelial cell permeability, invasion, and capillary formation. Blood. 120: 2745–2756.

7. Rathore, V.B., M. Okada, P.J. Newman, and D.K. Newman. 2007. Paxillin family members function as Csk-binding proteins that regulate Lyn activity in human and murine platelets. Biochem. J. 403: 275–281.

8. Lin, X., S. Lee, and G. Sun. 2003. Functions of the activation loop in Csk protein-tyrosine kinase. J. Biol. Chem. 278: 24072–24077.

9. Hughes, C.E., B.A. Finney, F. Koentgen, K.L. Lowe, and S.P. Watson. 2015. The N-terminal SH2 domain of Syk is required for (hem) ITAM , but not integrin , signaling in mouse platelets. Blood. 125: 144–155.

10. Severin, S., A.Y. Pollitt, L. Navarro-Nunez, C.A. Nash, D. Mour??o-S??, J.A. Eble, Y.A. Senis, and S.P. Watson. 2011. Syk-dependent phosphorylation of CLEC-2: A novel mechanism of hem-immunoreceptor tyrosine-based activation motif signaling. J. Biol. Chem. 286: 4107–4116.

11. Garzon Dasgupta, A.K., A.A. Martyanov, A.A. Filkova, M.A. Panteleev, and A.N. Sveshnikova. 2020. Development of a simple kinetic mathematical model of aggregation of proteins or clustering of receptors. Submiss. .

12. Pollitt, A.Y., N.S. Poulter, E. Gitz, L. Navarro-Nuñez, Y.J. Wang, C.E. Hughes, S.G. Thomas, B. Nieswandt, M.R. Douglas, D.M. Owen, D.G. Jackson, M.L. Dustin, and S.P. Watson. 2014. Syk and src family kinases regulate c-type lectin receptor 2 (clec-2)-mediated clustering of podoplanin and platelet adhesion to lymphatic endothelial cells. J. Biol. Chem. 289: 35695–35710.

13. Filkova, A.A., A.A. Martyanov, A.K. Garzon Dasgupta, M.A. Panteleev, and A.N. Sveshnikova. 2019. Quantitative dynamics of reversible platelet aggregation: mathematical modelling and experiments. Sci. Rep. 9: 6217.

14. Manne, B.K., T.M. Getz, C.E. Hughes, O. Alshehri, C. Dangelmaier, U.P. Naik, S.P. Watson, and S.P. Kunapuli. 2013. Fucoidan is a novel platelet agonist for the C-type lectin-like receptor 2 (CLEC-2). J. Biol. Chem. 288: 7717–7726.

15. Musumeci, L., M.J. Kuijpers, K. Gilio, A. Hego, E. Th????tre, L. Maurissen, M. Vandereyken, C. V. Diogo, C. Lecut, W. Guilmain, E. V. Bobkova, J.A. Eble, R. Dahl, P. Drion, J. Rascon, Y. Mostofi, H. Yuan, E. Sergienko, T.D.Y. Chung, M. Thiry, Y. Senis, M. Moutschen, T. Mustelin, P. Lancellotti, J.W.M. Heemskerk, L. Tautz, C. Oury, and S. Rahmouni. 2015. Dual-specificity phosphatase 3 deficiency or inhibition limits platelet activation and arterial thrombosis. Circulation. 131: 656–668.

16. Sveshnikova, A.N., A. V. Balatskiy, A.S. Demianova, T.O. Shepelyuk, S.S. Shakhidzhanov, M.N. Balatskaya, A. V. Pichugin, F.I. Ataullakhanov, and M.A. Panteleev. 2016. Systems biology insights into the meaning of the platelet's dual-receptor thrombin signaling. J. Thromb. Haemost. 14: 2045–2057.

17. Balabin, F.A., and A.N. Sveshnikova. 2016. Computational biology analysis of platelet signaling reveals roles of feedbacks through phospholipase C and inositol 1,4,5-trisphosphate 3-kinase in controlling amplitude and duration of calcium oscillations. Math. Biosci. 276: 67–74.

18. Dunster, J.L., F. Mazet, M.J. Fry, J.M. Gibbins, and M.J. Tindall. 2015. Regulation of Early Steps of GPVI Signal Transduction by Phosphatases: A Systems Biology Approach. PLoS Comput. Biol. 11: 1–26.

19. Sveshnikova, A.N., F.I. Ataullakhanov, and M.A. Panteleev. 2015. Compartmentalized calcium signaling triggers subpopulation formation upon platelet activation through PAR1. Mol. BioSyst. 11: 1052–1060.

20. Eckly, A., J.Y. Rinckel, F. Proamer, N. Ulas, S. Joshi, S.W. Whiteheart, and C. Gachet. 2016. Respective contributions of single and compound granule fusion to secretion by activated platelets. Blood. 128: 2538–2549.

21. Gitz, E., A.Y. Pollitt, J.J. Gitz-Francois, O. Alshehri, J. Mori, S. Montague, G.B. Nash, M.R. Douglas, E.E. Gardiner, R.K. Andrews, C.D. Buckley, P. Harrison, and S.P. Watson. 2014. CLEC-2 expression is maintained on activated platelets and on platelet microparticles. Blood. 124: 2262–2270.

22. Burkhart, J.M., M. Vaudel, S. Gambaryan, S. Radau, U. Walter, L. Martens, J. Geiger, A. Sickmann, and R.P. Zahedi. 2012. The first comprehensive and quantitative analysis of human platelet protein composition allows the comparative analysis of structural and functional pathways. Blood. 120.

23. Kemble, D.J., Y.H. Wang, and G. Sun. 2006. Bacterial expression and characterization of catalytic loop mutants of Src protein tyrosine kinase. Biochemistry. 45: 14749–14754.

24. Ren, L., X. Chen, R. Luechapanichkul, N.G. Selner, T.M. Meyer, A.-S. Wavreille, R. Chan, C. Iorio, X. Zhou, B.G. Neel, and D. Pei. 2011. Substrate Specificity of Protein Tyrosine Phosphatases 1B, RPTPα, SHP-1, and SHP-2.

Biochemistry. 50: 2339–2356.

25. Park, M.J., R. Sheng, A. Silkov, D.J. Jung, Z.G. Wang, Y. Xin, H. Kim, P. Thiagarajan-Rosenkranz, S. Song, Y. Yoon, W. Nam, I. Kim, E. Kim, D.G. Lee, Y. Chen, I. Singaram, L. Wang, M.H. Jang, C.S. Hwang, B. Honig, S. Ryu, J. Lorieau, Y.M. Kim, and W. Cho. 2016. SH2 Domains Serve as Lipid-Binding Modules for pTyr-Signaling Proteins. Mol. Cell. 62: 7–20.

26. Tsang, E., A.M. Giannetti, D. Shaw, M. Dinh, J.K.Y. Tse, S. Gandhi, A. Ho, S. Wang, E. Papp, and J.M. Bradshaw. 2008. Molecular mechanism of the Syk activation switch. J. Biol. Chem. 283: 32650–32659.

27. Hughes, C.E., U. Sinha, A. Pandey, J.A. Eble, C.A. O'Callaghan, and S.P. Watson. 2013. Critical role for an acidic amino acid region in platelet signaling by the HemITAM (hemi-immunoreceptor tyrosine-based activation motif) containing receptor CLEC-2 (C-type lectin receptor-2). J. Biol. Chem. 288: 5127–5135.

28. Dinh, M., D. Grunberger, H. Ho, S.Y. Tsing, D. Shaw, S. Lee, J. Barnett, R.J. Hill, D.C. Swinney, and J.M. Bradshaw. 2007. Activation Mechanism and Steady State Kinetics of Bruton's Tyrosine Kinase. J. Biol. Chem. 282: 8768–8776.

29. Hughes, C.E., A.Y. Pollitt, J. Mori, J.A. Eble, M.G. Tomlinson, J.H. Hartwig, C.A. O'Callaghan, K. Fütterer, and S.P. Watson. 2010. CLEC-2 activates Syk through dimerization. Blood. 115: 2947–2955.